



This is a post-print of an article published in eLife. The final authenticated version is available online at: <https://doi.org/10.7554/eLife.43284>

Arabidopsis RCD1 Coordinates Chloroplast and Mitochondrial Functions through Interaction with ANAC Transcription Factors

Short title: RCD1 and organellar redox status

Alexey Shapiguzov^{1,2*}, Julia P. Vainonen^{1*}, Kerri Hunter^{1**}, Helena Tossavainen^{3,4**}, Arjun Tiwari^{5**}, Sari Järvi^{5**}, Maarit Hellman⁴, Fayezeah Aarabi⁶, Saleh Alseekh^{6,7}, Brecht Wybouw^{8,9}, Katrien Van Der Kelen^{8,9,10}, Lauri Nikkanen⁵, Julia Krasensky-Wrzaczek¹, Nina Sipari¹¹, Markku Keinänen¹², Esa Tyystjärvi⁵, Eevi Rintamäki⁵, Bert De Rybel^{8,9}, Jarkko Salojärvi^{1,13}, Frank Van Breusegem^{8,9}, Alisdair R. Fernie^{6,7}, Mikael Brosché^{1,14}, Perttu Permi^{3,4,15}, Eva-Mari Aro⁵, Michael Wrzaczek¹, and Jaakko Kangasjärvi¹.

* These authors contributed equally to the manuscript.

** These authors contributed equally to the manuscript.

Author affiliations

1. Organismal and Evolutionary Biology Research Programme, Faculty of Biological and Environmental Sciences, and Viikki Plant Science Center, University of Helsinki, FI-00014 Helsinki, Finland.
2. Permanent address: Institute of Plant Physiology, Russian Academy of Sciences, Botanicheskaya Street, 35, 127276 Moscow, Russia.
3. Program in Structural Biology and Biophysics, Institute of Biotechnology, University of Helsinki, FI-00014 Helsinki, Finland.
4. Department of Chemistry, Nanoscience Center, University of Jyväskylä, FI-40014 Jyväskylä, Finland.
5. Department of Biochemistry / Molecular Plant Biology, University of Turku, FI-20014 Turku, Finland.
6. Max-Planck Institute for Molecular Plant Physiology, D-14476 Potsdam-Golm, Germany.

7. Center of Plant System Biology and Biotechnology, 4000 Plovdiv, Bulgaria.
8. Department of Plant Biotechnology and Bioinformatics, Ghent University, 9052 Ghent, Belgium.
9. VIB Center for Plant Systems Biology, 9052 Ghent, Belgium.
10. Current address: Sciensano. Rue Juliette Wytsmanstraat 14, 1050 Brussels, Belgium.
11. Viikki Metabolomics Unit, Organismal and Evolutionary Biology Research Programme, Faculty of Biological and Environmental Sciences, University of Helsinki, FI-00014 Helsinki, Finland.
12. Department of Environmental and Biological Sciences, University of Eastern Finland, FI-80101 Joensuu, Finland.
13. Current address: School of Biological Sciences, Nanyang Technological University, 60 Nanyang Drive, Singapore 637551, Singapore.
14. Institute of Technology, University of Tartu, 50411 Tartu, Estonia.
15. Department of Biological and Environmental Science, Nanoscience Center, University of Jyväskylä, FI-40014 Jyväskylä, Finland.

The author responsible for distribution of materials integral to the findings presented in this article is: Jaakko Kangasjärvi (jaakko.kangasjarvi@helsinki.fi), University of Helsinki.

Corresponding author email: jaakko.kangasjarvi@helsinki.fi

Abstract

Reactive oxygen species (ROS)-dependent signaling pathways from chloroplasts and mitochondria merge at the nuclear protein RADICAL-INDUCED CELL DEATH1 (RCD1). RCD1 interacts *in vivo* and suppresses the activity of the transcription factors ANAC013 and ANAC017, which mediate a ROS-related retrograde signal originating from mitochondrial complex III. Inactivation of *RCD1* leads to increased expression of mitochondrial dysfunction stimulon (MDS) genes regulated by ANAC013 and ANAC017. Accumulating MDS gene products, including alternative oxidases (AOXs), affect redox status of the chloroplasts, leading to changes in chloroplast ROS processing and increased protection of photosynthetic apparatus. ROS alter the abundance, thiol redox state and oligomerization of the RCD1 protein *in vivo*, providing feedback control on its function. RCD1-dependent regulation is linked to chloroplast signaling by 3'-phosphoadenosine 5'-phosphate (PAP). Thus, RCD1 integrates organellar signaling from chloroplasts and mitochondria to establish transcriptional control over the metabolic processes in both organelles.

Introduction

Cells of photosynthesizing eukaryotes are unique in harboring two types of energy organelles, the chloroplasts and the mitochondria, which interact at an operational level by the exchange of metabolites, energy and reducing power (Noguchi and Yoshida 2008, Cardol et al., 2009, Bailleul et al., 2015). Reducing power flows between the organelles through several pathways, including photorespiration (Watanabe et al., 2016), malate shuttles (Scheibe 2004, Zhao et al., 2018) and transport of carbon-rich metabolites from chloroplasts to mitochondria. At the signaling level, the so-called retrograde signaling pathways originating from the organelles influence the expression of nuclear genes (de Souza et al., 2016, Leister 2017, Waszczak et al., 2018). These pathways provide feedback communication between the organelles and the gene expression apparatus in the nucleus to adjust expression of genes encoding organelle components in accordance with changes in the developmental stage or environmental conditions.

Reactive oxygen species (ROS), inevitable by-products of aerobic energy metabolism, play pivotal roles in plant organellar signaling from both chloroplasts and mitochondria (Dietz et al., 2016, Noctor et al., 2017, Waszczak et al. 2018). Superoxide anion radical ($O_2^{\cdot-}$) is formed in the organelles by the transfer of electrons from the organellar electron transfer chains (ETCs) to molecular oxygen (O_2). In illuminated chloroplasts, superoxide anion formed from O_2 reduction by Photosystem I (PSI) is converted to hydrogen peroxide (H_2O_2) which is further reduced to water by chloroplastic H_2O_2 -scavenging systems during the water-water cycle (Asada 2006, Awad et al., 2015). Chloroplast production of ROS can be enhanced by application of methyl viologen (MV), a chemical that catalyzes shuttling of electrons from PSI to O_2 (Farrington et al., 1973). The immediate product of this reaction, $O_2^{\cdot-}$, is not likely to directly mediate organellar signaling; however, H_2O_2 is involved in many retrograde signaling pathways (Leister 2017, Mullineaux et al., 2018, Waszczak et al. 2018). Organellar H_2O_2 was suggested to translocate to the nucleus directly (Caplan et al., 2015, Exposito-Rodriguez et al., 2017). It can oxidize thiol groups of specific proteins, thereby converting the ROS signal into thiol redox signals (Moller and Kristensen 2004, Nietzel et al., 2017). One recently discovered process targeted by chloroplastic H_2O_2 is the metabolism of 3'-phosphoadenosine 5'-phosphate (PAP). PAP is a toxic by-product of sulfate metabolism produced when cytoplasmic sulfotransferases (SOTs, e.g., SOT12) transfer a sulfuryl group from PAP-sulfate (PAPS) to various target compounds (Klein and Papenbrock 2004). PAP is transported to chloroplasts where it is

detoxified by dephosphorylation to adenosine monophosphate in a reaction catalyzed by the adenosine bisphosphate phosphatase 1, SAL1 (Quintero et al., 1996, Chan et al., 2016). It has been proposed that oxidation of SAL1 thiols by chloroplastic H₂O₂ inactivates the enzyme, and accumulating PAP may act as a retrograde signal (Estavillo et al., 2011, Chan et al. 2016, Crisp et al., 2018).

ROS are also produced in the mitochondria, for example by complex III at the outer side of the inner mitochondrial membrane (Cvetkovska et al., 2013, Ng et al., 2014, Huang et al., 2016, Wang et al., 2018). Blocking electron transfer through complex III by application of the inhibitors antimycin A (AA) or myxothiazol (myx) enhances electron leakage and thus induces the retrograde signal. Two known mediators of this signal are the transcription factors ANAC013 (De Clercq et al., 2013) and ANAC017 (Ng et al., 2013, Van Aken et al., 2016) that are both bound to the endoplasmic reticulum (ER) by a transmembrane domain. Mitochondria-derived signals lead to proteolytic cleavage of this domain. The proteins are released from the ER and translocated to the nucleus where they activate the mitochondrial dysfunction stimulon (MDS) genes (De Clercq et al. 2013, Van Aken et al., 2016). MDS genes include the mitochondrial alternative oxidases (AOXs), *SOT12* and *ANAC013* itself, which provides positive feedback regulation and thus enhancement of the signal.

Whereas multiple retrograde signaling pathways have been described in detail (de Souza et al. 2016, Leister 2017, Waszczak et al. 2018), it is still largely unknown how the numerous chloroplast- and mitochondria-derived signals are integrated and processed by the nuclear gene expression system. Nuclear cyclin-dependent kinase E is implicated in the expression of both chloroplastic (*LHCB2.4*) and mitochondrial (*AOX1a*) components in response to perturbations of chloroplast ETC (Blanco et al., 2014), mitochondrial ETC, or H₂O₂ treatment (Ng et al., 2013). The transcription factor ABI4 is also suggested to respond to retrograde signals from both organelles (Giraud et al., 2009, Blanco et al. 2014), although its significance in chloroplast signaling has recently been disputed (Kacprzak et al., 2019). Mitochondrial signaling *via* ANAC017 was recently suggested to converge with chloroplast PAP signaling, based on similarities in their transcriptomic profiles (Van Aken and Pogson 2017). However, the mechanistic details underlying this convergence remain currently unknown.

Arabidopsis RADICAL-INDUCED CELL DEATH1 (RCD1) is a nuclear protein containing a WWE, a PARP-like [poly (ADP-ribose) polymerase-like], and a C-terminal RST domain (RCD1-SRO1-TAF4) (Overmyer et al., 2000, Ahlfors et al., 2004, Jaspers et al., 2009, Jaspers et al., 2010). In yeast two-hybrid studies RCD1 interacted with several transcription factors (Jaspers et al. 2009) including ANAC013, DREB2A (Vainonen et al., 2012), and Rap2.4a (Hiltscher et al., 2014) *via* the RST domain (Jaspers et al., 2010). In agreement with the numerous potential interaction partners of RCD1, the *rcd1* mutant demonstrates pleiotropic phenotypes in diverse stress and developmental responses (Jaspers et al. 2009). It has been identified in screens for sensitivity to ozone (Overmyer et al. 2000), tolerance to MV (Fujibe et al., 2004) and redox imbalance in the chloroplasts (Heiber et al., 2007, Hiltscher et al. 2014). RCD1 was found to complement the deficiency of the redox sensor YAP1 in yeast (Belles-Boix et al., 2000). Under standard growth conditions, the *rcd1* mutant displays differential expression of over 400 genes, including those encoding mitochondrial AOXs (Jaspers et al. 2009, Brosche et al., 2014) and the chloroplast 2-Cys peroxiredoxin (2-CP) (Heiber et al. 2007, Hiltscher et al. 2014).

Here we have addressed the role of RCD1 in the integration of ROS signals emitted by both mitochondria and chloroplasts. Abundance, redox status and oligomerization state of the nuclear-localized RCD1 protein changed in response to ROS generated in the chloroplasts. Furthermore, RCD1 directly interacted *in vivo* with ANAC013 and ANAC017 and appeared to function as a negative regulator of both transcription factors. The RST domain, mediating RCD1 interaction with ANAC transcription factors, was required for plant sensitivity to chloroplastic ROS. We demonstrate that RCD1 is a molecular component that integrates organellar signal input from both chloroplasts and mitochondria to exert its influence on nuclear gene expression.

Results

The response to chloroplastic ROS is compromised in *rcd1*

Methyl viologen (MV) enhances ROS generation in illuminated chloroplasts by catalyzing the transfer of electrons from Photosystem I (PSI) to molecular oxygen. This triggers a chain of reactions that ultimately inhibit Photosystem II (PSII) (Farrington et al. 1973, Nishiyama et al., 2011). To reveal the significance of nuclear protein RCD1 in these reactions, rosettes of *Arabidopsis* were pre-treated with MV in darkness. Without exposure to light, the plants displayed unchanged PSII photochemical yield (Fv/Fm). Illumination resulted in a decrease of Fv/Fm in wild type (Col-0), but not in the *rcd1* mutant (Fig. 1A), suggesting increased tolerance of *rcd1* to chloroplastic ROS production. Analysis of several independent *rcd1* complementation lines expressing different levels of HA-tagged RCD1 revealed that tolerance to MV inversely correlated with the amount of expressed RCD1 (Fig. 1 – figure supplements 1, 2). This suggests that RCD1 protein quantitatively lowered the resistance of the photosynthetic apparatus to ROS.

Treatment with MV leads to formation of superoxide that is enzymatically dismutated to the more long-lived H₂O₂. Chloroplastic production of H₂O₂ in the presence of MV was assessed by staining plants with 3,3'-diaminobenzidine (DAB) under light. Higher accumulation of H₂O₂ was evident in MV pre-treated rosettes of both Col-0 and *rcd1*. Longer illumination led to a time-dependent increase in the H₂O₂ accumulation in Col-0, but not in *rcd1* (Fig. 1 – figure supplement 3). In several MV-tolerant mutants, the resistance is based on restricted access of MV to chloroplasts (Hawkes 2014). However, in *rcd1* MV pre-treatment led to an initial increase in H₂O₂ production similar to that in the wild type (Fig. 1 – figure supplement 3), suggesting that resistance of *rcd1* was not due to lowered delivery of MV to PSI. To test this directly, the kinetics of PSI oxidation was assessed by *in vivo* spectroscopy using DUAL-PAM. As expected, pre-treatment of leaves with MV led to accelerated oxidation of PSI. This effect was identical in Col-0 and *rcd1*, indicating unrestricted access of MV to PSI in the *rcd1* mutant (Fig. 1B).

The MV toxicity was not associated with the changed stoichiometry of photosystems (Fig. 1 – figure supplement 4A). However, in Col-0 it coincided with progressive destabilization of PSII complex with its light-harvesting antennae (LHCII) and accumulation of PSII monomer (Fig. 1 – figure supplement 4B). No signs of PSI inhibition were evident either in DUAL-PAM (Fig. 1B) or in PSI immunoblotting assays (Fig. 1 – figure supplement 4B)

in either genotype. The fact that production of ROS affected PSII, but not PSI where these ROS are formed, suggests that PSII inhibition results from a regulated mechanism rather than uncontrolled oxidation by ROS, and that this mechanism requires the activity of RCD1.

Previous studies have described *rcd1* as a mutant with altered ROS metabolism and redox status of the chloroplasts, although the underlying mechanisms are unknown (Fujibe et al. 2004, Heiber et al. 2007, Hiltcher et al. 2014, Cui et al., 2018). No significant changes were detected in *rcd1* in transcript levels of chloroplast-related genes (Brosche et al. 2014). Analyses of the low molecular weight antioxidant compounds ascorbate and glutathione did not explain the tolerance of *rcd1* to chloroplastic ROS either (Heiber et al. 2007, Hiltcher et al. 2014). To understand the molecular basis of the RCD1-dependent redox alterations, the levels of chloroplast proteins related to photosynthesis and ROS scavenging were analyzed by immunoblotting. None of these showed significantly altered abundance in *rcd1* compared to Col-0 (Fig. 1 – figure supplement 5A). Furthermore, no difference was detected between the genotypes in abundance and subcellular distribution of the nucleotide redox couples NAD⁺/ NADH and NADP⁺/ NADPH (Fig. 1 – figure supplement 5B, C). Finally, the redox status of chloroplast thiol redox enzymes was addressed. The chloroplast stroma-localized 2-Cys peroxiredoxin (2-CP) is an abundant enzyme (Konig et al., 2002, Peltier et al., 2006, Liebthal et al., 2018) that was recently found to link chloroplast thiol redox system to ROS (Ojeda et al., 2018, Vaseghi et al., 2018, Yoshida et al., 2018). The level of the 2-CP protein was unchanged in *rcd1* (Fig. 1 – figure supplement 5A). To assess its redox state, protein extracts were subjected to thiol bond-specific labeling as described in Fig. 1C (Nikkanen et al., 2016). While in Col-0 the larger fraction of 2-CP was present as oxidized forms, in *rcd1* most 2-CP was reduced, both in the darkness and under light. Thus, RCD1 likely is involved in the regulation of the redox status of chloroplastic thiol enzymes.

Taken together, the results hinted that the mechanisms by which RCD1 regulates chloroplastic redox status are independent of the photosynthetic ETC, or steady-state levels and distribution of nucleotide electron carriers. However, they appear to be associated with changed thiol redox state of chloroplast enzymes.

RCD1 protein is sensitive to ROS

It was next tested whether the nuclear RCD1 protein could itself be sensitive to ROS, thus accounting for the observed alterations. For that, the RCD1-HA complementation line was used (line “a” in Fig. 1 – figure supplement 1). No changes were detected in RCD1-HA abundance during 5 hours amid the standard growth light period, or during 5-hour high light treatment. On the other hand, both MV and H₂O₂ treatments led to a gradual decrease in RCD1 abundance (Fig. 2A). When plant extracts from these experiments were separated in non-reducing SDS-PAGE, the RCD1-HA signal resolved into species of different molecular weights (Fig. 2B). Under standard growth conditions or high light, most RCD1-HA formed a reduced monomer. In contrast, treatment with MV under light or H₂O₂ resulted in the fast conversion of RCD1-HA monomers into high-molecular-weight aggregates (Fig. 2B). Importantly, MV-induced redox changes in RCD1-HA only occurred in light, but not in darkness, suggesting that the changes were mediated by increased chloroplastic ROS production (Fig. 2B and Fig. 4 – figure supplement 2B). To test whether oligomerization of RCD1 was thiol-regulated, a variant of RCD1-HA was generated where seven cysteines in the linkers between the RCD1 domains were substituted by alanines (RCD1Δ7Cys; Fig. 2 – figure supplement 1A). The treatments of *rcd1*: RCD1Δ7Cys-HA plants with MV or H₂O₂ led to significantly less aggregation of RCD1Δ7Cys-HA compared to RCD1-HA. In addition, the levels of RCD1Δ7Cys-HA were insensitive to MV or H₂O₂ (Fig. 2 – figure supplement 1B). In three independent complementation lines the RCD1Δ7Cys-HA variant accumulated to higher levels compared to RCD1-HA (Fig. 2 – figure supplement 1C). This suggests the involvement of the tested RCD1 cysteine residues in the regulation of the protein oligomerization and stability *in vivo*. However, the tolerance of the RCD1Δ7Cys-HA lines to chloroplastic ROS and the expression of the selected RCD1-regulated genes in response to MV treatment were comparable to that of the RCD1-HA lines or Col-0 (Fig. 2 – figure supplement 1C, D). These results suggest that the RCD1 protein is sensitive to chloroplastic ROS. However, the changes in RCD1 abundance and redox state did not explain the RCD1-dependent redox alternations observed in the chloroplasts.

Mitochondrial respiration is altered in *rcd1*

In further search for the mechanisms of RCD1-dependent redox alternations in the chloroplast (Fig.1), analysis of cell energy metabolism was performed by [U-¹⁴C] glucose

labeling of leaf discs from light- and dark-adapted Col-0 and *rcd1* plants. Distribution of radioactive label between emitted $^{14}\text{CO}_2$ and fractionated plant material was analyzed. This revealed significantly more active carbohydrate metabolism in *rcd1* (Fig. 3 supplemental dataset 1). The redistribution of radiolabel to sucrose, starch and cell wall was elevated in *rcd1* as were the corresponding deduced fluxes (Fig. 3), suggesting that *rcd1* displayed a higher respiration rate indicative of mitochondrial defects.

Indeed, earlier transcriptomic studies in *rcd1* have revealed increased expression of genes encoding mitochondrial functions, including mitochondrial alternative oxidases (AOXs) (Jaspers et al. 2009, Brosche et al. 2014). Immunoblotting of protein extracts from isolated mitochondria with an antibody recognizing all five isoforms of Arabidopsis AOX confirmed the increased abundance of AOX in *rcd1* (Fig. 4A). The most abundant AOX isoform in Arabidopsis is AOX1a. Accordingly, only a weak signal was detected in the *aox1a* mutant. However, in the *rcd1 aox1a* double mutant AOXs other than AOX1a were evident, thus the absence of RCD1 led to an increased abundance of several AOX isoforms.

To test whether the high abundance of AOXs in *rcd1* correlated with their increased activity, seedling respiration was assayed *in vivo*. Mitochondrial AOXs form an alternative respiratory pathway to the KCN-sensitive electron transfer through complex III and cytochrome C (Fig. 4B). Thus, after recording the initial rate of O_2 uptake, KCN was added to inhibit cytochrome-dependent respiration. In Col-0 seedlings KCN led to approximately 80 % decrease in O_2 uptake, *versus* only about 20 % in *rcd1*, revealing elevated AOX capacity of the mutant (Fig. 4C). The elevated AOX capacity of *rcd1* was similar to that of an *AOX1a*-OE overexpressor line (Umbach et al., 2005). In the *rcd1 aox1a* double mutant the AOX capacity was comparable to Col-0 or *aox1a* (Fig. 4C). Thus, elevated AOX respiration of *rcd1* seedlings was dependent on the AOX1a isoform. Importantly, however, metabolism of *rcd1 aox1a* was only slightly different from *rcd1* under light and indistinguishable from *rcd1* in the darkness (Fig. 3 – supplemental dataset 1). This again indicated that the studied phenotypes of *rcd1* are associated with the induction of more than one AOX isoform. Taken together, the results suggested that inactivation of *RCD1* led to increased expression and activity of AOX isoforms, which could contribute to the observed changes in energy metabolism of *rcd1* (Fig. 3).

Mitochondrial AOXs affect ROS processing in the chloroplasts

Inhibition of complex III by antimycin A (AA) or myxothiazol (myx) activates mitochondrial retrograde signaling (Fig. 4B). It leads to nuclear transcriptional reprogramming including induction of AOX genes (Clifton et al., 2006). Accordingly, overnight treatment with either of these chemicals significantly increased the abundance of AOXs in Col-0, *rcd1* and *rcd1 aox1a* (Fig. 4 – figure supplement 1). Thus, sensitivity of *rcd1* to the complex III retrograde signal was not compromised, rather continuously augmented. In addition, no major effect was observed on RCD1-HA protein level or redox state in the RCD1-HA line treated with AA or myx, suggesting that RCD1 acts as a modulator, and not the mediator, of the mitochondrial retrograde signal (Fig. 4 – figure supplement 2).

To assess whether increased AOX abundance affected chloroplast functions, PSII inhibition was assayed in the presence of MV in AA- or myx-pre-treated leaf discs. Pre-treatment of Col-0 with either AA or myx increased the resistance of PSII to inhibition by chloroplastic ROS (Fig. 4D), thus mimicking the *rcd1* phenotype. In addition to complex III, AA has been reported to inhibit plastid cyclic electron flow dependent on PGR5 (PROTON GRADIENT REGULATION 5). Thus, *pgr5* mutant was tested for its tolerance to chloroplastic ROS after AA pre-treatment. AA made *pgr5* more MV-tolerant similarly to the wild type, indicating that PGR5 is not involved in the observed gain in ROS tolerance (Fig. 4 – figure supplement 3A).

Mitochondrial complex III signaling induces expression of several genes other than AOX. To test whether accumulation of AOXs contributed to PSII protection from chloroplastic ROS or merely correlated with it, the AOX inhibitor salicylhydroxamic acid (SHAM) was used. Treatment of plants with SHAM alone resulted in very mild PSII inhibition, which was similar in *rcd1* and Col-0 (Fig. 4 – figure supplement 3B). However, pre-treatment with SHAM made both *rcd1* and Col-0 plants significantly more sensitive to chloroplastic ROS generated by MV (Fig. 4E), thereby partially abolishing MV tolerance of the *rcd1* mutant. Involvement of the plastid terminal oxidase PTOX (Fu et al., 2012) in this effect was excluded by using the *ptox* mutant (Fig. 4 – figure supplement 3C). Noteworthy, analyses of AOX1a-OE, *aox1a* and *rcd1 aox1a* lines demonstrated that AOX1a isoform was neither sufficient nor necessary for chloroplast ROS tolerance (Fig. 4 – figure supplement 4). Taken together, these results indicated that mitochondrial AOXs

contributed to resistance of PSII to chloroplastic ROS. We hypothesize that AOX isoforms other than AOX1a are implicated in this process.

Evidence for altered electron transfer between chloroplasts and mitochondria in *rcd1*

The pathway linking mitochondrial AOXs with chloroplastic ROS processing is likely to involve electron transfer between the two organelles. Chlorophyll fluorescence under light (Fs; Fig. 1 – figure supplement 2) inversely correlates with the rate of electron transfer from PSII to plastoquinone and thus can be used as a proxy of the reduction state of the chloroplast ETC. After combined treatment with SHAM and MV (as in Fig. 4E), Fs increased in *rcd1*, but not in Col-0 (Fig. 5A). This hinted at a pathway that in *rcd1* linked the chloroplast ETC to the activity of mitochondrial AOXs, with the latter functioning as an electron sink. When the AOX activity was inhibited by SHAM, electron flow along this pathway was blocked. This led to accumulation of electrons in the chloroplast ETC and hence to the observed rise in Fs. As a parallel approach, dynamics of PSII photochemical quenching was evaluated in MV-pre-treated Col-0 and *rcd1*. In both lines, this parameter dropped within the first 20 min upon exposure to light and then started to recover. Recovery was more pronounced and more suppressed by SHAM in *rcd1* (Fig. 5 – figure supplement 1). These experiments suggest that exposure of MV-pretreated plants to light triggered an adjustment of electron flows, which was compromised by SHAM. This was in line with the involvement of AOXs in photosynthetic electron transfer and chloroplast ROS maintenance.

One of the mediators of electron transfer between the organelles is the malate shuttle (Scheibe 2004, Zhao et al. 2018). Thus, malate concentrations were measured in total extracts from Col-0 and *rcd1* seedlings. Illumination of seedlings pre-treated with MV led to dramatic decrease in malate concentration in Col-0, but not in *rcd1* (Fig. 5B). Noteworthy, under standard light-adapted growth conditions, the concentration and the subcellular distribution of malate was unchanged in *rcd1* (Fig. 5 – figure supplement 2). These observations suggest that exposure to light of MV-pre-treated plants resulted in rearrangements of electron flows that were different in Col-0 and *rcd1*.

Next, the activity of another component of the malate shuttle, the NADPH-dependent malate dehydrogenase (NADPH-MDH), was measured. Chloroplast NADPH-MDH is a redox-regulated enzyme activated by reduction of thiol bridges. Thus, the initial NADPH-

MDH activity may reflect the *in vivo* thiol redox state of the cellular compartment from which it has been isolated. After measuring this parameter, thiol reductant was added to the extracts to reveal the total NADPH-MDH activity. Both values were higher in *rcd1* than in Col-0 (Fig. 5C). To determine the contribution of *in vivo* thiol redox state, the initial NADPH-MDH activity was divided by the total activity. This value, the activation state, was also increased in *rcd1* (Fig. 5C).

Taken together, our results suggested that mitochondria contributed to ROS processing in the chloroplasts *via* a mechanism involving mitochondrial AOXs and possibly malate shuttle. These processes appeared to be dynamically regulated in response to chloroplastic ROS production, and RCD1 was involved in this regulation.

Retrograde signaling from both chloroplasts and mitochondria is altered in *rcd1*

Our results demonstrated that absence of RCD1 caused physiological alterations in both chloroplasts and mitochondria. As RCD1 is a nuclear-localized transcriptional co-regulator (Jaspers et al. 2009, Jaspers et al. 2010), its involvement in retrograde signaling pathways from both organelles was assessed. Transcriptional changes observed in *rcd1* (Jaspers et al. 2009, Brosche et al. 2014) were compared to gene expression datasets obtained after perturbations in energy organelles. This revealed a striking similarity of genes differentially regulated in *rcd1* to those affected by disturbed organellar function (Fig. 6 – figure supplement 1). Analyzed perturbations included disruptions of mitochondrial genome stability (*msh1 recA3*), organelle translation (*mterf6*, *prors1*), activity of mitochondrial complex I (*ndufs4*, rotenone), complex III (AA), and ATP synthase function (oligomycin), as well as treatments and mutants related to chloroplastic ROS production (high light, MV, H₂O₂, *alx8/ fry1*, norflurazon).

In particular, a significant overlap was observed between genes mis-regulated in *rcd1* and the mitochondrial dysfunction stimulon (MDS) genes (De Clercq et al. 2013) (Fig. 6A). Consistently, *AOX1a* was among the genes induced by the majority of the treatments. To address the role of RCD1 protein in the induction of other MDS genes, transcription of some of them was assayed 3 hours after AA treatment (Fig. 6 – figure supplement 2). As expected, expression of all these genes was elevated in *rcd1* under control conditions. AA induced accumulation of MDS transcripts to similar levels in Col-0, *rcd1* and *rcd1*: RCD1-HA lines expressing low levels of RCD1. For one marker gene,

UPOX (*UP-REGULATED BY OXIDATIVE STRESS*), AA induction was impaired in the lines expressing higher levels of RCD1-HA or RCD1 Δ 7Cys-HA (Fig. 6 supplement 2).

In addition to MDS, the list of genes mis-regulated in *rcd1* overlapped with those affected by 3'-phosphoadenosine 5'-phosphate (PAP) signaling (Estavillo et al. 2011, Van Aken and Pogson 2017) (Fig. 6A). Given that PAP signaling is suppressed by the activity of SAL1, this signaling was increased in the mutants deficient in SAL1 (*alx8* and *fry1*, Fig. 6A, Fig. 6 supplement 1). One of the MDS genes with increased expression in *rcd1* encoded the sulfotransferase SOT12, an enzyme generating PAP. Accordingly, immunoblotting of total protein extracts with α SOT12 antibody demonstrated elevated SOT12 protein abundance in *rcd1* (Fig. 6B). To address the functional interaction of RCD1 with PAP signaling, *rcd1-4* was crossed with *alx8* (also known as *sal1-8*). The resulting *rcd1 sal1* mutant was severely affected in development (Fig. 6C). The effect of PAP signaling on the tolerance of PSII to chloroplastic ROS production was tested. The single *sal1* mutant was more tolerant to MV than Col-0, while under high MV concentration *rcd1 sal1* was even more MV-tolerant than *rcd1* (Fig. 6 – figure supplement 3). Together with transcriptomic similarities between *rcd1* and *sal1* mutants, these results further supported an overlap and/ or synergy of PAP and RCD1 signaling pathways.

RCD1 interacts with ANAC transcription factors *in vivo*

Expression of the MDS genes is regulated by the transcription factors ANAC013 and ANAC017 (De Clercq et al. 2013). The ANAC-responsive *cis*-element (De Clercq et al. 2013) was significantly enriched in promoter regions of *rcd1* mis-regulated genes (Fig. 6 – figure supplement 1). This suggested a functional connection between RCD1 and transcriptional regulation of the MDS genes by ANAC013/ ANAC017. In an earlier study, ANAC013 was identified among many transcription factors interacting with RCD1 in the yeast two-hybrid system (Jaspers et al. 2009). This prompted us to investigate further the connection between RCD1 and ANAC013 and the *in vivo* relevance of this interaction.

Association of RCD1 with ANAC transcription factors *in vivo* was tested in two independent pull-down experiments. To identify interaction partners of ANAC013, an Arabidopsis line expressing ANAC013-GFP (De Clercq et al. 2013) was used. ANAC013-GFP was purified with α GFP beads, and associated proteins were identified by mass spectrometry in three replicates. RCD1 and its closest homolog SRO1, as well as ANAC017, were identified as ANAC013 interacting proteins (see Table 1 for a list of

selected nuclear-localized interaction partners of ANAC013, and Fig. 7 – supplemental dataset 1 for the full list of identified proteins and mapped peptides). These data confirmed that ANAC013, RCD1 and ANAC017 are components of the same protein complex *in vivo*. In a reciprocal pull-down assay using transgenic Arabidopsis line expressing RCD1 tagged with triple Venus YFP under the control of *UBIQUITIN10* promoter, RCD1-3xVenus and interacting proteins were immunoprecipitated using α GFP (Table 1; Fig. 7 – supplemental dataset 2). ANAC017 was found among RCD1 interactors.

To test whether RCD1 directly interacts with ANAC013/ ANAC017 *in vivo*, the complex was reconstituted in the human embryonic kidney cell (HEK293T) heterologous expression system (details in Fig. 7 – figure supplement 1). Together with the results of *in vivo* pull-down assays, these experiments strongly supported the formation of a complex between RCD1 and ANAC013/ ANAC017 transcription factors.

Structural and functional consequences of RCD1-ANAC interaction

RCD1 interacts with many transcription factors belonging to different families (Jaspers et al. 2009, Jaspers et al. 2010, Bugge et al., 2018) *via* its RST domain. The strikingly diverse set of RCD1 interacting partners may be partially explained by disordered flexible regions present in the transcription factors (Kragelund et al., 2012, O'Shea et al., 2017, Bugge et al. 2018). To address structural details of this interaction, the C-terminal domain of RCD1 (residues 468-589) including the RST domain (RST_{RCD1}; 510-568) was purified and labeled with ¹³C and ¹⁵N for NMR spectroscopic study (Tossavainen et al., 2017) (details in Fig. 7 – figure supplement 2 and Fig. 7 – supplemental dataset 3). ANAC013 was shown to interact with RCD1 in yeast two-hybrid assays (Jaspers et al. 2009, O'Shea et al. 2017). Thus, ANAC013²³⁵⁻²⁸⁴ peptide was selected to address the specificity of the interaction of the RST domain with ANAC transcription factors using NMR (details in Fig. 7 – figure supplement 3A, B). Binding of RCD1⁴⁶⁸⁻⁵⁸⁹ to ANAC013²³⁵⁻²⁸⁴ caused profound changes in the HSQC spectrum of RCD1⁴⁶⁸⁻⁵⁸⁹ (Fig. 7A, Fig. 7 – figure supplement 3C). These data supported a strong and specific binary interaction between the RCD1 RST domain and the ANAC013 transcription factor.

To evaluate the physiological significance of this interaction, stable *rcd1* complementation lines expressing an HA-tagged RCD1 variant lacking the C-terminus (amino acids 462-589) were generated. The *rcd1*: RCD1 Δ RST-HA lines were characterized by increased

accumulation of AOXs in comparison with the *rcd1*: RCD1-HA lines (Fig. 7B). They also had *rcd1*-like tolerance of PSII to chloroplastic ROS (Fig. 7C).

Physiological outcomes of the interaction between RCD1 and ANAC transcription factors were further tested by reverse genetics. ANAC017 regulates the expression of *ANAC013* in the mitochondrial retrograde signaling cascade (Van Aken et al. 2016). Since ANAC017 precedes ANAC013 in the regulatory pathway and because no *anac013* knockout mutant is available, only the *rcd1-1 anac017* double mutant was generated. In this double mutant curly leaf habitus of *rcd1* was partially suppressed (Fig. 8A). The *rcd1-1 anac017* mutant was more sensitive to chloroplastic ROS than the parental *rcd1* line (Fig. 8B). The double mutant was characterized by lower abundance of AOX isoforms (Fig. 8C), dramatically decreased expression of MDS genes (Fig. 8 – figure supplement 1) and lower AOX respiration capacity (Fig. 8D) compared to *rcd1*. Thus, gene expression, developmental, chloroplast- and mitochondria-related phenotypes of *rcd1* were partially mediated by ANAC017. These observations suggested that the *in vivo* interaction of RCD1 with ANAC transcription factors mediated by the RCD1 C-terminal RST domain are necessary for regulation of mitochondrial respiration and chloroplast ROS processing.

Discussion

RCD1 integrates chloroplast and mitochondrial signaling pathways

Plant chloroplasts and mitochondria work together to supply the cell with energy and metabolites. In these organelles, ROS are formed as by-products of the electron transfer chains (photosynthetic in chloroplasts and respiratory in mitochondria). ROS serve as versatile signaling molecules regulating many aspects of plant physiology such as development, stress signaling, systemic responses, and programmed cell death (PCD) (Dietz et al. 2016, Noctor et al. 2017, Waszczak et al. 2018). This communication network also affects gene expression in the nucleus where numerous signals are perceived and integrated. However, the molecular mechanisms of the coordinated action of the two energy organelles in response to environmental cues are only poorly understood. Evidence accumulated in this and earlier studies revealed the nuclear protein RCD1 as a regulator of energy organelle communication with the nuclear gene expression apparatus.

The *rcd1* mutant displays alterations in both chloroplasts and mitochondria (Fujibe et al. 2004, Heiber et al. 2007, Jaspers et al. 2009, Brosche et al. 2014, Hiltcher et al. 2014), and transcriptomic outcomes of RCD1 inactivation share similarities with those triggered by disrupted functions of both organelles (Fig. 6). The results here suggest that RCD1 forms inhibitory complexes with components of mitochondrial retrograde signaling *in vivo*. Chloroplastic ROS appear to exhibit a direct influence on redox state and stability of RCD1 in the nucleus. This positions RCD1 within a regulatory system encompassing mitochondrial complex III signaling through ANAC013/ ANAC017 transcription factors and chloroplastic signaling by H₂O₂. The existence of such an inter-organellar regulatory system, integrating mitochondrial ANAC013 and ANAC017-mediated signaling (De Clercq et al. 2013, Ng et al. 2013) with the PAP-mediated chloroplastic signaling (Estavillo et al. 2011, Chan et al. 2016, Crisp et al. 2018) has been previously proposed on the basis of transcriptomic analyses (Van Aken and Pogson 2017). However, the underlying molecular mechanisms were unknown. Based on our results we propose that RCD1 may function at the intersection of mitochondrial and chloroplast signaling pathways and act as a nuclear integrator of both PAP and ANAC013 and ANAC017-mediated retrograde signals.

RCD1 has been proposed to act as a transcriptional co-regulator because of its interaction with many transcription factors in yeast-two-hybrid analyses (Jaspers et al. 2009). The *in vivo* interaction of RCD1 with ANAC013 and ANAC017 revealed in this study (Table 1, Fig. 7, 8) allows RCD1 to modulate expression of the MDS, a set of nuclear genes activated by ANAC013/ ANAC017 and mostly encoding mitochondrial components (De Clercq et al. 2013). *ANAC013* itself is an MDS gene, thus mitochondrial signaling through ANAC013/ ANAC017 establishes a self-amplifying loop. Transcriptomic and physiological data support the role of RCD1 as a negative regulator of these transcription factors (Fig. 6, 7, 8). Thus, RCD1 is likely involved in the negative regulation of the ANAC013/ ANAC017 self-amplifying loop and in preventing excessive expression of MDS genes under unstressed conditions.

Induction of genes in response to stress is commonly associated with rapid inactivation of a negative co-regulator. Accordingly, the RCD1 protein was sensitive to treatments triggering or mimicking chloroplastic ROS production. MV and H₂O₂ treatment of plants resulted in rapid oligomerization of RCD1 (Fig. 2). Involvement of chloroplasts is indicated by the fact that MV treatment led to redox changes of RCD1-HA only in light (Fig. 2B, Fig.

4 – figure supplement 2B). In addition, little change was observed with the mitochondrial complex III inhibitors AA or myx (Fig. 4 – figure supplement 2A, B). Together with the fact that MDS induction was not compromised in the *rcd1* mutant (Fig. 4 – figure supplement 1, Fig. 6 – figure supplement 2), this suggests that RCD1 may primarily function as a redox sensor of chloroplastic, rather than mitochondrial, ROS/ redox signaling. In addition to fast redox changes, the overall level of RCD1 gradually decreased during prolonged (5 hours) stress treatments. This suggests several independent modes of RCD1 regulation at the protein level.

The complicated post-translational regulation of RCD1 is reminiscent of another prominent transcriptional co-regulator protein NONEXPRESSER OF PR GENES 1 (NPR1). NPR1 exists as a high molecular weight oligomer stabilized by intermolecular disulfide bonds between conserved cysteine residues. Accumulation of salicylic acid and cellular redox changes lead to the reduction of cysteines and release of NPR1 monomers that translocate to the nucleus and activate expression of defense genes (Kinkema et al., 2000, Mou et al., 2003, Withers and Dong 2016). Similar to NPR1, RCD1 has a bipartite nuclear localization signal and, in addition, a putative nuclear export signal between the WWE and PARP-like domains. Like NPR1, RCD1 has several conserved cysteine residues. This could allow redox-controlled translocation of RCD1 between the nucleus and the cytoplasm, thus providing an additional mode of regulation. Changes of RCD1 localization between the nucleus and the cytosol in response to stress conditions have previously been described in transient expression systems (Katiyar-Agarwal et al., 2006). Interestingly, mutation of seven interdomain cysteines in RCD1 largely eliminated the fast *in vivo* effect of chloroplastic ROS on redox state and stability of RCD1; however, it did not significantly alter the plant response to MV (Fig. 2, Fig. 2 – figure supplement 1C, D). This suggests that redox-dependent oligomerization of RCD1 may serve to fine-tune its activity.

MDS genes are involved in interactions between the organelles

How the RCD1-dependent induction of MDS genes contributes to the energetic and signaling landscape of the plant cell remains to be investigated. Our results suggest that one component of this adaptation is the activity of mitochondrial alternative oxidases, which are part of the MDS regulon. Consequently, AOX proteins accumulate at higher amounts in *rcd1* (Fig. 4). Pretreatment of wild type plants with complex III inhibitors AA or

myx led to elevated AOX abundance coinciding with increased tolerance to chloroplastic ROS. Moreover, the AOX inhibitor SHAM made plants more sensitive to MV, indicating the direct involvement of AOX activity in the chloroplastic ROS processing. It thus appears that AOXs in the mitochondria form an electron sink that indirectly contributes to the oxidization of the electron acceptor side of PSI. In the *rcd1* mutant, this mechanism may be continuously active. The described inter-organellar electron transfer may decrease production of ROS by PSI (asterisk in Fig. 9). Furthermore, chloroplastic ROS are considered the main electron sink for oxidation of chloroplast thiol enzymes (Ojeda et al. 2018, Vaseghi et al. 2018, Yoshida et al. 2018). Thus, the redox status of these enzymes could depend on the proposed inter-organellar pathway. This is in line with higher reduction of the chloroplast enzymes 2-CP and NADPH-MDH observed in *rcd1* (Fig. 1C, Fig. 5C).

The malate shuttle was recently shown to mediate a chloroplast-to-mitochondria electron transfer pathway that caused ROS production by complex III and evoked mitochondrial retrograde signaling (Wu et al., 2015, Zhao et al. 2018). Altered levels of malate and increased activity of NADPH-dependent malate dehydrogenase in *rcd1* (Fig. 5) suggest that in this mutant the malate shuttle could act as an inter-organellar electron carrier.

Another MDS gene with more abundant mRNA levels in the *rcd1* mutant encodes sulfotransferase SOT12, an enzyme involved in PAP metabolism (Klein and Papenbrock 2004). Accordingly, SOT12 protein level was significantly increased in the *rcd1* mutant (Fig. 6B). Accumulation of SOT12 and similarities between transcript profiles of RCD1- and PAP-regulated genes suggest that PAP signaling is likely to be constitutively active in the *rcd1* mutant. Unbalancing this signaling by elimination of SAL1 leads to severe developmental defects, as evidenced by the stunted phenotype of the *rcd1 sal1* double mutant. Thus, the RCD1 and the PAP signaling pathways appear to be overlapping and somewhat complementary, but the exact molecular mechanisms remain to be explored.

RCD1 regulates stress responses and cell fate

The MDS genes represent only a fraction of genes showing differential regulation in *rcd1* (Fig. 6 – figure supplement 1). This likely reflects the fact that RCD1 interacts with many other protein partners in addition to ANACs. The C-terminal RST domain of RCD1 was shown to interact with transcription factors belonging to DREB, PIF, ANAC, Rap2.4 and other families (Jaspers et al. 2009, Vainonen et al. 2012, Hiltcher et al. 2014, Bugge et

al. 2018). Analyses of various transcription factors interacting with RCD1 revealed little structural similarity between their RCD1-interacting sequences (O'Shea et al. 2017). The flexible structure of the C-terminal domain of RCD1 probably determines the specificity and ability of RCD1 to interact with those different transcription factors. This makes RCD1 a hub in the crosstalk of organellar signaling with hormonal, photoreceptor, immune and other pathways and a likely mechanism by which these pathways are integrated and co-regulated.

The changing environment requires plants to continuously readjust their energy metabolism and ROS processing. On the one hand, this happens because of abiotic stress factors such as changing light intensity or temperature. For example, a sunlight fleck on a shade-adapted leaf can instantly alter excitation pressure on photosystems by two orders of magnitude (Allahverdiyeva et al., 2015). On the other hand, chloroplasts and mitochondria are implicated in plant immune reactions to pathogens, contributing to decisive checkpoints including PCD (Shapiguzov et al., 2012, Petrov et al., 2015, Wu et al. 2015, Van Aken and Pogson 2017, Zhao et al. 2018). In both scenarios, perturbations of organellar ETCs may be associated with increased production of ROS. However, the physiological outcomes of the two situations can be opposite: acclimation in one case and cell death in the other. The existence of molecular mechanisms that unambiguously differentiate one type of response from the other has been previously suggested (Trotta et al., 2014, Sowden et al., 2017, Van Aken and Pogson 2017). The ANAC017 transcription factor and MDS genes, as well as PAP signaling, were proposed as organelle-related components counteracting PCD during abiotic stress (Van Aken and Pogson 2017). This suggests that RCD1 is involved in the regulation of the cell fate checkpoint. Accordingly, the *rcd1* mutant is resistant to a number of abiotic stress treatments (Ahlfors et al. 2004, Fujibe et al. 2004, Jaspers et al. 2009).

Interestingly, in contrast to its resistance to abiotic stress, *rcd1* is more sensitive to treatments related to biotic stress. The *rcd1* mutant was originally identified in a forward genetic screen for sensitivity to ozone (Overmyer et al. 2000). Ozone decomposes in the plant cell wall to ROS mimicking formation of ROS by respiratory burst oxidases (RBOHs) in the course of plant immune reactions (Joo et al., 2005, Vainonen and Kangasjarvi 2015). The opposing roles of RCD1 in the cell fate may be related to its interaction with diverse transcription factor partners and/ or different regulation of its stability and abundance. For example, transcriptomic analyses showed that under standard growth

conditions, a cluster of genes associated with defense against pathogens had decreased expression in *rcd1* (Brosche et al. 2014), and no ANAC013/ ANAC017 *cis*-element motif is associated with these genes (Fig. 6 – figure supplement 1). In agreement with its role in biotic stress, RCD1 is a target for a fungal effector protein that prevents the activation of plant immunity (Wirthmueller et al., 2018). Another possible factor determining varying roles of RCD1 in the cell fate is differential regulation of RCD1 protein function by ROS/redox signals emitted by different subcellular compartments. The sensitivity of RCD1 to chloroplastic ROS (Fig. 2) can be interpreted as negative regulation of the pro-PCD component. We hypothesize that this inactivation can occur in environmental situations that require physiological adaptation rather than PCD. For example, an abrupt increase in light intensity can cause excessive electron flow in photosynthetic ETC and overproduction of reducing power. The resulting deficiency of PSI electron acceptors can lead to increased production of chloroplastic ROS, which *via* retrograde signaling might influence RCD1 stability and/ or redox status, inhibiting its activity and thus affecting adjustments in nuclear gene expression (Fig. 9). Among other processes, RCD1-mediated suppression of ANAC013/ ANAC017 transcription factors is released, leading to the induction of the MDS regulon. The consequent expression of AOXs together with increased chloroplast-to-mitochondrial electron transfer is likely to provide electron sink for photosynthesis, which could suppress chloroplast ROS production and contribute to the plant's survival under a changing environment (Fig. 9).

Materials and methods

Plants and mutants

Arabidopsis thaliana adult plants were grown on soil (peat : vermiculite = 1:1) in white luminescent light ($220\text{-}250\ \mu\text{mol m}^{-2}\ \text{s}^{-1}$) at a 12-hour photoperiod. Seedlings were grown for 14 days on 1 x MS basal medium (Sigma-Aldrich) with 0.5 % Phytigel (Sigma-Aldrich) without added sucrose in white luminescent light ($150\text{-}180\ \mu\text{mol m}^{-2}\ \text{s}^{-1}$) at a 12-hour photoperiod. *Arabidopsis rcd1-4* mutant (GK-229D11), *rcd1-1* (Overmyer et al. 2000), *aox1a* (SAIL_030_D08), *AOX1a*-OE (Umbach et al. 2005), *ptox* (Wetzel et al., 1994), *anac017* (SALK_022174), and *sal1-8* (Wilson et al., 2009) mutants are of Col-0 background; *pgr5* mutant is of *gl1* background (Munekage et al., 2002). ANAC013-GFP line is described in (De Clercq et al. 2013), RCD1-HA line labeled “a” in Fig. 1 – figure

supplement 1 is described in (Jaspers et al. 2009), *rcd1 aox1a* double mutant – in (Brosche et al. 2014). RCD1-3xVenus, RCD1 Δ 7Cys-HA, RCD1 Δ RST-HA lines are described in *Cloning*.

Cloning

rcd1 complementation line expressing RCD1 tagged with triple HA epitope on the C-terminus was described previously (Jaspers et al. 2009). In this line the genomic sequence of RCD1 was expressed under the control of the *RCD1* native promoter (3505 bp upstream the start codon). The RCD1 Δ 7Cys-HA construct was generated in the same way as RCD1-HA. The cysteine residues were mutated to alanines by sequential PCR-based mutagenesis of the genomic sequence of *RCD1* in the pDONR/Zeo vector followed by end-joining with In-Fusion (Clontech). The RCD1 Δ RST-HA variant was generated in the same vector by removal with a PCR reaction of the region corresponding to amino acid residues 462-589. The resulting construct was transferred to the pGWB13 binary vector by a Gateway reaction. To generate the RCD1-3xVenus construct, RCD1 cDNA was fused to the *UBIQUITIN10* promoter region and to the C-terminal triple Venus YFP tag in a MultiSite Gateway reaction as described in (Siligato et al. 2016). The vectors were introduced in the *rcd1-4* mutant by floral dipping. Homozygous single insertion Arabidopsis lines were obtained. They were defined as the lines demonstrating 1:3 segregation of marker antibiotic resistance in T2 generation and 100 % resistance to the marker antibiotic in T3 generation.

For HEK293T cell experiments codon-optimized N-terminal 3xHA-fusion of RCD1 and C-terminal 3xmyc-fusion of ANAC013 were cloned into pcDNA3.1(+). Full-length ANAC017 was cloned pcDNA3.1(-) in the Xho I/ Hind III sites, the double myc tag was introduced in the reverse primer sequence. The primer sequences used for the study are presented in the Supplemental table.

Generation of the α RCD1 antibody

α RCD1 specific antibody was raised in rabbit using denatured RCD1-6His protein as the antigen for immunization (Storkbio, Estonia). The final serum was purified using denatured RCD1-6His immobilized on nitrocellulose membrane, aliquoted and stored at -80 °C. For immunoblotting, 200 μ g of total protein were loaded per well, the antibody was used in dilution 1 : 500.

Inhibitor treatments

For PSII inhibition studies, leaf discs were let floating on Milli-Q water solution supplemented with 0.05 % Tween 20 (Sigma-Aldrich). Final concentration of AA and myx was 2.5 μM each, of SHAM – 2 mM. For transcriptomic experiments, plant rosettes were sprayed with water solution of 50 μM AA complemented with 0.01 % Silwet Gold (Nordisk Alkali). Stock solutions of these chemicals were prepared in DMSO, equal volumes of DMSO were added to control samples. Pre-treatment with chemicals was carried out in the darkness, overnight for MV, AA and myx, 1 hour for SHAM. After spraying plants with 50 μM AA they were incubated in growth light for 3 hours. For chemical treatment in seedlings grown on MS plates, 5 mL of Milli-Q water with or without 50 μM MV were poured in 9-cm plates at the end of the light period. The seedlings were kept in the darkness overnight, and light treatment was performed on the following morning. For H_2O_2 treatment, the seedlings were incubated in 5 mL of Milli-Q water with or without 100 mM H_2O_2 in light.

DAB staining

Plant rosettes were stained with 3,3'-diaminobenzidine (DAB) essentially as described in (Daudi et al., 2012) [Daudi, A. and O'Brien, J. A. (2012). Detection of Hydrogen Peroxide by DAB Staining in Arabidopsis Leaves. Bio-protocol 2(18): e263. DOI: 10.21769/BioProtoc.263.]. After vacuum infiltration of DAB-staining solution in the darkness, rosettes were exposed to light ($180 \mu\text{mol m}^{-2} \text{s}^{-1}$) for 20 min to induce production of chloroplastic ROS and then immediately transferred to the bleaching solution.

Spectroscopic measurements of photosynthesis

Chlorophyll fluorescence was measured by MAXI Imaging PAM (Walz, Germany). PSII inhibition protocol consisted of repetitive 1-hour periods of blue actinic light (450 nm , $80 \mu\text{mol m}^{-2} \text{s}^{-1}$) each followed by a 20-min dark adaptation, then F_o and F_m measurement. PSII photochemical yield was calculated as $F_v/F_m = (F_m - F_o)/F_m$ (Fig. 1 – figure supplement 2). To plot raw chlorophyll fluorescence kinetics under light (F_s) against time, the reads were normalized to dark-adapted F_o . For the measurements of photochemical quenching, F_m' was measured with saturating pulses triggered against the background of activating light (450 nm , $80 \mu\text{mol m}^{-2} \text{s}^{-1}$), and the following formulae were used: $qP = (F_m' - F_s)/(F_m' - F_o')$, where $F_o' \approx F_o / (((F_m - F_o) / F_m) + (F_o / F_m'))$ (Oxborough and Baker 1997). The assays were performed in 96-well plates. In each assay, leaf discs from

at least 4 individual plants were analyzed. Each assay was reproduced at least three times.

PSI (P700) oxidation was measured by DUAL-PAM-100 (Walz, Germany) as described (Tiwari et al., 2016). Leaves were pre-treated in 1 μM MV for 4 hours, then shifted to light ($160 \mu\text{mol m}^{-2} \text{s}^{-1}$) for indicated time. Oxidation of P700 was induced by PSI-specific far red light (FR, 720 nm). To determine fully oxidized P700 (Pm), a saturating pulse of actinic light was applied under continuous background of FR, followed by switching off both the actinic and FR light. The kinetics of P700⁺ reduction by intersystem electron transfer pool and re-oxidation by FR was determined by using a multiple turnover saturating flash of PSII light (635 nm) in the background of continuous FR.

Isolation, separation and detection of proteins and protein complexes

Thylakoids were isolated as described in (Jarvi et al., 2016). Chlorophyll content was determined according to (Porra et al., 1989) and protein content according to (Lowry et al., 1951). For immunoblotting of total plant extracts, the plant material was frozen immediately after treatments in liquid nitrogen and ground. Total proteins were extracted in SDS extraction buffer [50 mM Tris-HCl (pH 7.8), 2 % SDS, 1 x protease inhibitor cocktail (Sigma-Aldrich), 2 mg/ mL NaF] for 20 min at 37 °C and centrifuged at 18 000 x g for 10 min. Supernatants were normalized for protein concentration and resolved by SDS-PAGE. For separation of proteins, SDS-PAGE (10-12 % polyacrylamide) was used (Laemmli 1970). For thylakoid proteins, the gel was complemented with 6 M urea. To separate thylakoid membrane protein complexes, isolated thylakoids were solubilized with *n*-dodecyl β -D-maltoside (Sigma-Aldrich) and separated in BN-PAGE (5-12.5 % polyacrylamide) as described by (Jarvi et al. 2016). After electrophoresis, proteins were electroblotted to PVDF membrane and immunoblotted with specific antibodies. α SOT12 antibodies have Agrisera reference number AS16 3943. For quantification of immunoblotting signal, ImageJ software was used (<https://imagej.nih.gov/ij/>).

Analysis of protein thiol redox state by mobility shift assays

Thiol redox state of 2-CPs in detached Col-0 and *rcd1* leaves adapted to darkness or light (3 hours of $160 \mu\text{mol m}^{-2} \text{s}^{-1}$), was determined by alkylating free thiols in TCA-precipitated proteins with 50 mM N-ethylmaleimide in the buffer containing 8 M urea, 100 mM Tris-HCl (pH 7.5), 1 mM EDTA, 2% SDS, and 1/10 of protease inhibitor cocktail (Thermo Scientific), reducing *in vivo* disulfides with 100 mM DTT and then alkylating the newly reduced thiols with 10 mM methoxypolyethylene glycol maleimide of molecular weight 5

kDa (Sigma-Aldrich), as described in (Nikkanen et al. 2016). Proteins were then separated by SDS-PAGE and immunoblotted with a 2-CP-specific antibody.

Non-aqueous fractionation (NAF)

Leaves of Arabidopsis plants were harvested in the middle of the light period and snap-frozen in liquid nitrogen. Four grams of fresh weight of frozen plant material was ground to a fine powder using a mixer mill (Retsch), transferred to Falcon tubes and freeze-dried at 0.02 bar for 5 days in a lyophilizer, which had been pre-cooled to $-40\text{ }^{\circ}\text{C}$. The NAF-fractionation procedure was performed as described in (Krueger et al., 2011, Arrivault et al., 2014, Krueger et al., 2014) except that the gradient volume, composed of the solvents tetrachloroethylene (C_2Cl_4)/ heptane (C_7H_{16}), was reduced from 30 mL to 25 mL but with the same linear density. Leaf powder was resuspended in 20 mL C_2Cl_4 / C_7H_{16} mixture 66:34 (v/v; density $\rho = 1.3\text{ g cm}^{-3}$), and sonicated for 2 min, with 6×10 cycles at 65 % power. The sonicated suspension was filtered through a nylon net (20 μm pore size). The net was washed with 30 mL of heptane. The suspension was centrifuged for 10 min at $3\ 200 \times g$ at $4\text{ }^{\circ}\text{C}$ and the pellet was resuspended in 5 mL C_2Cl_4 / C_7H_{16} mixture 66:34. The gradient was formed in 38 mL polyallomer centrifugation tube using a peristaltic gradient pump (BioRad) generating a linear gradient from 70 % solvent A (C_2Cl_4 / C_7H_{16} mixture 66:34) to 100 % solvent B (100 % C_2Cl_4) with a flow rate of 1.15 mL min^{-1} , resulting in a density gradient from 1.43 g cm^{-3} to 1.62 g cm^{-3} . Five mL suspension containing the sample was loaded on top of the gradient and centrifuged for 55 min at $5\ 000 \times g$ at $4\text{ }^{\circ}\text{C}$ using a swing-out rotor with acceleration and deceleration of 3:3 (brakes off). Each of the compartment-enriched fractions (F1 to F8) were transferred carefully from the top of the gradient into a 50-mL Falcon tube, filled up with heptane to a volume of 20 mL and centrifuged at $3\ 200 \times g$ for 10 min. The pellet was resuspended in 6 mL of heptane and subsequently divided into 6 aliquots of equal volume (950 μL). The pellets had been dried in a vacuum concentrator without heating and stored at $-80\text{ }^{\circ}\text{C}$ until further use. Subcellular compartmentation of markers or the metabolites of our interest was calculated by BestFit method as described in (Krueger et al. 2011, Krueger et al. 2014). Percentage values (% of the total found in all fractions) of markers and metabolites have been used to make the linear regressions for subcellular compartments using BestFit.

Marker measurements for non-aqueous fractionation

Before enzyme and metabolite measurements, dried pellets were homogenized in the corresponding extraction buffer by the addition of one steel ball (2-mm diameter) to each

sample and shaking at 25 Hz for 1 min in a mixer mill. Enzyme extracts were prepared as described in (Gibon et al., 2004) with some modifications. The extraction buffer contained 50 mM HEPES-KOH (pH 7.5), 10 mM MgCl₂, 1 mM EDTA, 1 mM EGTA, 1 mM benzamidine, 1 mM ε-aminocaproic acid, 0.25 % (w/v) BSA, 20 μM leupeptin, 0.5 mM DTT, 1 mM phenylmethylsulfonyl fluoride (PMSF), 1 % (v/v) Triton X-100, 20 % glycerol. The extract was centrifuged (14 000 rpm at 4 °C for 10 min) and the supernatant was used directly for the enzymatic assays. The activities of adenosine diphosphate glucose pyrophosphorylase (AGPase) and phosphoenolpyruvate carboxylase (PEPC) were determined as described in (Gibon et al. 2004) but without using the robot-based platform. Chlorophyll was extracted twice with 80 % (v/v) and once with 50 % (v/v) hot ethanol/ 10 mM HEPES (pH 7.0) followed by 30-min incubation at 80 °C and determined as described in (Cross et al., 2006). Nitrate was measured by the enzymatic reaction as described in (Cross et al. 2006).

Incubation of Arabidopsis leaf discs with [U-¹⁴C] glucose

For the light experiment, leaf discs were incubated in light in 5 mL 10 mM MES-KOH (pH 6.5), containing 1.85 MBq/ mmol [U-¹⁴C] glucose (Hartmann Analytic) in a final concentration of 2 mM. In the dark experiment, leaf discs were incubated under green light for 150 min. Leaf discs were placed in a sieve, washed several times in double-distilled water, frozen in liquid nitrogen, and stored at -80 °C until further analysis. All incubations were performed in sealed flasks under green light and shaken at 100 rpm. The evolved ¹⁴CO₂ was collected in 0.5 mL of 10 % (w/v) KOH.

Fractionation of ¹⁴C-labeled tissue extracts and measurement of metabolic fluxes

Extraction and fractionation were performed according to (Obata et al., 2017). Frozen leaf discs were extracted with 80 % (v/v) ethanol at 80 °C (1 mL per sample) and re-extracted in two subsequent steps with 50 % (v/v) ethanol (1 mL per sample for each step), and the combined supernatants were dried under an air stream at 35 °C and resuspended in 1 mL of water (Fernie et al., 2001). The soluble fraction was subsequently separated into neutral, anionic, and basic fractions by ion-exchange chromatography; the neutral fraction (2.5 mL) was freeze-dried, resuspended in 100 μL of water, and further analyzed by enzymatic digestion followed by a second ion-exchange chromatography step (Carrari et al., 2006). To measure phosphate esters, samples (250 μL) of the soluble fraction were incubated in 50 μL of 10 mM MES-KOH (pH 6.0), with or without 1 unit of potato acid phosphatase (grade II; Boehringer Mannheim) for 3 hours at 37 °C, boiled for 2 min, and

analyzed by ion-exchange chromatography (Fernie et al. 2001). The insoluble material left after ethanol extraction was homogenized, resuspended in 1 mL of water, and counted for starch (Fernie et al. 2001). Fluxes were calculated as described following the assumptions detailed by Geigenberger *et al* (Geigenberger et al., 1997, Geigenberger et al., 2000). Unfortunately, the discontinued commercial availability of the required positionally radiolabeled glucoses prevented us from analyzing fermentative fluxes more directly.

Preparation of crude mitochondria

Crude mitochondria were isolated from *Arabidopsis* rosette leaves as described in (Keech et al., 2005).

Measurements of AOX capacity in vivo

Seedling respiration and AOX capacity were assessed by measuring O₂ consumption in the darkness using a Clark electrode as described in (Schwarzlander et al., 2009).

Metabolite extraction

Primary metabolites were analyzed with GC-MS according to (Roessner et al., 2000). GC-MS analysis was executed from the plant extracts of eight biological replicates (pooled samples). Plant material was homogenized in a Qiagen TissueLyser II bead mill (Qiagen, Germany) with 1-1.5 mm Retsch glass beads. Soluble metabolites were extracted from plant material in two steps, first with 1 mL of 100 % methanol (Merck) and second with 1 mL of 80 % (v/v) aqueous methanol. During the first extraction step, 5 μ L of internal standard solution (0.2 mg mL⁻¹ of benzoic-d₅ acid, 0.1 mg mL⁻¹ of glycerol-d₈, 0.2 mg mL⁻¹ of 4-methylumbelliferone in methanol) was added to each sample. During both extraction steps, the samples were vortexed for 30 min and centrifuged for 5 min at 13 000 rpm (13 500 \times g) at 4 °C. The supernatants were then combined for metabolite analysis. The extracts (2 mL) were dried in a vacuum concentrator (MiVac Duo, Genevac Ltd, Ipswich, UK), the vials were degassed with nitrogen and stored at -80 °C prior to derivatization and GC-MS analysis.

Dried extracts were re-suspended in 500 μ L of methanol. Aliquot of 200 μ L was transferred to a vial and dried in a vacuum. The samples were derivatized with 40 μ L of methoxyamine hydrochloride (MAHC, Sigma-Aldrich) (20 mg mL⁻¹) in pyridine (Sigma-Aldrich) for 90 min at 30 °C at 150 rpm, and with 80 μ L N-methyl-N-(trimethylsilyl) trifluoroacetamide with 1 % trimethylchlorosilane (MSTFA with 1 % TMCS, Thermo

Scientific) for 120 min at 37 °C at 150 rpm. Alkane series (10 µL, C10–C40, Supelco) in hexane (Sigma-Aldrich) and 100 µL of hexane was added to each sample before GC-MS analysis.

Metabolite analysis by gas chromatography-mass spectrometry

The GC-MS system consisted of Agilent 7890A gas chromatograph with 7000 Triple quadrupole mass spectrometer and GC PAL autosampler and injector (CTC Analytics). Splitless injection (1 µL) was employed using a deactivated single tapered splitless liner with glass wool (Topaz, 4 mm ID, Restek). Helium flow in the column (Agilent HP-5MS Ultra Inert, length 30 m, 0.25 mm ID, 0.25 µm film thickness combined with Agilent Ultimate Plus deactivated fused silica, length 5 m, 0.25 mm ID) was 1.2 mL min⁻¹ and purge flow at 0.60 min was 50 mL min⁻¹. The injection temperature was set to 270 °C, MS interface 180 °C, source 230 °C and quadrupole 150 °C. The oven temperature program was as follows: 2 min at 50 °C, followed by a 7 °C min⁻¹ ramp to 260 °C, 15 °C min⁻¹ ramp to 325 °C, 4 min at 325 °C and post-run at 50 °C for 4.5 min. Mass spectra were collected with a scan range of 55-550 *m/z*.

Metabolite Detector (versions 2.06 beta and 2.2N) (Hiller et al., 2009) and AMDIS (version 2.68, NIST) were used for deconvolution, component detection and quantification. Malate levels were calculated as the peak area of the metabolite normalized with the peak area of the internal standard, glycerol-d₈, and the fresh weight of the sample.

Measurements of NADPH-MDH activity

From light-adapted plants grown for 5 weeks (100-120 µmol m⁻² s⁻¹ at an 8-hour day photoperiod), total extracts were prepared as for non-aqueous fractionation in the extraction buffer supplemented with 250 µM DTT. In microplates, 5 µL of the extract (diluted x 500) were mixed with 20 µL of activation buffer (0.1 M Tricine-KOH (pH 8.0), 180 mM KCl, 0.5 % Triton X-100). Initial activity was measured immediately after, while total activity was measured after incubation for 2 hours at room temperature in presence of additional 150 mM DTT. Then assay mix was added consisting of 20 µL of assay buffer [0.5 M Tricine-KOH (pH 8.0), 0.25 % Triton X-100, 0.5 mM EDTA], 9 µL of water, and 1 µL of 50 mM NADPH (prepared in 50 mM NaOH), after which 45 µL of 2.5 mM oxaloacetate or water control was added. The reaction was mixed, and light absorbance at 340-nm wavelength was measured at 25 °C.

Analysis of rcd1 misregulated genes in microarray experiments related to chloroplast or mitochondrial dysfunction

Genes with misregulated expression in *rcd1* were selected from our previous microarray datasets (Brosche et al. 2014) with the cutoff, absolute value of logFC < 0.5. These genes were subsequently clustered with the *rcd1* gene expression dataset together with various Affymetrix datasets related to chloroplast or mitochondrial dysfunction from the public domain using bootstrapped Bayesian hierarchical clustering as described in (Wrzaczek et al., 2010). Affymetrix raw data (.cel files) were normalized with Robust Multi-array Average normalization, and manually annotated to control and treatment conditions, or mutant *versus* wild type.

Affymetrix ATH1-121501 data were from the following sources: Gene Expression Omnibus <https://www.ncbi.nlm.nih.gov/geo/>, AA 3 hours (in figures labelled as experiment 1), GSE57140 (Ivanova et al., 2014); AA and H₂O₂, 3 hour treatments (in figures labelled as experiment 2), GSE41136 (Ng et al. 2013); MV 3 hours, GSE41963 (Sharma et al., 2013); *mterf6-1*, GSE75824 (Leister and Kleine 2016); *prors1-2*, GSE54573 (Leister et al., 2014); H₂O₂ 30 min, GSE43551 (Gutierrez et al., 2014); high light 1 hour (in figures labelled as experiment 1), GSE46107 (Van Aken et al., 2013); high light 30 min in cell culture, GSE22671 (Gonzalez-Perez et al., 2011); high light 3 hours (in figures labelled as experiment 2), GSE7743 (Kleine et al., 2007); oligomycin 1 and 4 hours, GSE38965 (Geisler et al., 2012); norflurazon – 5 day-old seedlings grown on plates with norflurazon, GSE12887 (Koussevitzky et al., 2007); *msh1 recA3* double mutant, GSE19603 (Shedge et al., 2010). AtGenExpress oxidative time series, MV 12 and 24 hours,

http://www.arabidopsis.org/servlets/TairObject?type=expression_set&id=1007966941.

ArrayExpress, <https://www.ebi.ac.uk/arrayexpress/>: rotenone, 3 and 12 hours, E-MEXP-1797 (Garmier et al., 2008); *alx8* and *fry1*, E-MEXP-1495 (Wilson et al. 2009); *ndufs4*, E-MEXP-1967 (Meyer et al., 2009).

Quantitative PCR

Quantitative PCR was performed essentially as described in (Brosche et al. 2014). The data were normalized with three reference genes, *PP2AA3*, *TIP41* and *YLS8*. Relative expression of the genes *RCD1*, *AOX1a*, *UPOX*, *ANAC013*, *At5G24640* and *ZAT12* was calculated in qBase+ 3.2 (Biogazelle, <https://www.qbaseplus.com/>). The primer sequences and primer efficiencies are presented in the Supplemental table.

Identification of interacting proteins using IP/MS-MS

Immunoprecipitation experiments were performed in three biological replicates as described previously (De Rybel et al., 2013), using 3 g of rosette leaves from p35S: ANAC013-GFP and 2.5 g of rosette leaves from pUBI10: RCD1-3xVenus transgenic lines. Interacting proteins were isolated by applying total protein extracts to α GFP-coupled magnetic beads (Milteny Biotech). Three replicates of p35S: ANAC013-GFP or pUBI10: RCD1-3xVenus were compared to three replicates of Col-0 controls. Tandem mass spectrometry (MS) and statistical analysis using MaxQuant and Perseus software was performed as described previously (Wendrich et al., 2017).

HEK293T human embryonic kidney cell culture and transfection

HEK293T cells were maintained at 37 °C and 5 % CO₂ in Dulbecco's Modified Eagle's Medium F12-HAM, supplemented with 10 % fetal bovine serum, 15 mM HEPES, and 1 % penicillin/ streptomycin. Cells were transiently transfected using GeneJuice (Novagen) according to the manufacturer's instructions.

For co-immunoprecipitation experiments, HEK293T cells were co-transfected with plasmids encoding HA-RCD1 and ANAC013-myc or ANAC017-myc. Forty hours after transfection, cells were lysed in TNE buffer [50 mM Tris-HCl (pH 7.4), 150 mM NaCl, 5 mM EDTA, 1 % Triton X-100, 1 x protease inhibitor cocktail, 50 μ M proteasome inhibitor MG132 (Sigma-Aldrich)]. After incubation for 2 hours at 4 °C, lysates were cleared by centrifugation at 18 000 x *g* for 10 min at 4 °C. For co-immunoprecipitation, cleared cell lysates were incubated with either α HA or α myc antibody immobilized on agarose beads overnight at 4 °C. Beads were washed six times with the lysis buffer. The bound proteins were dissolved in SDS sample buffer, resolved by SDS-PAGE, and immunoblotted with the specified antibodies.

Protein expression and purification

The C-terminal domain of RCD1 for NMR study was expressed as GST-fusion protein in *E.coli* BL21 (DE3) Codon Plus strain and purified using GSH-Sepharose beads (GE Healthcare) according to the manufacturer's instruction. Cleavage of GST tag was performed with thrombin (GE Healthcare, 80 units per mL of beads) for 4 hours at room temperature and the C-terminal domain of RCD1 was eluted from the beads with PBS buffer (137 mM NaCl, 2.7 mM KCl, 10 mM Na₂HPO₄, 1.8 mM KH₂PO₄, pH 7.4). The protein was further purified by gel filtration with HiLoad 16/600 Superdex 75 column (GE

Healthcare) equilibrated with 20 mM sodium phosphate buffer (pH 6.4), 50 mM NaCl at 4 °C.

Peptide synthesis

ANAC013 peptides of > 98 % purity for surface plasmon resonance and NMR analysis were purchased from Genecust, dissolved in water to 5 mM final concentration and stored at -80 °C before analyses.

Surface plasmon resonance

The C-terminal domain of RCD1 was covalently coupled to a Biacore CM5 sensor chip *via* amino-groups. 500 nM of ANAC013 peptides were then profiled at a flow rate of 30 $\mu\text{L min}^{-1}$ for 300 s, followed by 600 s flow of running buffer. Analysis was performed at 25 °C in the running buffer containing 10 mM HEPES (pH 7.4), 150 mM NaCl, 3 mM EDTA, 0.05 % surfactant P20 (Tween-20). After analysis in BiaEvaluation (Biacore) software, the normalized resonance units were plotted over time with the assumption of one-to-one binding.

NMR spectroscopy

NMR sample production and chemical shift assignment have been described in (Tossavainen et al. 2017). A Bruker Avance III HD 800 MHz spectrometer equipped with a TCI $^1\text{H}/^{13}\text{C}/^{15}\text{N}$ cryoprobe was used to acquire spectra for structure determination of RCD1⁴⁶⁸⁻⁵⁸⁹. Peaks were manually picked from three NOE spectra, a ^1H , ^{15}N NOESY-HSQC and ^1H , ^{13}C NOESY-HSQC spectra for the aliphatic and aromatic ^{13}C regions. CYANA 2.1 (Lopez-Mendez and Guntert 2006) automatic NOE peak assignment – structure calculation routine was used to generate 300 structures from which 30 were further refined in explicit water with AMBER 16 (Case et al., 2005). Assignments of three NOE peaks were kept fixed using the KEEP subroutine in CYANA. These NOE peaks restrained distances between the side chains of W507 and M508 and adjacent helices 1 and 4, respectively. Fifteen lowest AMBER energy structures were chosen to represent of RCD1⁴⁶⁸⁻⁵⁸⁹ structure in solution.

Peptide binding experiment was carried out by preparing a sample containing of RCD1⁴⁶⁸⁻⁵⁸⁹ and ANAC013²³⁵⁻²⁸⁴ peptide in an approximately 1:2 concentration ratio, and recording a ^1H , ^{15}N HSQC spectrum. Amide peak positions were compared with those of the free RCD1⁴⁶⁸⁻⁵⁸⁹.

Acknowledgements

We thank Dr. Olga Blokhina, Dr. Bernadette Gehl and Manuel Saornil for the help in studies of mitochondria, Katariina Vuorinen for genotyping *rcd1-1 anac017*, Richard Gossens for critical comments on the manuscript. Prof. F. J. Cejudo (Institute of Plant Biochemistry, University of Sevilla) for the α -CP antibody. Dr. Saijaliisa Kangasjärvi for the α SOT12 antibody. We acknowledge CSC – IT Center for Science, Finland, for computational resources. This work was supported by the University of Helsinki (JK); the Academy of Finland Centre of Excellence programs (2006-11; JK and 2014-19; JK, EMA) and Research Grant (Decision 250336; JK); Academy of Finland fellowships (Decisions 275632, 283139 and 312498; MW); Academy of Finland Research Grant (Decision 288235; PP); by The Research Foundation – Flanders (FWO; Odysseus II G0D0515N and Post-doc grant 12D1815N; BW and BDR); PlantaSYST project by the European Union's Horizon 2020 research and innovation programme (SGA-CSA No 664621 and No 739582 under FPA No. 664620; SA and ARF); Deutsche Forschungsgemeinschaft (DFG TRR 175 The Green Hub – Central Coordinator of Acclimation in Plants; FA and ARF); the Research Foundation – Flanders (Excellence of Science project no 30829584; FVB).

Author contributions

J.K., A.S., M.W., S.J., J.P.V., M.B., A.R.F., E.R., E.-M.A., F.B., and P.P. designed the research. J.P.V., K.H., B.W., K.V.D.K., B.D.R., F.B., and M.W. carried out *in vivo* pull-down experiments of RCD1 and ANACs. A.S., J.P.V., S.J., A.T., L.N., E.T., E.R., and E.-M.A. performed studies of photosynthesis and respiration. A.R.F., F.A., S.A., N.S., A.S., and M.K. conducted metabolomic studies. J.P.V., H.T., M.H., and P.P. carried out structural analyses of RCD1. J.S. and M.B. performed bioinformatic studies. A.S., J.P.V., M.W., J.K.-W., M.B., A.R.F., and J.K. wrote the manuscript.

References

- Ahlfors, R., S. Lang, K. Overmyer, P. Jaspers, M. Brosche, A. Tauriainen, H. Kollist, H. Tuominen, E. Belles-Boix, M. Piippo, D. Inze, E. T. Palva and J. Kangasjarvi. Arabidopsis RADICAL-INDUCED CELL DEATH1 belongs to the WWE protein-protein interaction domain protein family and modulates abscisic acid, ethylene, and methyl jasmonate responses. (2004) **Plant Cell** 16(7): 1925-1937.
- Allahverdiyeva, Y., M. Suorsa, M. Tikkanen and E. M. Aro. Photoprotection of photosystems in fluctuating light intensities. (2015) **J Exp Bot** 66(9): 2427-2436.

- Ap Rees, T. Assessment of the contribution of metabolic pathways to plant respiration (1978) **Metabolism and Respiration. A Comprehensive Treatise. Edited by David D. Davies. Academic Press Inc. San Diego.** : 1-27.
- Arrivault, S., M. Guenther, A. Florian, B. Encke, R. Feil, D. Vosloh, J. E. Lunn, R. Sulpice, A. R. Fernie, M. Stitt and W. X. Schulze. Dissecting the subcellular compartmentation of proteins and metabolites in arabidopsis leaves using non-aqueous fractionation. (2014) **Mol Cell Proteomics** 13(9): 2246-2259.
- Asada, K. Production and scavenging of reactive oxygen species in chloroplasts and their functions. (2006) **Plant Physiol** 141(2): 391-396.
- Awad, J., H. U. Stotz, A. Fekete, M. Krischke, C. Engert, M. Havaux, S. Berger and M. J. Mueller. 2-cysteine peroxiredoxins and thylakoid ascorbate peroxidase create a water-water cycle that is essential to protect the photosynthetic apparatus under high light stress conditions. (2015) **Plant Physiol** 167(4): 1592-1603.
- Bailleul, B., N. Berne, O. Murik, D. Petroutsos, J. Prihoda, A. Tanaka, V. Villanova, R. Bligny, S. Flori, D. Falconet, A. Krieger-Liszky, S. Santabarbara, F. Rappaport, P. Joliot, L. Tirichine, P. G. Falkowski, P. Cardol, C. Bowler and G. Finazzi. Energetic coupling between plastids and mitochondria drives CO₂ assimilation in diatoms. (2015) **Nature** 524(7565): 366-369.
- Belles-Boix, E., E. Babiychuk, M. Van Montagu, D. Inze and S. Kushnir. CEO1, a new protein from Arabidopsis thaliana, protects yeast against oxidative damage. (2000) **FEBS Lett** 482(1-2): 19-24.
- Blanco, N. E., M. Guinea-Diaz, J. Whelan and A. Strand. Interaction between plastid and mitochondrial retrograde signalling pathways during changes to plastid redox status. (2014) **Philos Trans R Soc Lond B Biol Sci** 369(1640): 20130231.
- Brosche, M., T. Blomster, J. Salojarvi, F. Cui, N. Sipari, J. Leppala, A. Lamminmaki, G. Tomai, S. Narayanasamy, R. A. Reddy, M. Keinanen, K. Overmyer and J. Kangasjarvi. Transcriptomics and functional genomics of ROS-induced cell death regulation by RADICAL-INDUCED CELL DEATH1. (2014) **PLoS Genet** 10(2): e1004112.
- Bugge, K., L. Staby, K. R. Kemplen, C. O'Shea, S. K. Bendtsen, M. K. Jensen, J. G. Olsen, K. Skriver and B. B. Kragelund. Structure of Radical-Induced Cell Death1 Hub Domain Reveals a Common alpha-alpha-Scaffold for Disorder in Transcriptional Networks. (2018) **Structure** 26(5): 734-746 e737.
- Caplan, J. L., A. S. Kumar, E. Park, M. S. Padmanabhan, K. Hoban, S. Modla, K. Czymmek and S. P. Dinesh-Kumar. Chloroplast Stromules Function during Innate Immunity. (2015) **Dev Cell** 34(1): 45-57.
- Cardol, P., J. Alric, J. Girard-Bascou, F. Franck, F. A. Wollman and G. Finazzi. Impaired respiration discloses the physiological significance of state transitions in Chlamydomonas. (2009) **Proc Natl Acad Sci U S A** 106(37): 15979-15984.
- Carrari, F., C. Baxter, B. Usadel, E. Urbanczyk-Wochniak, M. I. Zanon, A. Nunes-Nesi, V. Nikiforova, D. Centero, A. Ratzka, M. Pauly, L. J. Sweetlove and A. R. Fernie. Integrated analysis of metabolite and transcript levels reveals the metabolic shifts that underlie tomato fruit development and highlight regulatory aspects of metabolic network behavior. (2006) **Plant Physiol** 142(4): 1380-1396.
- Case, D. A., T. E. Cheatham, 3rd, T. Darden, H. Gohlke, R. Luo, K. M. Merz, Jr., A. Onufriev, C. Simmerling, B. Wang and R. J. Woods. The Amber biomolecular simulation programs. (2005) **J Comput Chem** 26(16): 1668-1688.
- Chan, K. X., P. D. Mabbitt, S. Y. Phua, J. W. Mueller, N. Nisar, T. Gigolashvili, E. Stroehrer, J. Grassl, W. Arlt, G. M. Estavillo, C. J. Jackson and B. J. Pogson. Sensing and signaling of oxidative stress in chloroplasts by inactivation of the SAL1 phosphoadenosine phosphatase. (2016) **Proc Natl Acad Sci U S A** 113(31): E4567-4576.
- Clifton, R., A. H. Millar and J. Whelan. Alternative oxidases in Arabidopsis: a comparative analysis of differential expression in the gene family provides new insights into function of non-phosphorylating bypasses. (2006) **Biochim Biophys Acta** 1757(7): 730-741.
- Crisp, P. A., A. B. Smith, D. R. Ganguly, K. D. Murray, S. R. Eichten, A. A. Millar and B. J. Pogson. RNA Polymerase II read-through promotes expression of neighboring genes in SAL1-PAP-XRN retrograde signaling. (2018) **Plant Physiol**.

- Cross, J. M., M. von Korff, T. Altmann, L. Bartzetko, R. Sulpice, Y. Gibon, N. Palacios and M. Stitt. Variation of enzyme activities and metabolite levels in 24 *Arabidopsis* accessions growing in carbon-limited conditions. (2006) **Plant Physiol** 142(4): 1574-1588.
- Cui, F., M. Brosché, A. Shapiguzov, X.-Q. He, J. P. Vainonen, J. Leppälä, A. Trotta, S. Kangasjärvi, J. Salojärvi, J. Kangasjärvi and K. Overmyer. Methyl viologen can affect mitochondrial function in *Arabidopsis*. (2018) <https://www.biorxiv.org/content/early/2018/10/07/436543>.
- Cvetkovska, M., N. A. Alber and G. C. Vanlerberghe. The signaling role of a mitochondrial superoxide burst during stress. (2013) **Plant Signal Behav** 8(1): e22749.
- Daudi, A., Z. Cheng, J. A. O'Brien, N. Mammarella, S. Khan, F. M. Ausubel and G. P. Bolwell. The apoplastic oxidative burst peroxidase in *Arabidopsis* is a major component of pattern-triggered immunity. (2012) **Plant Cell** 24(1): 275-287.
- De Clercq, I., V. Vermeirssen, O. Van Aken, K. Vandepoele, M. W. Murcha, S. R. Law, A. Inze, S. Ng, A. Ivanova, D. Rombaut, B. van de Cotte, P. Jaspers, Y. Van de Peer, J. Kangasjärvi, J. Whelan and F. Van Breusegem. The membrane-bound NAC transcription factor ANAC013 functions in mitochondrial retrograde regulation of the oxidative stress response in *Arabidopsis*. (2013) **Plant Cell** 25(9): 3472-3490.
- De Rybel, B., B. Moller, S. Yoshida, I. Grabowicz, P. Barbier de Reuille, S. Boeren, R. S. Smith, J. W. Borst and D. Weijers. A bHLH complex controls embryonic vascular tissue establishment and indeterminate growth in *Arabidopsis*. (2013) **Dev Cell** 24(4): 426-437.
- de Souza, A., J. Z. Wang and K. Dehesh. Retrograde Signals: Integrators of Interorganellar Communication and Orchestrators of Plant Development. (2016) **Annu Rev Plant Biol**.
- Dietz, K. J., R. Mittler and G. Noctor. Recent Progress in Understanding the Role of Reactive Oxygen Species in Plant Cell Signaling. (2016) **Plant Physiol** 171(3): 1535-1539.
- Estavillo, G. M., P. A. Crisp, W. Pornsiriwong, M. Wirtz, D. Collinge, C. Carrie, E. Giraud, J. Whelan, P. David, H. Javot, C. Brearley, R. Hell, E. Marin and B. J. Pogson. Evidence for a SAL1-PAP chloroplast retrograde pathway that functions in drought and high light signaling in *Arabidopsis*. (2011) **Plant Cell** 23(11): 3992-4012.
- Exposito-Rodriguez, M., P. P. Laissue, G. Yvon-Durocher, N. Smirnov and P. M. Mullineaux. Photosynthesis-dependent H₂O₂ transfer from chloroplasts to nuclei provides a high-light signalling mechanism. (2017) **Nat Commun** 8(1): 49.
- Farrington, J. A., M. Ebert, E. J. Land and K. Fletcher. Bipyridylum quaternary salts and related compounds. V. Pulse radiolysis studies of the reaction of paraquat radical with oxygen. Implications for the mode of action of bipyridyl herbicides. (1973) **Biochim Biophys Acta** 314(3): 372-381.
- Fernie, A. R., A. Roscher, R. G. Ratcliffe and N. J. Kruger. Fructose 2,6-bisphosphate activates pyrophosphate: fructose-6-phosphate 1-phosphotransferase and increases triose phosphate to hexose phosphate cycling in heterotrophic cells. (2001) **Planta** 212(2): 250-263.
- Fettke, J., N. Eckermann, A. Tiessen, P. Geigenberger and M. Steup. Identification, subcellular localization and biochemical characterization of water-soluble heteroglycans (SHG) in leaves of *Arabidopsis thaliana* L.: distinct SHG reside in the cytosol and in the apoplast. (2005) **Plant J** 43(4): 568-585.
- Fu, A., H. Liu, F. Yu, S. Kambakam, S. Luan and S. Rodermel. Alternative oxidases (AOX1a and AOX2) can functionally substitute for plastid terminal oxidase in *Arabidopsis* chloroplasts. (2012) **Plant Cell** 24(4): 1579-1595.
- Fujibe, T., H. Saji, K. Arakawa, N. Yabe, Y. Takeuchi and K. T. Yamamoto. A methyl viologen-resistant mutant of *Arabidopsis*, which is allelic to ozone-sensitive *rcd1*, is tolerant to supplemental ultraviolet-B irradiation. (2004) **Plant Physiol** 134(1): 275-285.
- Garmier, M., A. J. Carroll, E. Delannoy, C. Vallet, D. A. Day, I. D. Small and A. H. Millar. Complex I dysfunction redirects cellular and mitochondrial metabolism in *Arabidopsis*. (2008) **Plant Physiol** 148(3): 1324-1341.

- Geigenberger, P., A. R. Fernie, Y. Gibon, M. Christ and M. Stitt. Metabolic activity decreases as an adaptive response to low internal oxygen in growing potato tubers. (2000) **Biological Chemistry** 381(8): 723-740.
- Geigenberger, P., R. Reimholz, M. Geiger, L. Merlo, V. Canale and M. Stitt. Regulation of sucrose and starch metabolism in potato tubers in response to short-term water deficit. (1997) **Planta** 201(4): 502-518.
- Geisler, D. A., C. Papke, T. Obata, A. Nunes-Nesi, A. Matthes, K. Schneitz, E. Maximova, W. L. Araujo, A. R. Fernie and S. Persson. Downregulation of the delta-subunit reduces mitochondrial ATP synthase levels, alters respiration, and restricts growth and gametophyte development in Arabidopsis. (2012) **Plant Cell** 24(7): 2792-2811.
- Gibon, Y., O. E. Blaesing, J. Hannemann, P. Carillo, M. Hohne, J. H. Hendriks, N. Palacios, J. Cross, J. Selbig and M. Stitt. A Robot-based platform to measure multiple enzyme activities in Arabidopsis using a set of cycling assays: comparison of changes of enzyme activities and transcript levels during diurnal cycles and in prolonged darkness. (2004) **Plant Cell** 16(12): 3304-3325.
- Giraud, E., O. Van Aken, L. H. Ho and J. Whelan. The transcription factor ABI4 is a regulator of mitochondrial retrograde expression of ALTERNATIVE OXIDASE1a. (2009) **Plant Physiol** 150(3): 1286-1296.
- Gonzalez-Perez, S., J. Gutierrez, F. Garcia-Garcia, D. Osuna, J. Dopazo, O. Lorenzo, J. L. Revuelta and J. B. Arellano. Early transcriptional defense responses in Arabidopsis cell suspension culture under high-light conditions. (2011) **Plant Physiol** 156(3): 1439-1456.
- Gutierrez, J., S. Gonzalez-Perez, F. Garcia-Garcia, C. T. Daly, O. Lorenzo, J. L. Revuelta, P. F. McCabe and J. B. Arellano. Programmed cell death activated by Rose Bengal in Arabidopsis thaliana cell suspension cultures requires functional chloroplasts. (2014) **J Exp Bot** 65(12): 3081-3095.
- Hawkes, T. R. Mechanisms of resistance to paraquat in plants. (2014) **Pest Manag Sci** 70(9): 1316-1323.
- Heiber, I., E. Stroher, B. Raatz, I. Busse, U. Kahmann, M. W. Bevan, K. J. Dietz and M. Baier. The redox imbalanced mutants of Arabidopsis differentiate signaling pathways for redox regulation of chloroplast antioxidant enzymes. (2007) **Plant Physiol** 143(4): 1774-1788.
- Hiller, K., J. Hangebrauk, C. Jager, J. Spura, K. Schreiber and D. Schomburg. MetaboliteDetector: comprehensive analysis tool for targeted and nontargeted GC/MS based metabolome analysis. (2009) **Anal Chem** 81(9): 3429-3439.
- Hiltscher, H., R. Rudnik, J. Shaikhali, I. Heiber, M. Mellenthin, I. Meirelles Duarte, G. Schuster, U. Kahmann and M. Baier. The radical induced cell death protein 1 (RCD1) supports transcriptional activation of genes for chloroplast antioxidant enzymes. (2014) **Front Plant Sci** 5: 475.
- Huang, S., O. Van Aken, M. Schwarzlander, K. Belt and A. H. Millar. The Roles of Mitochondrial Reactive Oxygen Species in Cellular Signaling and Stress Response in Plants. (2016) **Plant Physiol** 171(3): 1551-1559.
- Ivanova, A., S. R. Law, R. Narsai, O. Duncan, J. H. Lee, B. Zhang, O. Van Aken, J. D. Radomiljac, M. van der Merwe, K. Yi and J. Whelan. A Functional Antagonistic Relationship between Auxin and Mitochondrial Retrograde Signaling Regulates Alternative Oxidase1a Expression in Arabidopsis. (2014) **Plant Physiol** 165(3): 1233-1254.
- Jarvi, S., M. Suorsa, V. Paakkarinen and E. M. Aro. Optimized native gel systems for separation of thylakoid protein complexes: novel super- and mega-complexes. (2011) **Biochem J** 439(2): 207-214.
- Jarvi, S., M. Suorsa, L. Tadini, A. Ivanauskaite, S. Rantala, Y. Allahverdiyeva, D. Leister and E. M. Aro. Thylakoid-Bound FtsH Proteins Facilitate Proper Biosynthesis of Photosystem I. (2016) **Plant Physiol** 171(2): 1333-1343.
- Jaspers, P., T. Blomster, M. Brosche, J. Salojarvi, R. Ahlfors, J. P. Vainonen, R. A. Reddy, R. Immink, G. Angenent, F. Turck, K. Overmyer and J. Kangasjarvi. Unequally redundant RCD1 and SRO1 mediate stress and developmental responses and interact with transcription factors. (2009) **Plant J** 60(2): 268-279.
- Jaspers, P., M. Brosche, K. Overmyer and J. Kangasjarvi. The transcription factor interacting protein RCD1 contains a novel conserved domain. (2010) **Plant Signal Behav** 5(1): 78-80.

- Jaspers, P., K. Overmyer, M. Wrzaczek, J. P. Vainonen, T. Blomster, J. Salojarvi, R. A. Reddy and J. Kangasjarvi. The RST and PARP-like domain containing SRO protein family: analysis of protein structure, function and conservation in land plants. **(2010) BMC Genomics** 11: 170.
- Joo, J. H., S. Wang, J. G. Chen, A. M. Jones and N. V. Fedoroff. Different signaling and cell death roles of heterotrimeric G protein alpha and beta subunits in the Arabidopsis oxidative stress response to ozone. **(2005) Plant Cell** 17(3): 957-970.
- Kacprzak, S. M., N. Mochizuki, B. Naranjo, D. Xu, D. Leister, T. Kleine, H. Okamoto and M. J. Terry. Plastid-to-Nucleus Retrograde Signalling during Chloroplast Biogenesis Does Not Require ABI4. **(2019) Plant Physiol** 179(1): 18-23.
- Katiyar-Agarwal, S., J. Zhu, K. Kim, M. Agarwal, X. Fu, A. Huang and J. K. Zhu. The plasma membrane Na⁺/H⁺ antiporter SOS1 interacts with RCD1 and functions in oxidative stress tolerance in Arabidopsis. **(2006) Proc Natl Acad Sci U S A** 103(49): 18816-18821.
- Keech, O., P. Dizengremel and P. Gardestrom. Preparation of leaf mitochondria from Arabidopsis thaliana. **(2005) Physiologia Plantarum** 124(4): 403-409.
- Kinkema, M., W. Fan and X. Dong. Nuclear localization of NPR1 is required for activation of PR gene expression. **(2000) Plant Cell** 12(12): 2339-2350.
- Klein, M. and J. Papenbrock. The multi-protein family of Arabidopsis sulphotransferases and their relatives in other plant species. **(2004) J Exp Bot** 55(404): 1809-1820.
- Kleine, T., P. Kindgren, C. Benedict, L. Hendrickson and A. Strand. Genome-wide gene expression analysis reveals a critical role for CRYPTOCHROME1 in the response of Arabidopsis to high irradiance. **(2007) Plant Physiol** 144(3): 1391-1406.
- Konert, G., A. Trotta, P. Kouvonen, M. Rahikainen, G. Durian, O. Blokhina, K. Fagerstedt, D. Muth, G. L. Corthals and S. Kangasjarvi. Protein phosphatase 2A (PP2A) regulatory subunit B'gamma interacts with cytoplasmic ACONITASE 3 and modulates the abundance of AOX1A and AOX1D in Arabidopsis thaliana. **(2015) New Phytol** 205(3): 1250-1263.
- Konig, J., M. Baier, F. Horling, U. Kahmann, G. Harris, P. Schurmann and K. J. Dietz. The plant-specific function of 2-Cys peroxiredoxin-mediated detoxification of peroxides in the redox-hierarchy of photosynthetic electron flux. **(2002) Proc Natl Acad Sci U S A** 99(8): 5738-5743.
- Koussevitzky, S., A. Nott, T. C. Mockler, F. Hong, G. Sachetto-Martins, M. Surpin, J. Lim, R. Mittler and J. Chory. Signals from chloroplasts converge to regulate nuclear gene expression. **(2007) Science** 316(5825): 715-719.
- Kragelund, B. B., M. K. Jensen and K. Skriver. Order by disorder in plant signaling. **(2012) Trends Plant Sci** 17(11): 625-632.
- Krueger, S., P. Giavalisco, L. Krall, M. C. Steinhauser, D. Bussis, B. Usadel, U. I. Flugge, A. R. Fernie, L. Willmitzer and D. Steinhauser. A topological map of the compartmentalized Arabidopsis thaliana leaf metabolome. **(2011) PLoS One** 6(3): e17806.
- Krueger, S., D. Steinhauser, J. Lisec and P. Giavalisco. Analysis of subcellular metabolite distributions within Arabidopsis thaliana leaf tissue: a primer for subcellular metabolomics. **(2014) Methods Mol Biol** 1062: 575-596.
- Laemmli, U. K. Cleavage of structural proteins during the assembly of the head of bacteriophage T4. **(1970) Nature** 227(5259): 680-685.
- Leister, D. Piecing the Puzzle Together: The Central Role of Reactive Oxygen Species and Redox Hubs in Chloroplast Retrograde Signaling. **(2017) Antioxid Redox Signal**.
- Leister, D. and T. Kleine. Definition of a core module for the nuclear retrograde response to altered organellar gene expression identifies GLK overexpressors as gun mutants. **(2016) Physiol Plant** 157(3): 297-309.
- Leister, D., I. Romani, L. Mittermayr, F. Paieri, E. Fenino and T. Kleine. Identification of target genes and transcription factors implicated in translation-dependent retrograde signaling in Arabidopsis. **(2014) Mol Plant** 7(7): 1228-1247.

- Liebthal, M., D. Maynard and K. J. Dietz. Peroxiredoxins and Redox Signaling in Plants. **(2018) *Antioxid Redox Signal* 28(7): 609-624.**
- Lopez-Mendez, B. and P. Guntert. Automated protein structure determination from NMR spectra. **(2006) *J Am Chem Soc* 128(40): 13112-13122.**
- Lowry, O. H., N. J. Rosebrough, A. L. Farr and R. J. Randall. Protein Measurement with the Folin Phenol Reagent. **(1951) *Journal of Biological Chemistry* 193(1): 265-275.**
- Meyer, E. H., T. Tomaz, A. J. Carroll, G. Estavillo, E. Delannoy, S. K. Tanz, I. D. Small, B. J. Pogson and A. H. Millar. Remodeled respiration in *ndufs4* with low phosphorylation efficiency suppresses Arabidopsis germination and growth and alters control of metabolism at night. **(2009) *Plant Physiol* 151(2): 603-619.**
- Moller, I. M. and B. K. Kristensen. Protein oxidation in plant mitochondria as a stress indicator. **(2004) *Photochem Photobiol Sci* 3(8): 730-735.**
- Mou, Z., W. Fan and X. Dong. Inducers of plant systemic acquired resistance regulate NPR1 function through redox changes. **(2003) *Cell* 113(7): 935-944.**
- Mullineaux, P. M., M. Exposito-Rodriguez, P. P. Laissue and N. Smirnov. ROS-dependent signalling pathways in plants and algae exposed to high light: Comparisons with other eukaryotes. **(2018) *Free Radic Biol Med* 122: 52-64.**
- Munekage, Y., M. Hojo, J. Meurer, T. Endo, M. Tasaka and T. Shikanai. PGR5 is involved in cyclic electron flow around photosystem I and is essential for photoprotection in Arabidopsis. **(2002) *Cell* 110(3): 361-371.**
- Ng, S., I. De Clercq, O. Van Aken, S. R. Law, A. Ivanova, P. Willems, E. Giraud, F. Van Breusegem and J. Whelan. Anterograde and retrograde regulation of nuclear genes encoding mitochondrial proteins during growth, development, and stress. **(2014) *Mol Plant* 7(7): 1075-1093.**
- Ng, S., E. Giraud, O. Duncan, S. R. Law, Y. Wang, L. Xu, R. Narsai, C. Carrie, H. Walker, D. A. Day, N. E. Blanco, A. Strand, J. Whelan and A. Ivanova. Cyclin-dependent kinase E1 (CDKE1) provides a cellular switch in plants between growth and stress responses. **(2013) *J Biol Chem* 288(5): 3449-3459.**
- Ng, S., A. Ivanova, O. Duncan, S. R. Law, O. Van Aken, I. De Clercq, Y. Wang, C. Carrie, L. Xu, B. Kmiec, H. Walker, F. Van Breusegem, J. Whelan and E. Giraud. A membrane-bound NAC transcription factor, ANAC017, mediates mitochondrial retrograde signaling in Arabidopsis. **(2013) *Plant Cell* 25(9): 3450-3471.**
- Nietzel, T., J. Mostertz, F. Hochgrafe and M. Schwarzlander. Redox regulation of mitochondrial proteins and proteomes by cysteine thiol switches. **(2017) *Mitochondrion* 33: 72-83.**
- Nikkanen, L., J. Toivola and E. Rintamaki. Crosstalk between chloroplast thioredoxin systems in regulation of photosynthesis. **(2016) *Plant Cell Environ* 39(8): 1691-1705.**
- Nishiyama, Y., S. I. Allakhverdiev and N. Murata. Protein synthesis is the primary target of reactive oxygen species in the photoinhibition of photosystem II. **(2011) *Physiol Plant* 142(1): 35-46.**
- Noctor, G., J. P. Reichheld and C. H. Foyer. ROS-related redox regulation and signaling in plants. **(2017) *Semin Cell Dev Biol*.**
- Noguchi, K. and K. Yoshida. Interaction between photosynthesis and respiration in illuminated leaves. **(2008) *Mitochondrion* 8(1): 87-99.**
- O'Shea, C., L. Staby, S. K. Bendson, F. G. Tidemand, A. Redsted, M. Willemoes, B. B. Kragelund and K. Skriver. Structures and Short Linear Motif of Disordered Transcription Factor Regions Provide Clues to the Interactome of the Cellular Hub Protein Radical-induced Cell Death1. **(2017) *J Biol Chem* 292(2): 512-527.**
- Obata, T., L. Rosado-Souza and A. R. Fernie. Coupling Radiotracer Experiments with Chemical Fractionation for the Estimation of Respiratory Fluxes. **(2017) *Methods Mol Biol* 1670: 17-30.**
- Ojeda, V., J. M. Perez-Ruiz and F. J. Cejudo. 2-Cys Peroxiredoxins Participate in the Oxidation of Chloroplast Enzymes in the Dark. **(2018) *Mol Plant*.**
- Overmyer, K., H. Tuominen, R. Kettunen, C. Betz, C. Langebartels, H. Sandermann, Jr. and J. Kangasjarvi. Ozone-sensitive arabidopsis *rcd1* mutant reveals opposite roles for ethylene and jasmonate signaling pathways in regulating superoxide-dependent cell death. **(2000) *Plant Cell* 12(10): 1849-1862.**

- Oxborough, K. and N. R. Baker. Resolving chlorophyll a fluorescence images of photosynthetic efficiency into photochemical and non-photochemical components - calculation of qP and F_v'/F_m' without measuring F_o' . (1997) **Photosynthesis Research** 54(2): 135-142.
- Peltier, J. B., Y. Cai, Q. Sun, V. Zabrouskov, L. Giacomelli, A. Rudella, A. J. Ytterberg, H. Rutschow and K. J. van Wijk. The oligomeric stromal proteome of *Arabidopsis thaliana* chloroplasts. (2006) **Mol Cell Proteomics** 5(1): 114-133.
- Petrov, V., J. Hille, B. Mueller-Roeber and T. S. Gechev. ROS-mediated abiotic stress-induced programmed cell death in plants. (2015) **Front Plant Sci** 6: 69.
- Porra, R. J., W. A. Thompson and P. E. Kriedemann. Determination of Accurate Extinction Coefficients and Simultaneous-Equations for Assaying Chlorophyll-a and Chlorophyll-B Extracted with 4 Different Solvents - Verification of the Concentration of Chlorophyll Standards by Atomic-Absorption Spectroscopy. (1989) **Biochimica Et Biophysica Acta** 975(3): 384-394.
- Quintero, F. J., B. Garciadeblas and A. Rodriguez-Navarro. The SAL1 gene of *Arabidopsis*, encoding an enzyme with 3'(2'),5'-bisphosphate nucleotidase and inositol polyphosphate 1-phosphatase activities, increases salt tolerance in yeast. (1996) **Plant Cell** 8(3): 529-537.
- Roessner, U., C. Wagner, J. Kopka, R. N. Trethewey and L. Willmitzer. Technical advance: simultaneous analysis of metabolites in potato tuber by gas chromatography-mass spectrometry. (2000) **Plant J** 23(1): 131-142.
- Scheibe, R. Malate valves to balance cellular energy supply. (2004) **Physiol Plant** 120(1): 21-26.
- Schwarzlander, M., M. D. Fricker and L. J. Sweetlove. Monitoring the in vivo redox state of plant mitochondria: effect of respiratory inhibitors, abiotic stress and assessment of recovery from oxidative challenge. (2009) **Biochim Biophys Acta** 1787(5): 468-475.
- Shapiguzov, A., J. P. Vainonen, M. Wrzaczek and J. Kangasjarvi. ROS-talk - how the apoplast, the chloroplast, and the nucleus get the message through. (2012) **Front Plant Sci** 3: 292.
- Sharma, R., P. Priya and M. Jain. Modified expression of an auxin-responsive rice CC-type glutaredoxin gene affects multiple abiotic stress responses. (2013) **Planta** 238(5): 871-884.
- Shedge, V., J. Davila, M. P. Arrieta-Montiel, S. Mohammed and S. A. Mackenzie. Extensive rearrangement of the *Arabidopsis* mitochondrial genome elicits cellular conditions for thermotolerance. (2010) **Plant Physiol** 152(4): 1960-1970.
- Siligato, R., X. Wang, S. R. Yadav, S. Lehesranta, G. Ma, R. Ursache, I. Sevilem, J. Zhang, M. Gorte, K. Prasad, M. Wrzaczek, R. Heidstra, A. Murphy, B. Scheres and A. P. Mahonen. MultiSite Gateway-Compatible Cell Type-Specific Gene-Inducible System for Plants. (2016) **Plant Physiol** 170(2): 627-641.
- Sowden, R. G., S. J. Watson and P. Jarvis. The role of chloroplasts in plant pathology. (2017) **Essays Biochem**.
- Sugimoto, K., Y. Okegawa, A. Tohri, T. A. Long, S. F. Covert, T. Hisabori and T. Shikanai. A single amino acid alteration in PGR5 confers resistance to antimycin A in cyclic electron transport around PSI. (2013) **Plant Cell Physiol** 54(9): 1525-1534.
- Tiwari, A., F. Mamedov, M. Grieco, M. Suorsa, A. Jajoo, S. Styring, M. Tikkanen and E. M. Aro. Photodamage of iron-sulphur clusters in photosystem I induces non-photochemical energy dissipation. (2016) **Nat Plants** 2: 16035.
- Tossavainen, H., M. Hellman, J. P. Vainonen, J. Kangasjarvi and P. Permi. (1)H, (13)C and (15)N NMR chemical shift assignments of *A. thaliana* RCD1 RST. (2017) **Biomol NMR Assign** 11(2): 207-210.
- Trotta, A., M. Rahikainen, G. Konert, G. Finazzi and S. Kangasjarvi. Signalling crosstalk in light stress and immune reactions in plants. (2014) **Philos Trans R Soc Lond B Biol Sci** 369(1640): 20130235.
- Umbach, A. L., F. Fiorani and J. N. Siedow. Characterization of transformed *Arabidopsis* with altered alternative oxidase levels and analysis of effects on reactive oxygen species in tissue. (2005) **Plant Physiol** 139(4): 1806-1820.
- Vainonen, J. P., P. Jaspers, M. Wrzaczek, A. Lamminmaki, R. A. Reddy, L. Vaahtera, M. Brosche and J. Kangasjarvi. RCD1-DREB2A interaction in leaf senescence and stress responses in *Arabidopsis thaliana*. (2012) **Biochem J** 442(3): 573-581.

- Vainonen, J. P. and J. Kangasjarvi. Plant signalling in acute ozone exposure. (2015) **Plant Cell Environ** 38(2): 240-252.
- Van Aken, O., I. De Clercq, A. Ivanova, S. R. Law, F. Van Breusegem, A. H. Millar and J. Whelan. Mitochondrial and Chloroplast Stress Responses Are Modulated in Distinct Touch and Chemical Inhibition Phases. (2016) **Plant Physiol** 171(3): 2150-2165.
- Van Aken, O., E. Ford, R. Lister, S. Huang and A. H. Millar. Retrograde signalling caused by heritable mitochondrial dysfunction is partially mediated by ANAC017 and improves plant performance. (2016) **Plant J** 88(4): 542-558.
- Van Aken, O. and B. J. Pogson. Convergence of mitochondrial and chloroplastic ANAC017/PAP-dependent retrograde signalling pathways and suppression of programmed cell death. (2017) **Cell Death Differ**.
- Van Aken, O., B. Zhang, S. Law, R. Narsai and J. Whelan. AtWRKY40 and AtWRKY63 modulate the expression of stress-responsive nuclear genes encoding mitochondrial and chloroplast proteins. (2013) **Plant Physiol** 162(1): 254-271.
- van Leeuwen, L. A. G., E. C. Hinchy, M. P. Murphy, E. L. Robb and H. M. Cocheme. Click-PEGylation - A mobility shift approach to assess the redox state of cysteines in candidate proteins. (2017) **Free Radic Biol Med** 108: 374-382.
- Vaseghi, M. J., K. Chibani, W. Telman, M. F. Liebthal, M. Gerken, H. Schnitzer, S. M. Mueller and K. J. Dietz. The chloroplast 2-cysteine peroxiredoxin functions as thioredoxin oxidase in redox regulation of chloroplast metabolism. (2018) **Elife** 7.
- Wang, Y., O. Berkowitz, J. Selinski, Y. Xu, A. Hartmann and J. Whelan. Stress responsive mitochondrial proteins in *Arabidopsis thaliana*. (2018) **Free Radic Biol Med** 122: 28-39.
- Waszczak, C., M. Carmody and J. Kangasjarvi. Reactive Oxygen Species in Plant Signaling. (2018) **Annu Rev Plant Biol**.
- Watanabe, C. K., W. Yamori, S. Takahashi, I. Terashima and K. Noguchi. Mitochondrial Alternative Pathway-Associated Photoprotection of Photosystem II is Related to the Photorespiratory Pathway. (2016) **Plant Cell Physiol**.
- Wendrich, J. R., S. Boeren, B. K. Moller, D. Weijers and B. De Rybel. In Vivo Identification of Plant Protein Complexes Using IP-MS/MS. (2017) **Methods Mol Biol** 1497: 147-158.
- Wetzel, C. M., C. Z. Jiang, L. J. Meehan, D. F. Voytas and S. R. Rodermel. Nuclear-organelle interactions: the immutans variegation mutant of *Arabidopsis* is plastid autonomous and impaired in carotenoid biosynthesis. (1994) **Plant J** 6(2): 161-175.
- Wilson, P. B., G. M. Estavillo, K. J. Field, W. Pornsiriwong, A. J. Carroll, K. A. Howell, N. S. Woo, J. A. Lake, S. M. Smith, A. Harvey Millar, S. von Caemmerer and B. J. Pogson. The nucleotidase/phosphatase SAL1 is a negative regulator of drought tolerance in *Arabidopsis*. (2009) **Plant J** 58(2): 299-317.
- Wirthmueller, L., S. Asai, G. Rallapalli, J. Sklenar, G. Fabro, D. S. Kim, R. Lintermann, P. Jaspers, M. Wrzaczek, J. Kangasjarvi, D. MacLean, F. L. H. Menke, M. J. Banfield and J. D. G. Jones. *Arabidopsis* downy mildew effector HaRxL106 suppresses plant immunity by binding to RADICAL-INDUCED CELL DEATH1. (2018) **New Phytol** 220(1): 232-248.
- Withers, J. and X. Dong. Posttranslational Modifications of NPR1: A Single Protein Playing Multiple Roles in Plant Immunity and Physiology. (2016) **PLoS Pathog** 12(8): e1005707.
- Wrzaczek, M., M. Brosche, J. Salojarvi, S. Kangasjarvi, N. Idanheimo, S. Mersmann, S. Robatzek, S. Karpinski, B. Karpinska and J. Kangasjarvi. Transcriptional regulation of the CRK/DUF26 group of receptor-like protein kinases by ozone and plant hormones in *Arabidopsis*. (2010) **BMC Plant Biol** 10: 95.
- Wu, J., Y. Sun, Y. Zhao, J. Zhang, L. Luo, M. Li, J. Wang, H. Yu, G. Liu, L. Yang, G. Xiong, J. M. Zhou, J. Zuo, Y. Wang and J. Li. Deficient plastidic fatty acid synthesis triggers cell death by modulating mitochondrial reactive oxygen species. (2015) **Cell Res** 25(5): 621-633.
- Yoshida, K., A. Hara, K. Sugiura, Y. Fukaya and T. Hisabori. Thioredoxin-like2/2-Cys peroxiredoxin redox cascade supports oxidative thiol modulation in chloroplasts. (2018) **Proc Natl Acad Sci U S A** 115(35): E8296-E8304.

Zhao, Y., L. Luo, J. Xu, P. Xin, H. Guo, J. Wu, L. Bai, G. Wang, J. Chu, J. Zuo, H. Yu, X. Huang and J. Li. Malate transported from chloroplast to mitochondrion triggers production of ROS and PCD in *Arabidopsis thaliana*. (2018) **Cell Res.**

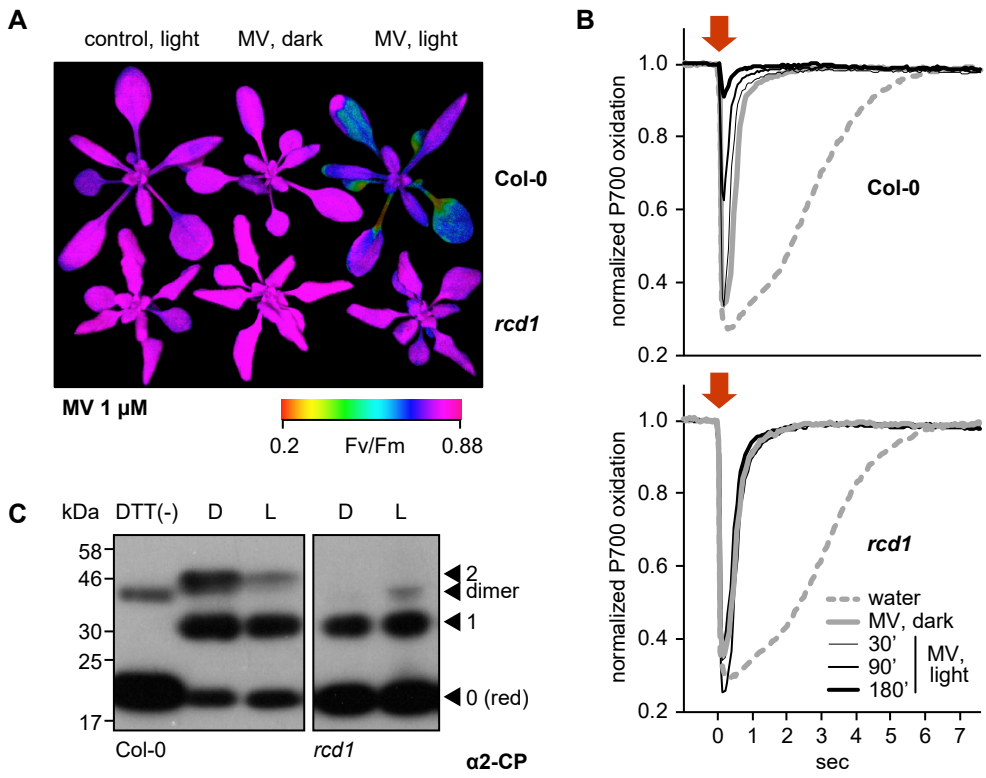


Figure 1

Figure 1. RCD1 controls tolerance of photosynthetic apparatus to ROS.

- (A) MV treatment results in PSII inhibition under light, which is suppressed in the *rcd1* mutant. PSII Photochemical yield (Fv/Fm) was measured in rosettes pre-treated overnight in darkness with 1 μM MV and then exposed to 3 hours of continuous light ($80 \mu\text{mol m}^{-2} \text{s}^{-1}$). Representative false-color image of Fv/Fm is shown.
- (B) MV access to electron-acceptor side of PSI is unaltered in *rcd1*. Treatment with MV led to similar changes in kinetics of PSI oxidation in Col-0 and *rcd1*. Oxidation of PSI reaction center (P700) was measured using DUAL-PAM. Leaves were first adapted to far-red light that is more efficiently used by PSI than PSII. In these conditions PSI is producing electrons at a faster rate than they are supplied by PSII, thus P700 is oxidized. Then a flash of orange light was provided that is efficiently absorbed by PSII (orange arrow). Electrons generated by PSII transiently reduced PSI, after which the kinetics of PSI re-oxidation was followed. Note the progressive decrease in the effect of the orange flash occurring in Col-0 at later time points, which suggests deterioration in PSII function. This was not observed in *rcd1*. Three leaves from three individual plants were used for each measurement. The experiment was repeated three times with similar results.
- (C) Redox state of the chloroplast enzyme 2-Cys peroxiredoxin (2-CP) assessed by thiol bond-specific labeling in Col-0 (left) and *rcd1* (right). Total protein was isolated from leaves incubated in darkness (D), or under light (L). Free sulfhydryls were blocked with N-ethylmaleimide, then *in vivo* thiol bridges were reduced with DTT, and finally the newly exposed sulfhydryls were labeled with methoxypolyethylene glycol maleimide of molecular weight 5 kDa. The labeled protein extracts were separated by SDS-PAGE and immunoblotted with α 2-CP antibody. DTT (-) control contained predominantly unlabeled form. Unlabeled reduced (red), singly and doubly labeled oxidized forms and the putative dimer were annotated as in (Nikkanen et al. 2016). Apparent molecular weight increment after the labeling of one thiol bond appears on SDS-PAGE higher than 10 kDa because of steric hindrance exerted on branched polymers during gel separation (van Leeuwen et al., 2017). The experiment was repeated three times with similar results.

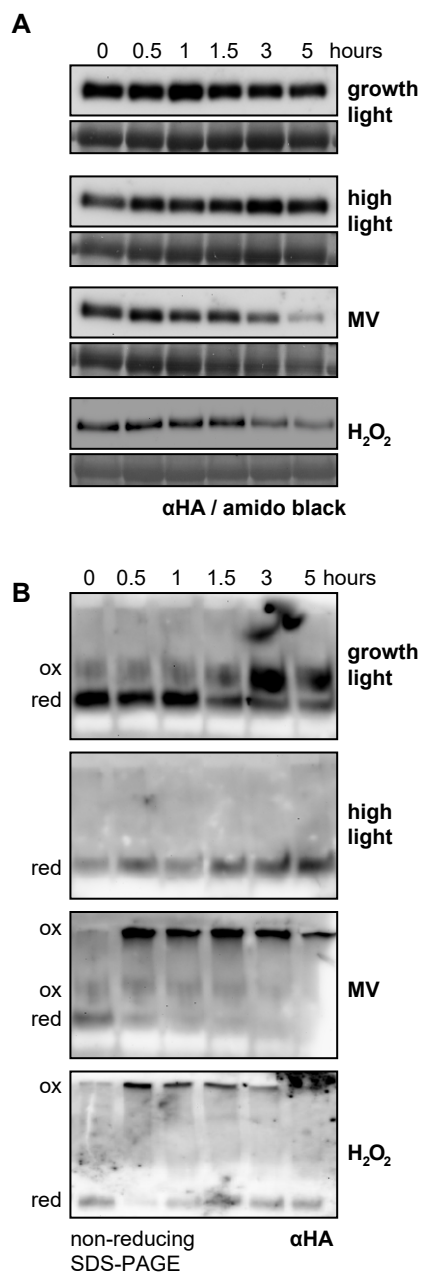


Figure 2

Figure 2. RCD1 protein is sensitive to chloroplastic ROS.

- (A) The *rcd1*: RCD1-HA complementation line was used to assess RCD1-HA abundance. It gradually decreased in response to chloroplastic ROS. Leaf discs from plants expressing HA-tagged RCD1 were treated with 5-hour growth light ($150 \mu\text{mol m}^{-2} \text{s}^{-1}$), high light ($1\ 300 \mu\text{mol m}^{-2} \text{s}^{-1}$), MV ($1 \mu\text{M}$) in light, or H_2O_2 (100 mM). The levels of RCD1-HA were monitored by immunoblotting with αHA at indicated time points. Rubisco large subunit (RbcL) detected by amido black staining is shown as a control for equal protein loading. The “0” time point of the MV time course represents dark-adapted leaf discs pre-treated with MV overnight. The experiment was performed four times with similar results.
- (B) Chloroplastic ROS caused oligomerization of RCD1-HA. Total protein extracts from the plants treated as in panel (A) were separated by non-reducing PAGE and immunoblotted with αHA antibody. Reduced (red) and oxidized (ox) forms of the protein are labeled. To ascertain that all HA-tagged protein including that forming high-molecular-weight aggregates has been detected by immunoblotting, the transfer to a membrane was performed using the entire SDS-PAGE gel including the stacking gel and the well pockets. The experiment was performed four times with similar results.

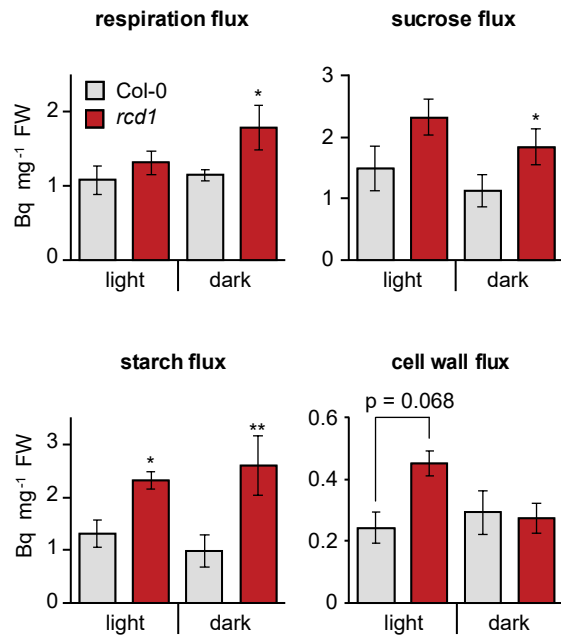


Figure 3

Figure 3. Altered energy metabolism of *rcd1*. Deduced metabolic fluxes in light- and dark- adapted Col-0 and *rcd1* rosettes were assessed by fractionation of the extracts of leaves treated with [U-¹⁴C] glucose. Increased respiration flux and higher amount of total metabolized glucose (Fig. 3 supplemental dataset 1) in *rcd1* suggest a more active glycolytic pathway. Higher cell wall metabolic flux in *rcd1* provided indirect support of increased operation of the oxidative pentose phosphate pathway which is required for generating pentoses used in cell wall biosynthesis (Ap Rees 1978). Mean ± SE are presented. Asterisks indicate values significantly different from the wild type, **P value < 0.01, *P value < 0.05, Student's t-test. Source data and statistics are presented in Figure 3 – supplemental dataset 2.

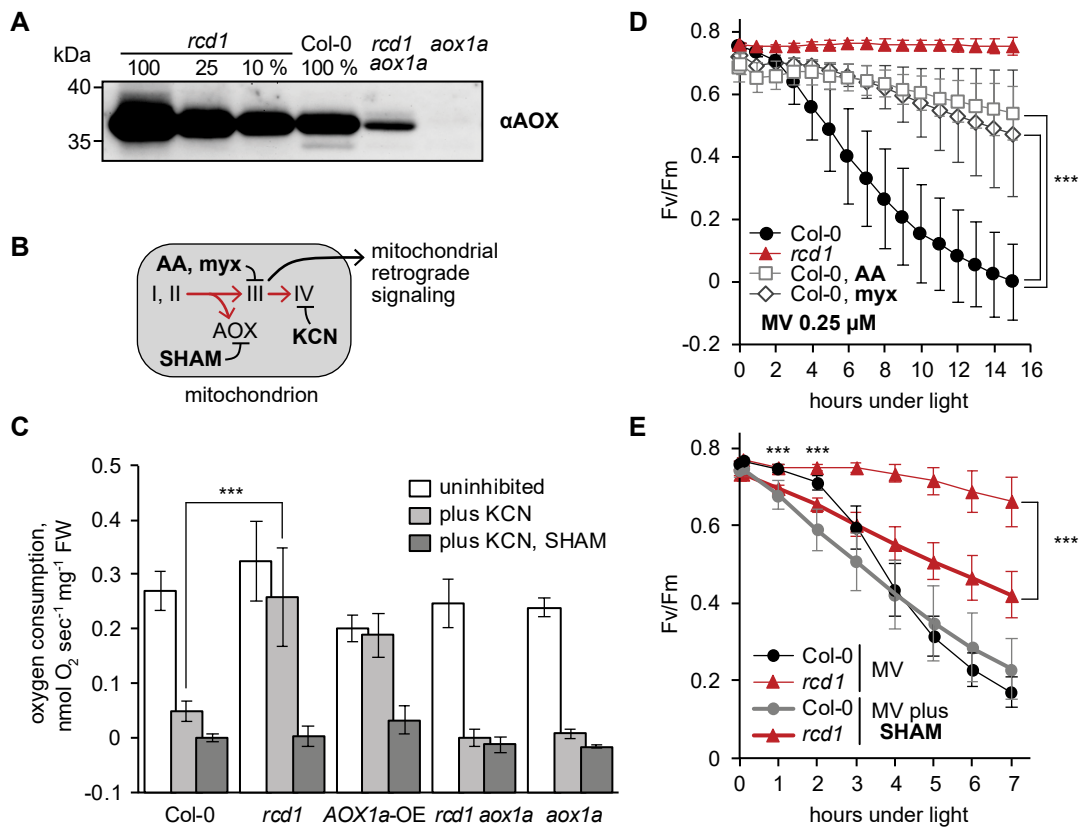


Figure 4

Figure 4. Mitochondrial AOXs affect energy metabolism of *rcd1* and alter response to chloroplastic ROS. Source data and statistics are presented in Figure 4 – supplemental dataset 1.

- (A) Expression of AOXs is induced in *rcd1*. Abundance of AOX isoforms in mitochondrial preparations was assessed by immunoblotting with α AOX antibody that recognizes AOX1a, -b, -c, -d, and AOX2 isoforms. 100 % corresponds to 15 μ g of mitochondrial protein.
- (B) Two mitochondrial respiratory pathways (red arrows) and sites of action of mitochondrial inhibitors. KCN inhibits complex IV (cytochrome c oxidase). Salicylhydroxamic acid (SHAM) inhibits AOX activity. Antimycin A (AA) and myxothiazol (myx) block electron transfer through complex III (ubiquinol-cytochrome c oxidoreductase), creating ROS-related mitochondrial retrograde signal.
- (C) AOX capacity is significantly increased in *rcd1*. Oxygen uptake by seedlings was measured in the darkness in presence of KCN and SHAM. Addition of KCN blocked respiration through complex IV, thus revealing the capacity of the alternative respiratory pathway through AOXs. Data is presented as mean \pm SD, asterisks denote selected values that are significantly different (P value < 0.001, one-way ANOVA with Bonferroni post hoc correction). Each measurement was performed on 10-15 pooled seedlings and repeated at least three times.
- (D) Inhibitors of mitochondrial complex III increase plant tolerance to chloroplastic ROS. Effect of pre-treatment with 2.5 μ M AA or 2.5 μ M myx on PSII inhibition (Fv/Fm) by MV. For each experiment, leaf discs from at least four individual rosettes were used. The experiment was performed four times with similar results. Mean \pm SD are shown. Asterisks indicate selected treatments that are significantly different (P value < 0.001, Bonferroni post hoc correction). AOX abundance in the leaf discs treated in the same way was quantified by immunoblotting (Fig. 4 – figure supplement 1).
- (E) AOX inhibitor SHAM decreases plant tolerance to chloroplastic ROS. 1-hour pre-treatment with 2 mM SHAM inhibited tolerance to 1 μ M MV both in Col-0 and *rcd1* as measured by Fv/Fm. SHAM stock solution was prepared in DMSO, thus pure DMSO was added in the SHAM-minus controls. For each experiment, leaf discs from at least four individual rosettes were used. The experiment was performed four times with similar results. Mean \pm SD are shown. Asterisks indicate significant difference in the

treatments of the same genotype at the selected time points (P value < 0.001, Bonferroni post hoc correction).

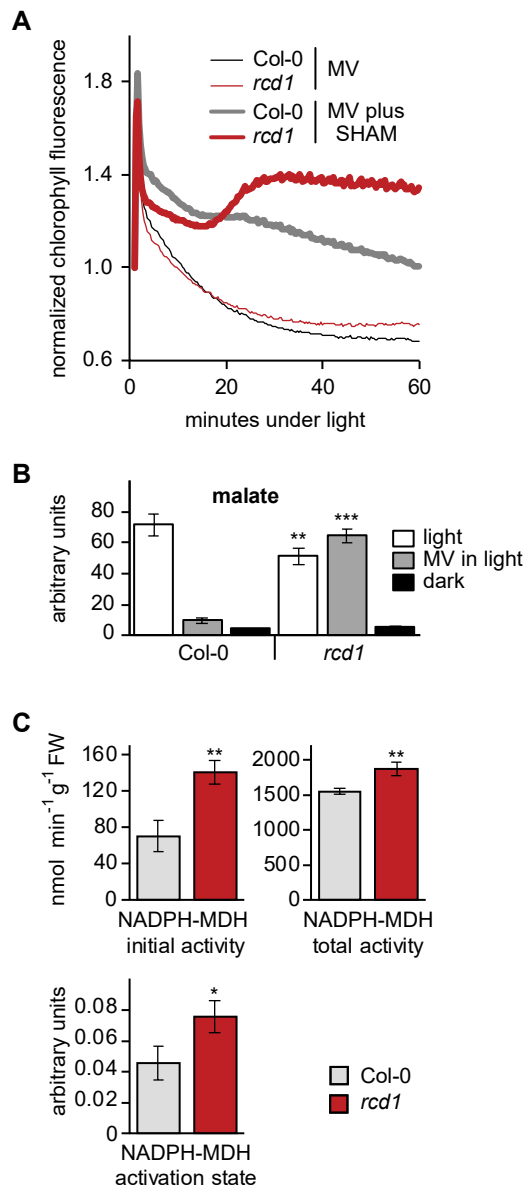


Figure 5

Figure 5. Altered electron transfer between the organelles in *rcd1*.

- (A) Leaf discs were pre-treated with 1 μM MV or MV plus 2 mM SHAM for 1 hour in the darkness. Then light was turned on ($80 \mu\text{mol m}^{-2} \text{s}^{-1}$) and chlorophyll fluorescence under light (F_s) was recorded by Imaging PAM. Application of the two chemicals together caused F_s rise in *rcd1*, but not Col-0, suggesting increase in the reduction state of the chloroplast ETC in *rcd1*. For analysis of photochemical quenching see Fig. 5 – figure supplement 1.
- (B) Malate levels are significantly decreased in Col-0 but not in *rcd1* after MV treatment in light. Malate level was measured in extracts from Col-0 and *rcd1* seedlings that were pre-treated overnight with 50 μM MV or water control and collected either dark-adapted or after exposure to 4 hours of light. Mean \pm SE are shown. Asterisks indicate values significantly different from those in the similarly treated wild type, ***P value < 0.001, **P value < 0.01, Student's t-test). For statistics see Fig. 5 – supplemental dataset 1.
- (C) NADPH-MDH activity is increased in *rcd1*. To measure the activity of chloroplastic NADPH-MDH, plants were grown at $100\text{-}120 \mu\text{mol m}^{-2} \text{s}^{-1}$ at an 8-hour day photoperiod, leaves were collected in the middle of the day and freeze-dried. The extracts were prepared in the buffer supplemented with 250 μM thiol-reducing agent DTT, and initial activity was measured (top left). The samples were then incubated for 2 hours in the presence of additional 150 mM DTT, and total activity was measured (top right). The activation state of NADPH-MDH (bottom) is presented as the ratio of the initial and the total activity. Mean \pm SE are shown. Asterisks indicate values significantly different from the wild type, **P value < 0.01, *P value < 0.05, Student's t-test. For statistics see Fig. 5 – supplemental dataset 1.

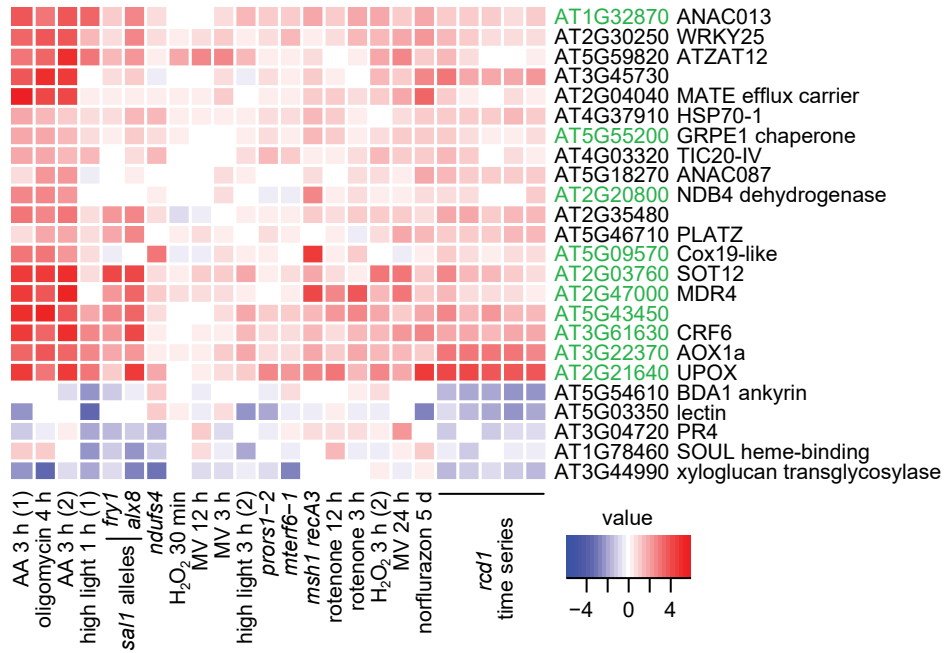
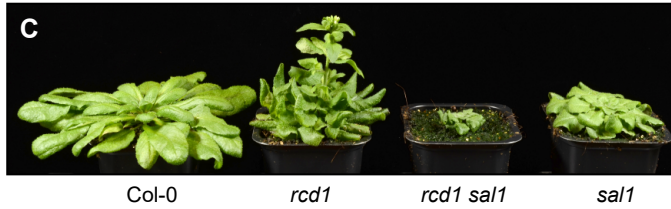
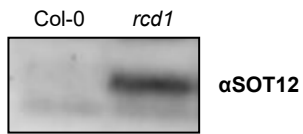
A**B****Figure 6**

Figure 6. RCD1 is involved in mitochondrial dysfunction, chloroplast ROS and PAP signaling pathways.

- (A) Regulation of *rcd1* mis-expressed genes under perturbations of organellar functions in the selected subset of genes. A complete list of *rcd1*-misexpressed genes is presented in Fig. 6 – figure supplement 1. Similar transcriptomic changes are observed between the genes differentially regulated in *rcd1* and the genes affected by disturbed chloroplastic or mitochondrial functions. Mitochondrial dysfunction stimulon (MDS) genes regulated by ANAC013/ ANAC017 transcription factors, are labeled green.
- (B) Sulfotransferase SOT12 encoded by an MDS gene accumulated in *rcd1* under standard growth conditions, as revealed by immunoblotting with the specific antibody.
- (C) Phenotype of the *rcd1 sal1* double mutant under standard growth conditions (12-hour photoperiod with white luminescent light of 220-250 $\mu\text{mol m}^{-2} \text{s}^{-1}$).

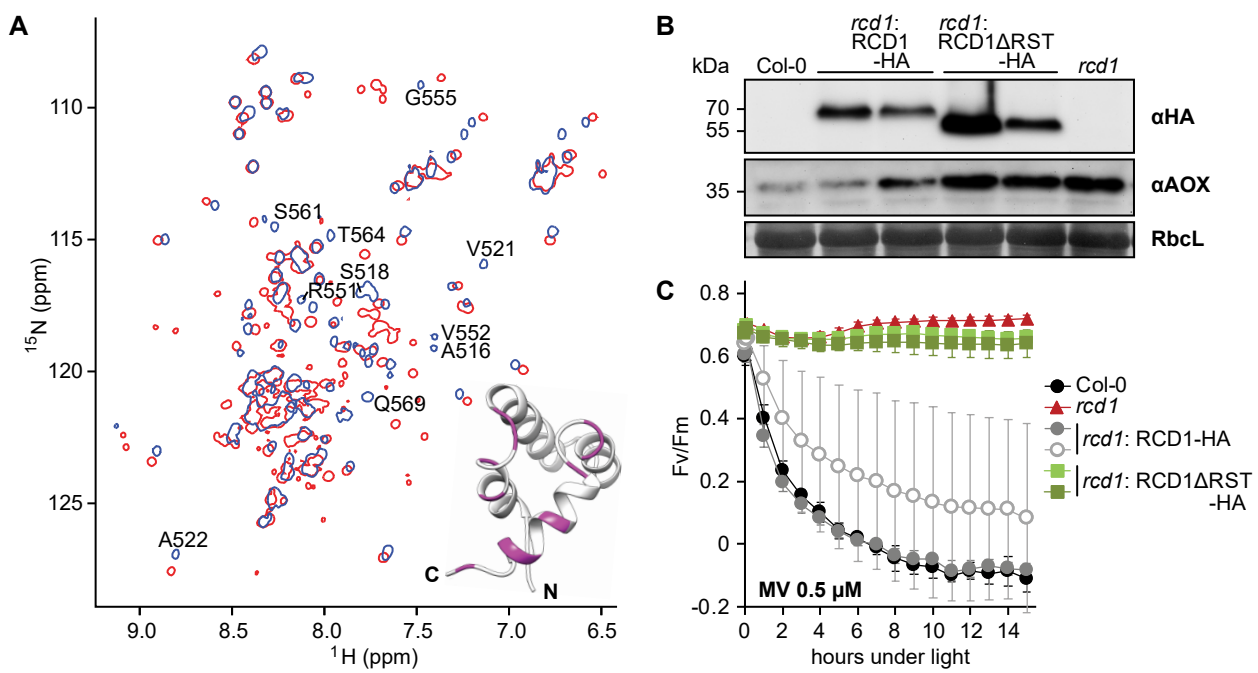


Figure 7

Figure 7. RST domain of RCD1 binds to ANAC transcription factors and is necessary for RCD1 function *in vivo*. Source data and statistics are presented in Fig. 7 – supplemental dataset 4.

- (A) Biochemical interaction of ANAC013 with the RST domain of RCD1 *in vitro*. Superimposed ^1H , ^{15}N HSQC spectra of the C-terminal domain of RCD1 acquired in absence (blue) and presence (red) of approximately two-fold excess of the ANAC013²³⁵⁻²⁸⁴ peptide. Interaction of RCD1⁴⁶⁸⁻⁵⁸⁹ with ANAC013²³⁵⁻²⁸⁴ caused peptide-induced chemical shift changes in the ^1H , ^{15}N correlation spectrum of RCD1, which were mapped on the structure of the RST domain (inset). Inset: RST_{RCD1} structure with highlighted residues demonstrating the largest chemical shift perturbations ($\Delta\delta \geq 0.10$ ppm) between the free and bound forms (details in Fig. 7 – figure supplement 3C), which probably corresponds to ANAC013-interaction site.
- (B) Stable expression in *rcd1* of the HA-tagged RCD1 variant lacking its C-terminus under the control of the native *RCD1* promoter does not complement *rcd1* phenotypes. In the independent complementation lines RCD1 Δ RST-HA was expressed at the levels comparable to those in the RCD1-HA lines (upper panel). However, in *rcd1*: RCD1 Δ RST-HA lines abundance of AOXs (middle panel) was similar to that in *rcd1*.
- (C) Tolerance of PSII to chloroplastic ROS was similar in the *rcd1*: RCD1 Δ RST-HA lines and *rcd1*. For each PSII inhibition experiment, leaf discs from at least four individual rosettes were used. The experiment was performed three times with similar results. Mean \pm SD are shown.

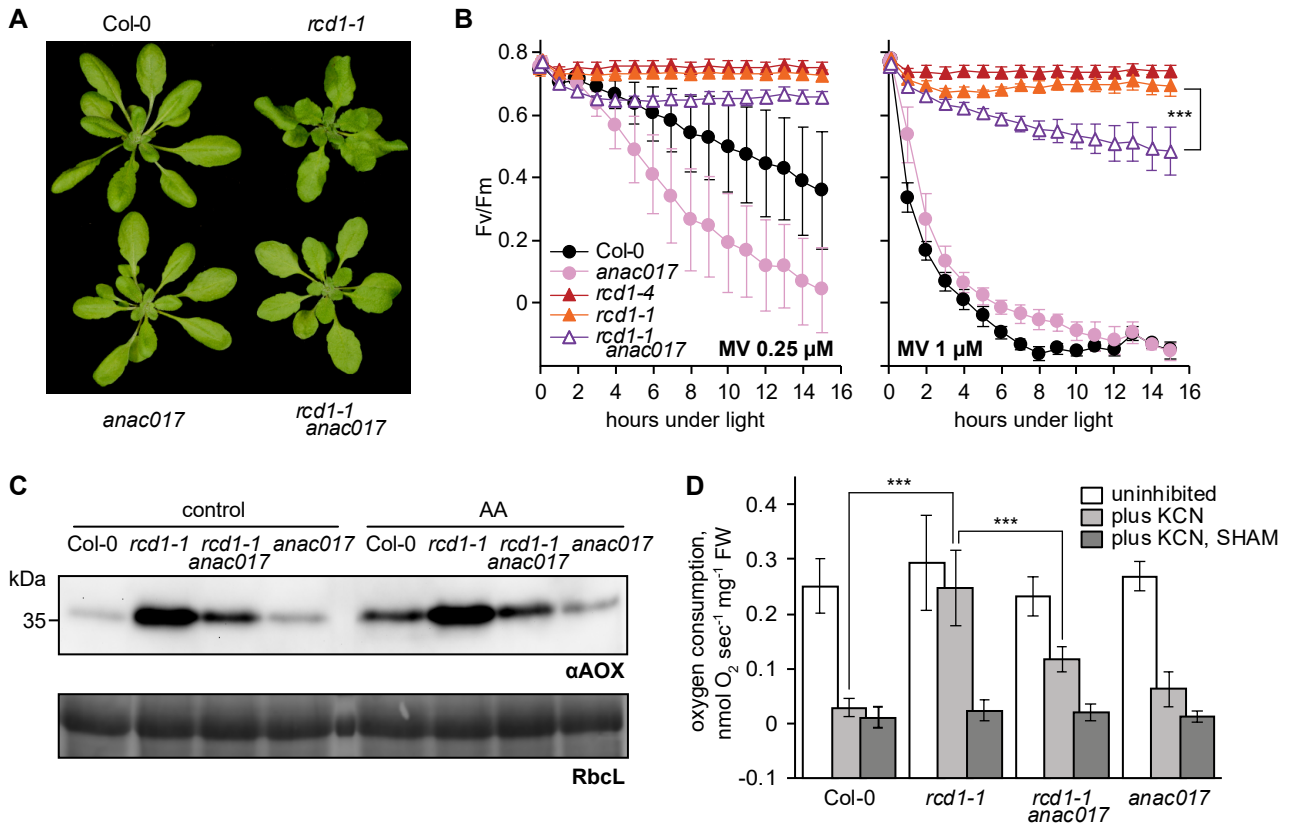


Figure 8

Figure 8. Developmental, chloroplast- and mitochondria-related phenotypes of *rcd1* are partially mediated by ANAC017. Source data and statistics are presented in Fig. 8 – supplemental dataset 1.

- (A) Introducing *anac017* mutation in the *rcd1* background partially suppressed the curly leaf phenotype of *rcd1*.
- (B) The *anac017* mutation partially suppressed tolerance of *rcd1* to chloroplastic ROS. PSII inhibition by ROS was measured in *rcd1 anac017* double mutant by using 0.25 μ M or 1 μ M MV (left and right panel, accordingly). For each experiment, leaf discs from at least four individual rosettes were used. The experiment was performed three times with similar results. Mean \pm SD are shown. Asterisks denote values significantly different from those in the similarly treated wild type at the last time point of the assay (P value < 0.001, two-way ANOVA with Bonferroni post hoc correction).
- (C) The *anac017* mutation partially suppressed mitochondrial phenotypes of *rcd1*. Total AOX protein levels were lowered in *rcd1 anac017* double mutant as compared to *rcd1* both after the overnight treatment with 2.5 μ M AA and in the untreated control.
- (D) Oxygen uptake by *rcd1 anac017* seedlings was measured in the darkness in presence of mitochondrial respiration inhibitors as described in Fig. 4C. The *rcd1 anac017* mutant demonstrated lower KCN-insensitive AOX respiration capacity than *rcd1*. Each measurement was performed on 10-15 pooled seedlings and repeated at least three times. Mean \pm SD are shown. Asterisks denote selected values that are significantly different (P value < 0.001, one-way ANOVA with Bonferroni post hoc correction).

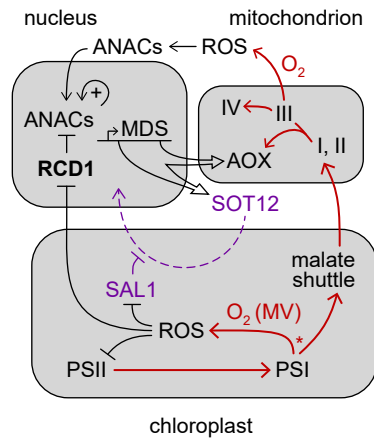


Figure 9

Figure 9. The hypothetical role of RCD1 in organelle signaling and energy metabolism. RCD1 is the direct suppressor of ANAC transcription factors that is itself subject to redox regulation. Chloroplastic ROS likely affect RCD1 protein redox state and abundance. Inactivation of RCD1 leads to induction of ANAC-controlled MDS regulon. Expression of MDS genes is possibly feedback-regulated *via* the PAP retrograde signaling (purple). Resulting activation of mitochondrial AOXs and other MDS components is likely to affect electron flows (red) and ROS signaling in mitochondria and in chloroplasts. Putative competition of AOX-directed electron transfer with the formation of ROS at PSI is labeled with an asterisk.

Supplementary Information

Figure 1 - supplemental dataset 1. Source data and statistics.

Figure 2 - supplemental dataset 1. Source data and statistics.

Figure 3 – supplemental dataset 1. Metabolic analyses.

Distribution of radioactive label was analyzed after feeding plants with ^{14}C -labeled glucose. Metabolic fluxes in light- and dark-adapted Col-0, *rcd1*, *rcd1 aox1a*, and *aox1a* plants were deduced.

Figure 3 – supplemental dataset 2. Source data and statistics.

Figure 4 – supplemental dataset 1. Source data and statistics.

Figure 5 – supplemental dataset 1. Source data and statistics.

Figure 6 - supplemental dataset 1. Source data and statistics.

Figure 7 – supplemental dataset 1. *In vivo* interaction partners of ANAC013.

From Arabidopsis line expressing ANAC013-GFP, ANAC013-GFP and associated proteins were purified with αGFP antibody and identified by mass spectrometry. Identified proteins (Perseus analysis, ANAC013) and mapped peptides (peptide IDs) are shown.

Figure 7 – supplemental dataset 2. *In vivo* interaction partners of RCD1.

From Arabidopsis line expressing RCD1-3xVenus, RCD1-3xVenus and associated proteins were purified with αGFP antibody and identified by mass spectrometry. Identified proteins (Perseus analysis, RCD1) and mapped peptides (peptide IDs) are shown.

Figure 7 – supplemental dataset 3. NMR constraints and structural statistics for the ensemble of the 15 lowest-energy structures of RCD1 RST.

Figure 7 – supplemental dataset 4. Source data and statistics.

Figure 8 – supplemental dataset 1. Source data and statistics.

Supplemental table. Primers used in the study.

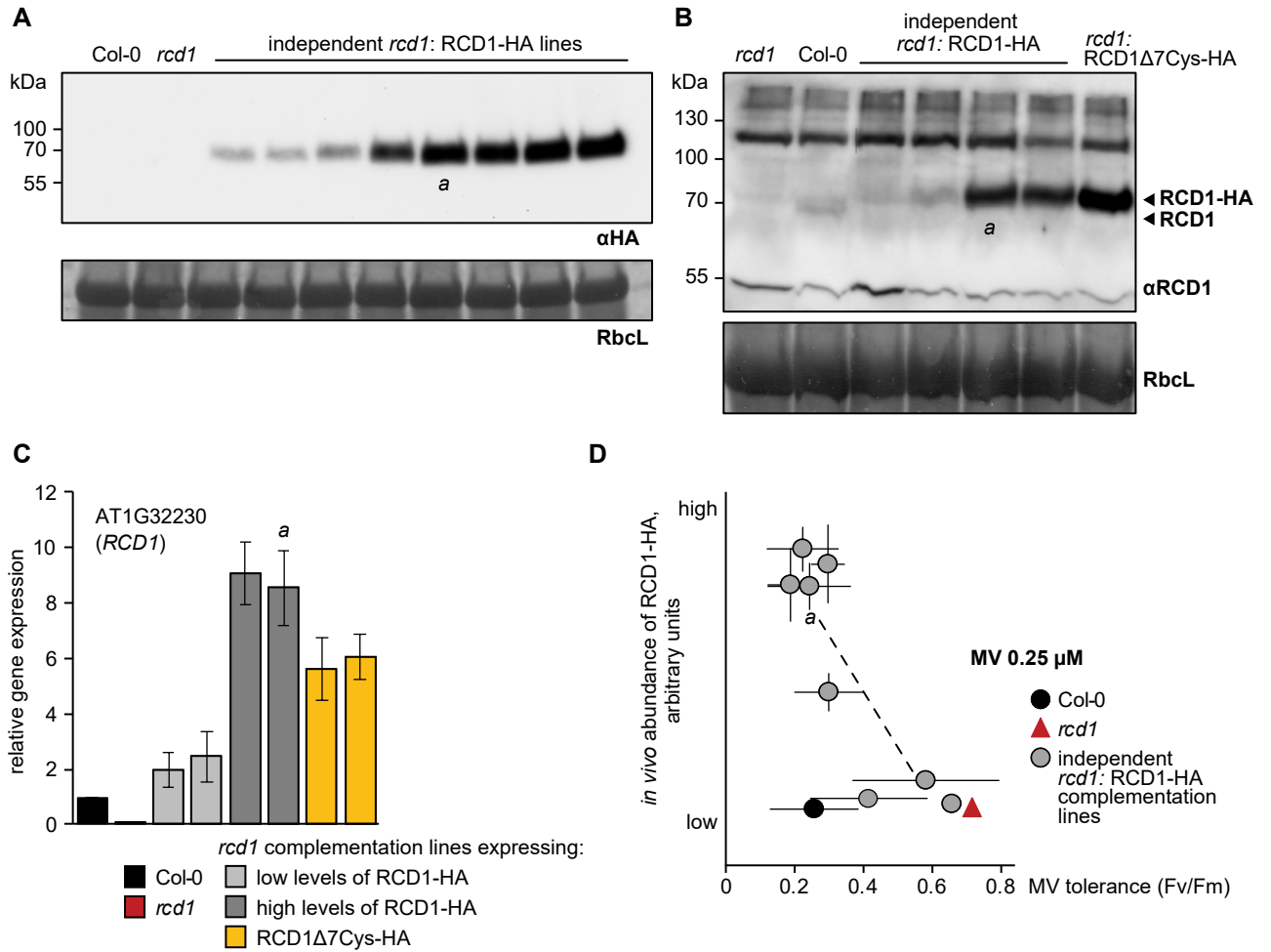


Figure 1 – figure supplement 1

Figure 1 – figure supplement 1. Inverse correlation of RCD1 abundance with tolerance to chloroplastic ROS.

- (A) Several independent *rcd1* complementation lines were generated in which HA-tagged RCD1 was reintroduced under the *RCD1* native promoter. Immunoblotting of protein extracts from these lines with α HA antibody revealed different levels of RCD1-HA under standard light-adapted growth conditions. This was presumably due to different transgene insertion sites in the genome. Line “a” was described in (Jaspers et al. 2009). Rubisco large subunit (RbcL) detected by amido black staining is shown as a control for equal protein loading.
- (B) An antibody was raised against the full-size RCD1 protein. This allowed comparing abundance of RCD1 in independent *rcd1*: RCD1-HA complementation lines described in the panel (A) versus Col-0 (two *rcd1*: RCD1-HA lines with the lowest and two with the higher levels of RCD1-HA are shown). In the complementation lines the RCD1 signal was detected at higher molecular weight due to the triple HA tag. The *rcd1*: RCD1 Δ 7Cys-HA line will be addressed below.
- (C) Expression of *RCD1* gene was measured by real time quantitative PCR in Col-0 and in four independent complementation lines described in the panel (A), two with the lowest and two with the higher levels of RCD1-HA. Results in panels (B) and (C) demonstrated that the levels of RCD1 protein and mRNA were about 10 times higher in the high-expressing complementation lines than in Col-0. Relative expression was calculated from three biological repeats and the data is scaled relative to Col-0. Source data is presented in Figure 6 – supplemental dataset 1.
- (D) Sensitivity of PSII to chloroplastic ROS in the *rcd1* complementation lines was assessed using time-resolved analysis described in Figure 1 – figure supplement 2. For that, leaf discs were pre-treated with 0.25 μ M MV overnight in the darkness. PSII photochemical yield after two 1-hour light cycles was plotted against abundance of RCD1-HA in the individual lines as determined in panel (A). Line “a” was described in (Jaspers et al. 2009). Five individual plants were taken per each line. The experiment was repeated three times with similar results. Source data and statistics are presented in Figure 1 – supplemental dataset 1.

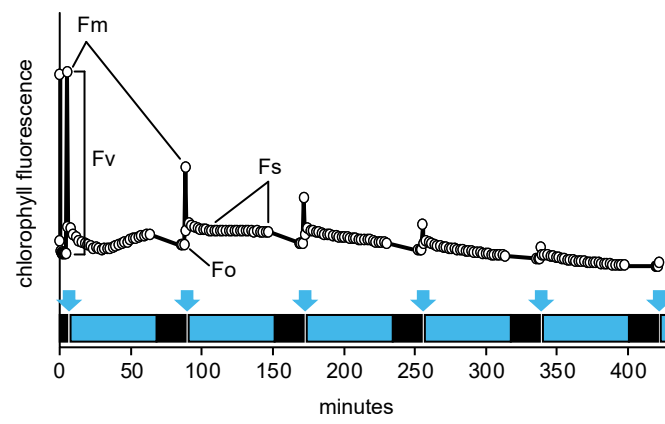


Figure 1 – figure supplement 2

Figure 1 – figure supplement 2. The Imaging PAM protocol developed to monitor kinetics of PSII inhibition by repetitive 1-hour light cycles. Plants dark-adapted for at least 20 min were first exposed to a saturating light pulse to measure F_m . Then the blue actinic light (450 nm, $80 \mu\text{mol m}^{-2} \text{s}^{-1}$) was turned on for 1 hour, over which time chlorophyll fluorescence under light (F_s) was followed by measuring flashes given once in 2 minutes. Then the actinic light was turned off to allow for 20-min dark adaptation, after which F_o and F_m were measured. Following the F_m measurement, the next light cycle was initiated. Saturating light pulses to measure F_m are depicted by blue arrows, actinic light periods by blue boxes, and dark adaptation by black boxes. PSII photochemical yield was calculated as $F_v/F_m = (F_m - F_o)/F_m$. To study different levels of MV tolerance, different concentrations of MV were employed throughout the study, as indicated in the figures or figure legends.

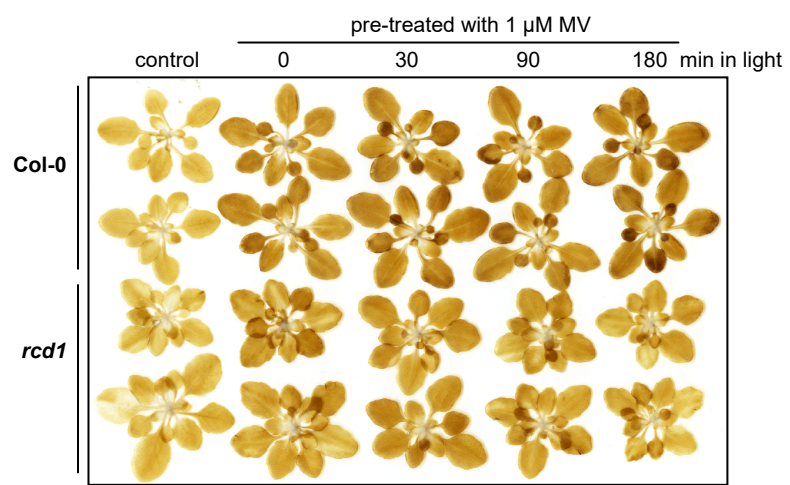


Figure 1 – figure supplement 3

Figure 1 – figure supplement 3. Accumulation of hydrogen peroxide in Col-0 and *rcd1* during illumination of MV-pre-treated rosettes. Col-0 and *rcd1* rosettes were pre-treated with 1 μM MV overnight in the darkness. Then they were exposed to light for indicated time. After this, the rosettes were infiltrated with DAB staining solution and exposed to 20 minutes of light ($180 \mu\text{mol m}^{-2} \text{s}^{-1}$). Similar initial increase in H_2O_2 production was observed in MV-pre-treated dark-adapted Col-0 and *rcd1*. During longer incubation under light the production of H_2O_2 further increased in Col-0, but decreased in *rcd1*. The experiment was performed three times with similar results.

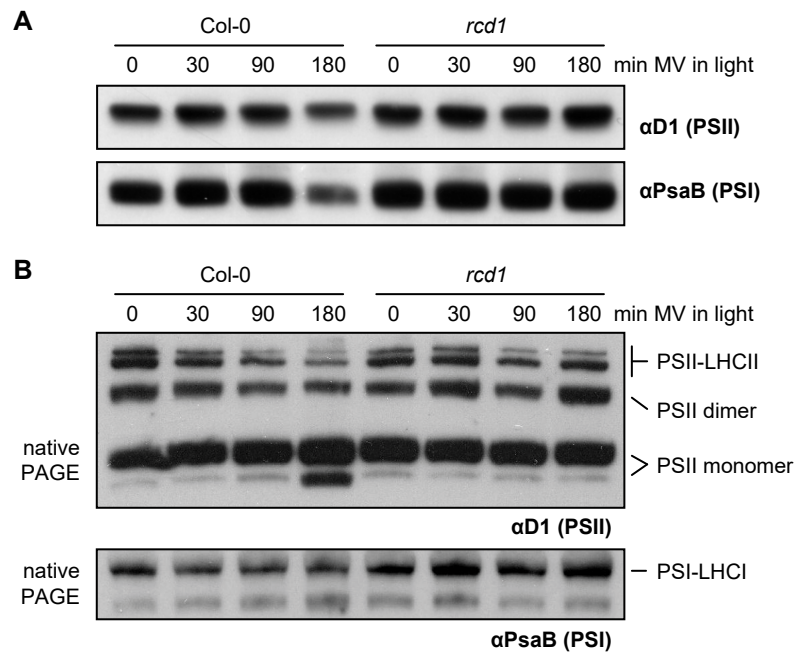


Figure 1 – figure supplement 4

Figure 1 – figure supplement 4. Altered resistance of *rcd1* photosynthetic apparatus to chloroplastic ROS.

- (A) Protein extracts from Col-0 and *rcd1* leaves pre-treated with 1 μ M MV and exposed to light for indicated time, were separated by SDS-PAGE followed by immunoblotting with antibodies against the PSII subunit D1 and the PSI subunit PsaB. No significant differences in stoichiometry of photosystems were detected.
- (B) Thylakoid protein complexes isolated from leaves treated as above were separated by native PAGE. Immunoblotting with α D1 antibody revealed PSII species of diverse molecular weights that were annotated as in (Jarvi et al., 2011). The largest of the complexes corresponds to PSII associated with its light-harvesting antennae complex (LHCII) while the smallest are the PSII monomers (top panel). Incubation under light in presence of MV led to destabilization of PSII-LHCII complexes in Col-0, but not in *rcd1*. At the same time, immunoblotting with α PsaB antibody showed no changes in PSI complex (bottom panel).

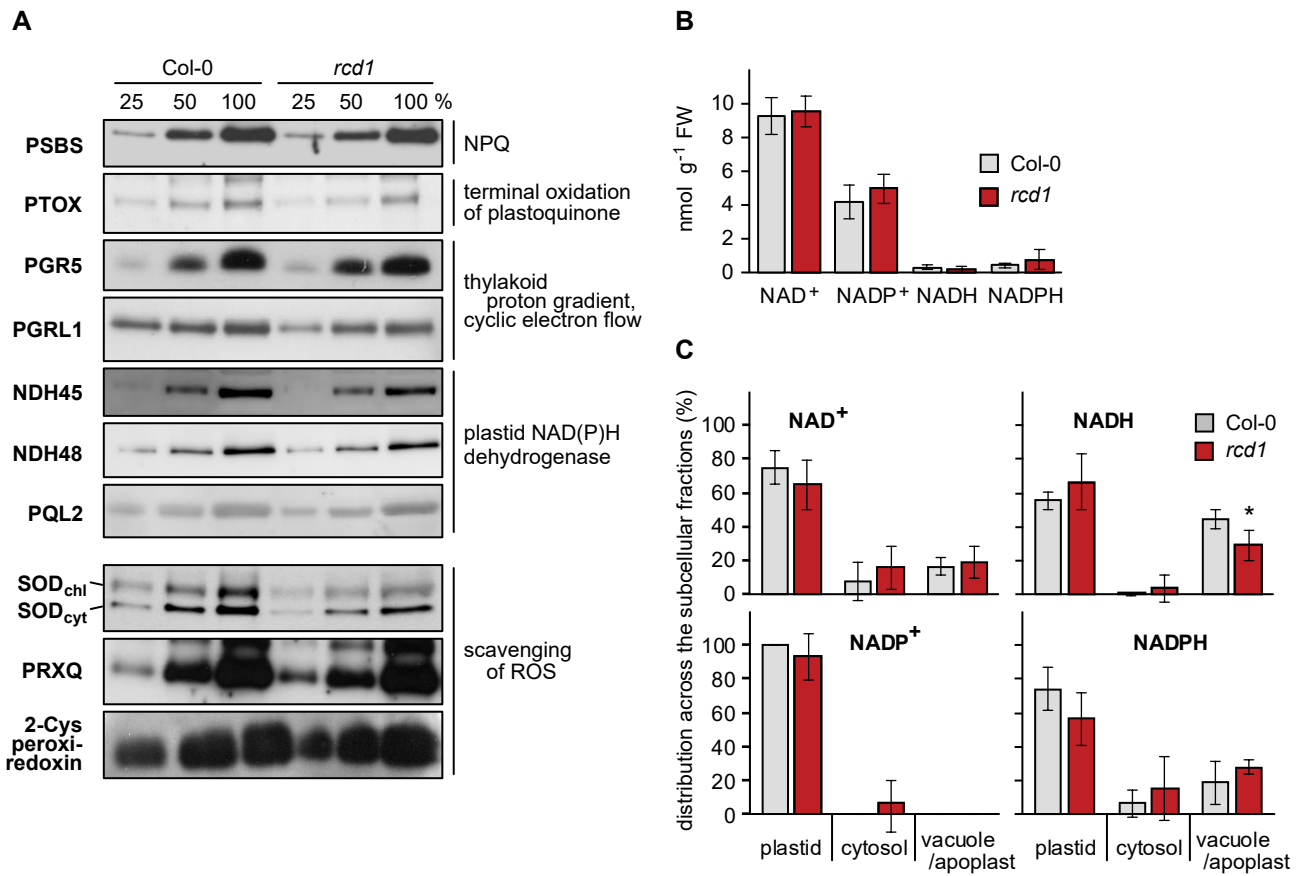


Figure 1 – figure supplement 5

Figure 1 – figure supplement 5. Components of photosynthetic electron transfer and chloroplast ROS scavenging; abundance and distribution of NAD⁺/ NADH and NADP⁺/ NADPH redox couples in Col-0 and *rcd1*.

- (A) Abundance of proteins related to photosynthetic electron transfer or chloroplast ROS scavenging was assessed by separating Col-0 and *rcd1* protein extracts (in dilution series) by SDS-PAGE and immunoblotting with specific antibodies, as indicated. 100 % corresponds to 20 µg of thylakoid protein. No difference was observed between Col-0 and *rcd1*.
- (B) Abundance of nucleotides NAD⁺, NADP⁺, NADH and NADPH in total leaf extracts isolated from Col-0 and *rcd1* (mean ± SE). No difference was observed between the genotypes. Source data and statistics are presented in Figure 1 – supplemental dataset 1.
- (C) Distribution of NAD⁺/ NADH and NADP⁺/ NADPH redox couples in various cellular compartments of Col-0 and *rcd1* was assessed by non-aqueous fractionation metabolomics (mean ± SE, an asterisk indicates the value significantly different from that in the corresponding wild type, *P value < 0.05, Student's t-test). In brief, the light-adapted rosettes were harvested in the middle of the light period, freeze-dried, homogenated and separated on non-aqueous density gradient, which allowed for enrichment in specific membrane compartments. No major difference was detected between Col-0 and *rcd1*. Note that the method does not allow for separation of apoplastic and vacuolar compartments or reliable definition of the mitochondria (Fettke et al., 2005). Source data and statistics are presented in Figure 1 – supplemental dataset 1.

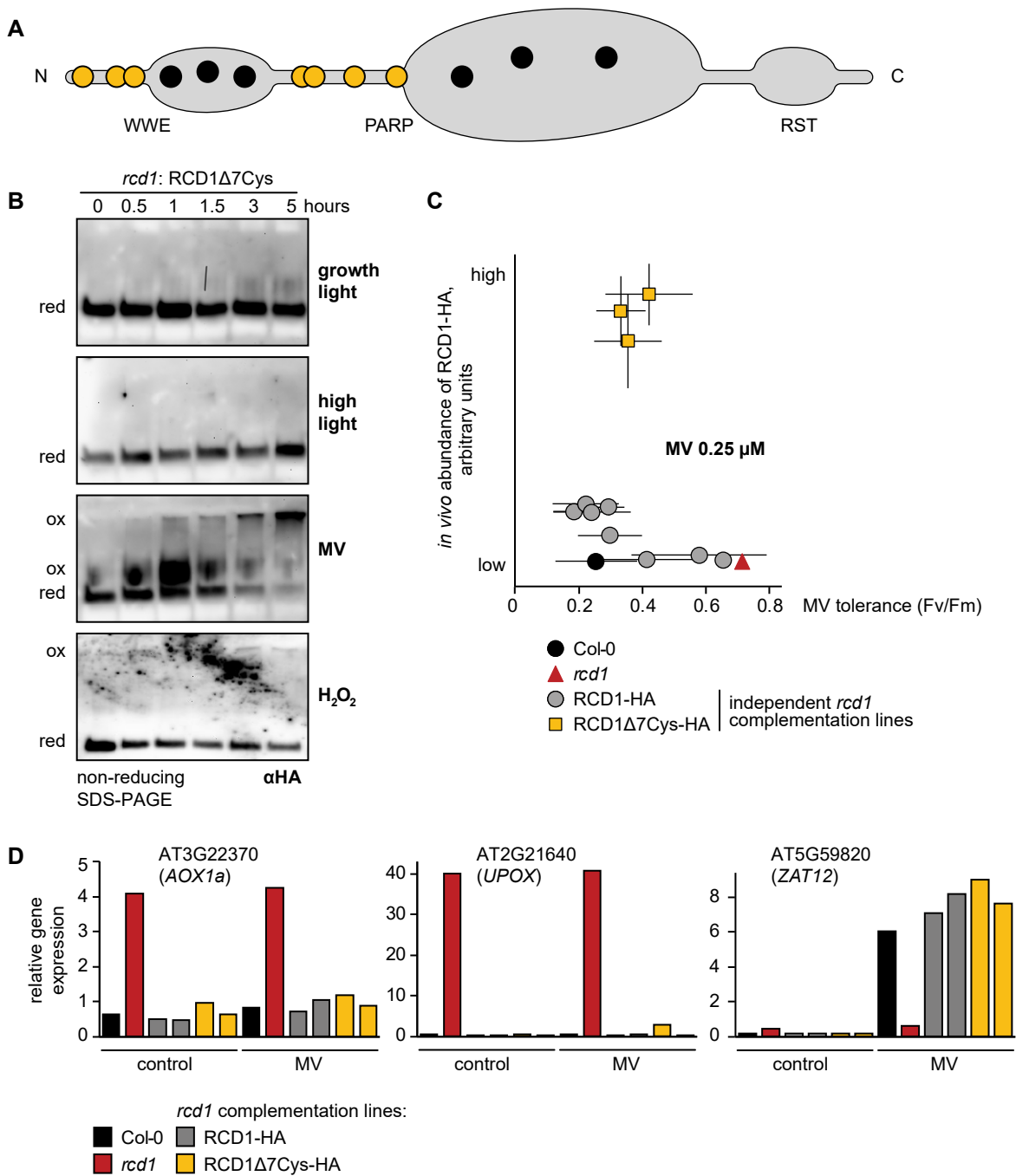
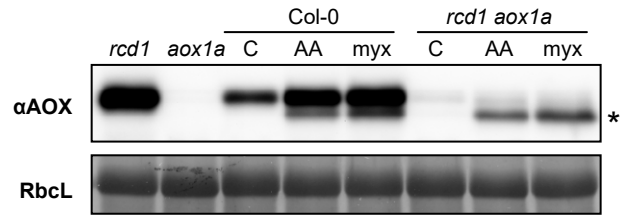


Figure 2 – figure supplement 1

Figure 2 – figure supplement 1. Characterization of the *rcd1*: RCD1 Δ 7Cys-HA lines.

- (A) Domain structure of RCD1 with the positions of cysteine residues shown with circles. Interdomain cysteines mutated in the RCD1 Δ 7Cys-HA lines (RCD1 Δ 7Cys = RCD1 C14A-C37A-C50A-C175A-C179A-C212A-C243A) are shown in yellow.
- (B) The *rcd1* complementation line expressing the RCD1 Δ 7Cys-HA variant under the control of the native *RCD1* promoter was treated with high light, MV or H₂O₂ as described in Fig. 2. In this line accumulation of high-molecular-weight RCD1 aggregates observed in RCD1-HA line (Fig. 2B) was largely abolished. Reduced (red) and oxidized (ox) forms of the protein are labeled. To ascertain that all HA-tagged protein including that forming high-molecular-weight aggregates has been detected by immunoblotting, the transfer to a membrane was performed using the entire SDS-PAGE gel including the stacking gel and the well pockets. The experiment was performed three times with similar results.
- (C) Independent single-insertion homozygous *rcd1* complementation lines expressing RCD1 Δ 7Cys-HA were compared to those expressing RCD1-HA as described in Fig. 1 – figure supplement 1D. In all the tested lines, RCD1 Δ 7Cys-HA accumulated to higher amounts than the wild-type RCD1-HA as revealed by immunoblotting with α HA antibody. MV tolerance of the RCD1 Δ 7Cys-HA lines was not different from that of the RCD1-HA lines or Col-0. Source data and statistics are presented in Figure 2 – supplemental dataset 1.
- (D) Expression of RCD1-regulated genes was measured by real time quantitative PCR in Col-0, *rcd1*, two *rcd1*: RCD1-HA lines expressing high levels of RCD1-HA and two lines expressing RCD1 Δ 7Cys-HA. No difference in expression of the selected RCD1-regulated genes *AOX1a* (AT3G22370), *UPOX* (AT2G21640), or the stress-induced gene *ZAT12* (AT5G59820) was detected in the *rcd1*: RCD1 Δ 7Cys-HA line as compared to *rcd1*: RCD1-HA or Col-0. For MV treatment detached rosettes were soaked in 1 μ M MV overnight in the darkness and then exposed to 1 hour of white luminescent light of 220-250 μ mol m⁻² s⁻¹. Note that inactivation of *RCD1* prevented induction of a general stress marker gene *ZAT12* in response to MV. Five rosettes were pooled together for each sample. The experiment was repeated twice with similar results. Source data and statistics are presented in Figure 2 – supplemental dataset 1.

A



B

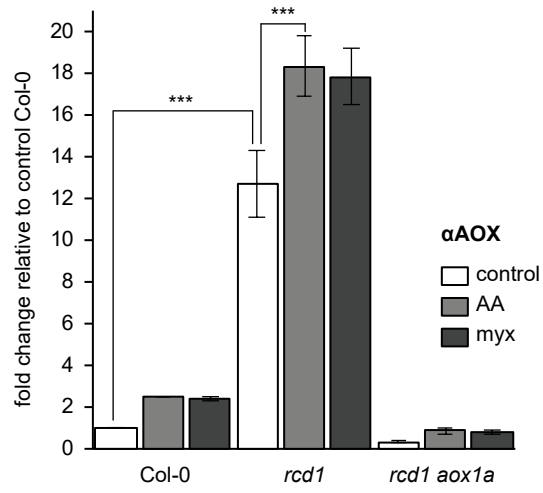


Figure 4 – figure supplement 1

Figure 4 – figure supplement 1. Effect of mitochondrial complex III inhibitors on expression of AOXs in Col-0 and *rcd1*.

- (A) Changes in AOX abundance after overnight pre-treatment of leaf discs with 2.5 μ M AA or 2.5 μ M myx (C – control treatment with no inhibitor). Notably, *rcd1 aox1a* double mutant accumulated AOXs other than AOX1a, including putative AOX1d (Konert et al., 2015) (labeled with asterisk).
- (B) Quantification of α AOX immunoblotting signal after pre-treatment with 2.5 μ M AA or myx. To avoid saturation of α AOX signal in *rcd1*, a dilution series of protein extracts was made. Quantification was performed using ImageJ. Mean \pm SD are shown, asterisks denote selected values that are significantly different (P value < 0.001, Bonferroni post hoc correction, for source data and statistics see Figure 4 – supplemental dataset 1).

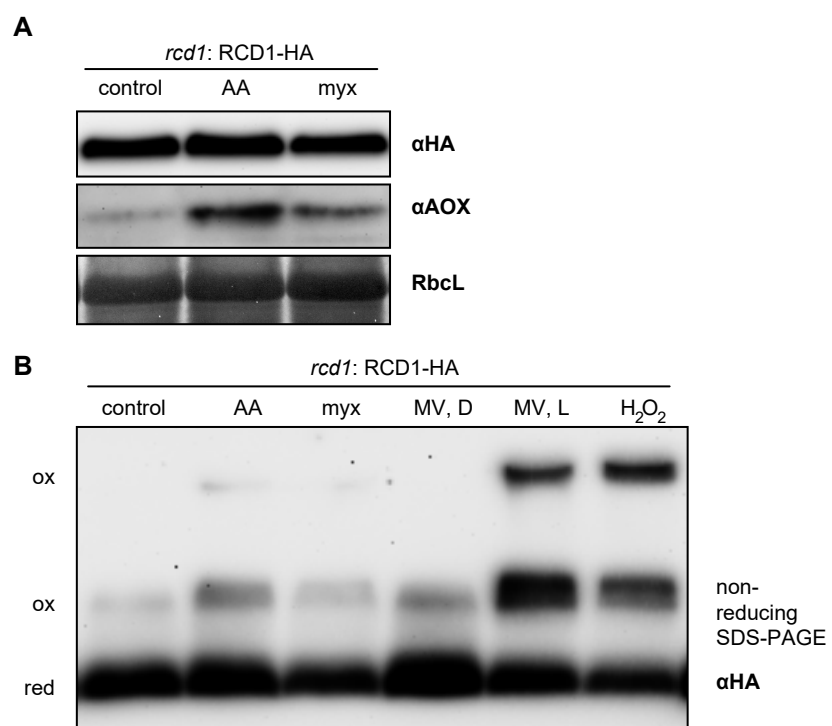


Figure 4 – figure supplement 2

Figure 4 – figure supplement 2. Effect of mitochondrial complex III inhibitors on abundance and redox state of the RCD1 protein.

- (A) Chemical induction of mitochondrial dysfunction signaling did not alter abundance of the RCD1 protein. Leaf discs were treated with 2.5 μ M AA or 2.5 μ M myx overnight. Then total protein extracts were isolated and separated in SDS-PAGE. Levels of RCD1-HA and of AOXs were assessed by immunoblotting with the specific antibodies as indicated.
- (B) Redox state of RCD1 protein was only very mildly altered by mitochondrial complex III inhibitors or by MV in the darkness. Treatment with AA or myx was performed as in panel (A). MV, D – leaf discs after overnight pre-treatment with 1 μ M MV in the darkness; MV, L – leaf discs after overnight pre-treatment with MV followed by 30 min of illumination; H₂O₂ – leaf discs after 30 min of incubation in presence of 100 mM H₂O₂ under light. Reduced (red) and oxidized (ox) forms of the protein are labelled.

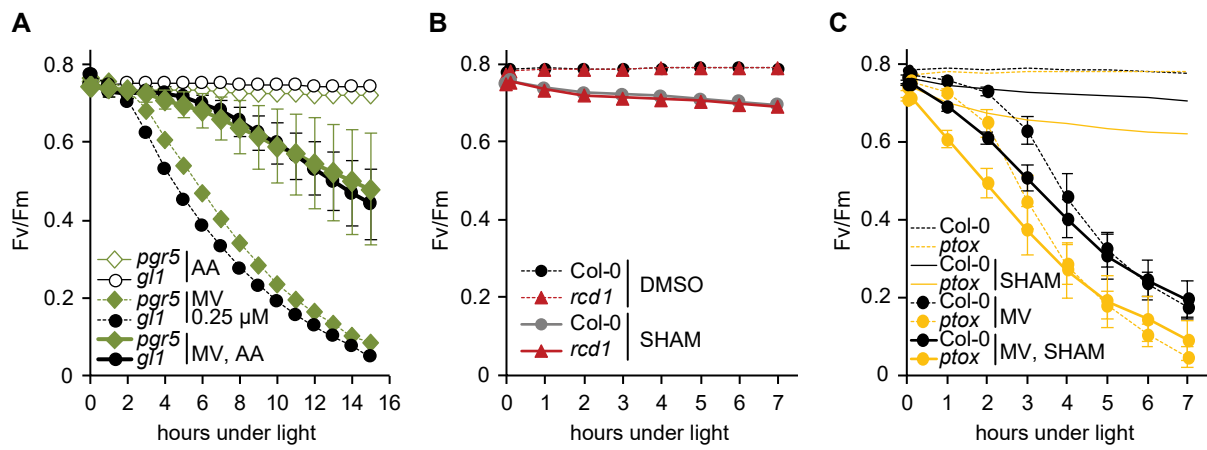


Figure 4 – figure supplement 3

Figure 4 – figure supplement 3. Specificity of inhibitor treatments. All chlorophyll fluorescence analyses are presented as mean \pm SD, for source data and statistics see Fig. 4 – supplemental dataset 1.

- (A) Interaction of AA with cyclic electron flow through binding to chloroplastic protein PGR5 (Sugimoto et al., 2013) is not the reason of AA-induced ROS tolerance. Possible off-target effect of AA was assessed by using the *pgr5* mutant. Pre-treatment with 2.5 μ M AA made both *pgr5* and its background wild type *g1* equally more tolerant to chloroplastic ROS. For each experiment leaf discs from at least four individual rosettes were used. The experiment was performed three times with similar results.
- (B) SHAM treatment results in only slight PSII inhibition both in Col-0 and *rcd1*. Fv/Fm was monitored under light after 1-hour pre-treatment with 2 mM SHAM. No significant difference was detected between Col-0 and *rcd1*. SHAM stock solution was prepared in DMSO, thus pure DMSO was added in the SHAM-minus controls. For each experiment leaf discs from at least four individual rosettes were used. The experiment was performed three times with similar results.
- (C) PTOX, plastid terminal oxidase analogous to AOX, is not involved in the SHAM-induced decrease of ROS tolerance. To exclude possible involvement of PTOX in MV-induced PSII inhibition, green sectors of the *ptox* mutant leaves were treated with 2 mM SHAM, 1 μ M MV, or both chemicals together. *ptox* mutant was responsive to SHAM treatment similarly to Col-0. For each experiment leaf discs from at least four individual rosettes were used. The experiment was performed twice with similar results.

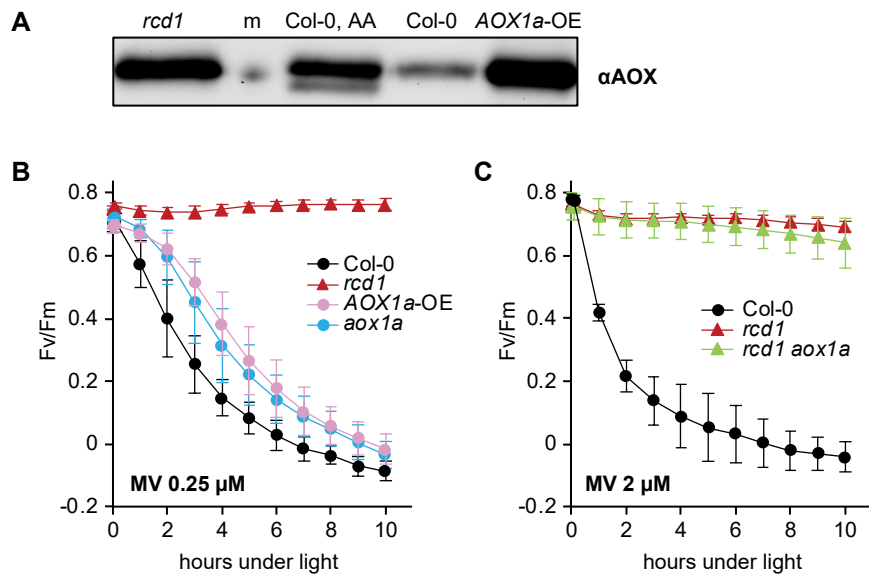


Figure 4 – figure supplement 4

Figure 4 – figure supplement 4. Irrelevance of AOX1a isoform for MV tolerance. All chlorophyll fluorescence analyses are presented as mean \pm SD, for source data and statistics see Fig. 4 – supplemental dataset 1.

- (A) Abundance of total AOX in the *AOX1a*-overexpressor line (*AOX1a*-OE) as assessed by immunoblotting was comparable to that in *rcd1* (m – molecular weight marker; AA – overnight treatment with 2.5 μ M AA).
- (B) Increased expression of AOX1a isoform is not sufficient to provide ROS tolerance. MV-induced PSII inhibition in the *AOX1a*-OE and *aox1a* lines was monitored by Fv/Fm. No significant difference was observed between *AOX1a*-OE and *aox1a* at any time point of the experiment.
- (C) AOX1a isoform is not necessary for chloroplastic ROS tolerance. MV-induced PSII inhibition in *rcd1 aox1a* double mutant was monitored by Fv/Fm. No significant difference was detected between *rcd1 aox1a* and *rcd1*.

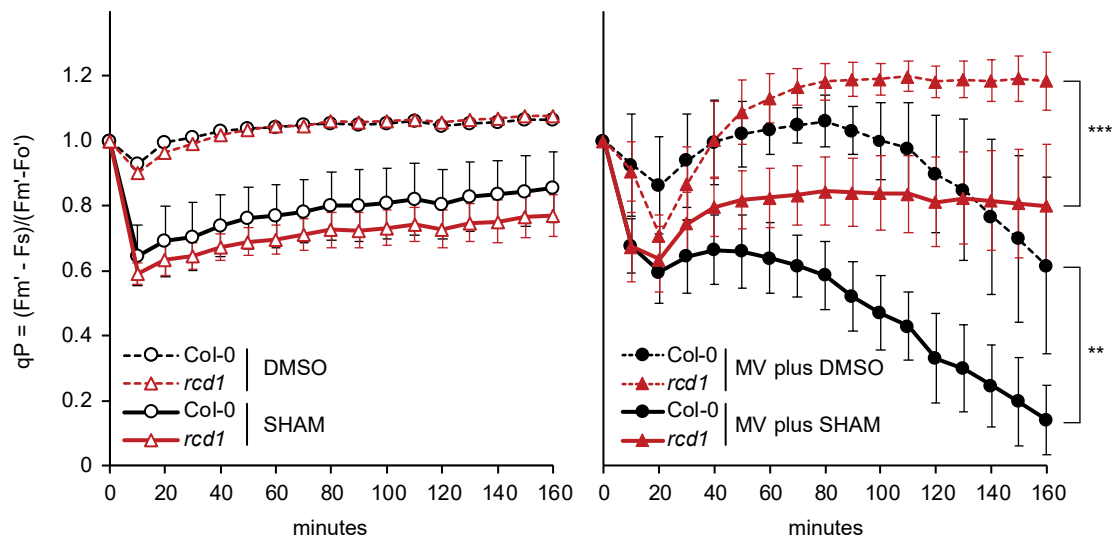


Figure 5 – figure supplement 1

Figure 5 – figure supplement 1. Alternations in chloroplast electron transfer induced by MV and SHAM. During the first 20 minutes of light exposure, MV-pre-treated Col-0 and *rcd1* experienced transient decrease in PSII photochemical quenching (qP). Within the next hour, photosynthesis recovered in *rcd1* to the level observed in the non-treated control, while only very mild recovery was observed in Col-0. In *rcd1*, the recovery was significantly inhibited by co-application of SHAM together with MV. Leaf discs were pre-treated with MV and SHAM for 1 hour in the darkness. SHAM stock solution was prepared in DMSO, thus pure DMSO was added in the SHAM-minus controls. To calculate qP, F_s was recorded as in Fig. 5A; saturating pulses were introduced every 10 minutes to measure F_m' . Data is presented as mean \pm SD, for source data and statistics see Fig. 5 – supplemental dataset 1.

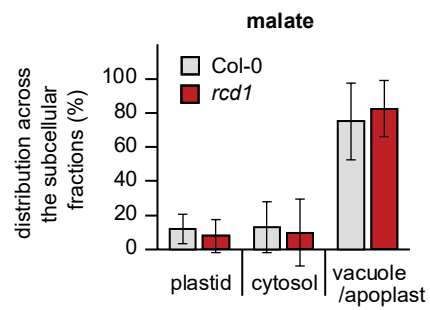


Figure 5 – figure supplement 2

Figure 5 – figure supplement 2. Distribution of malate in subcellular compartments of Col-0 and *rcd1*. Distribution of malate was assessed by non-aqueous fractionation metabolomics as described in Fig. 1 – figure supplement 5C. Mean values \pm SE are presented. For source data and statistics see Fig. 5 – supplemental dataset 1.

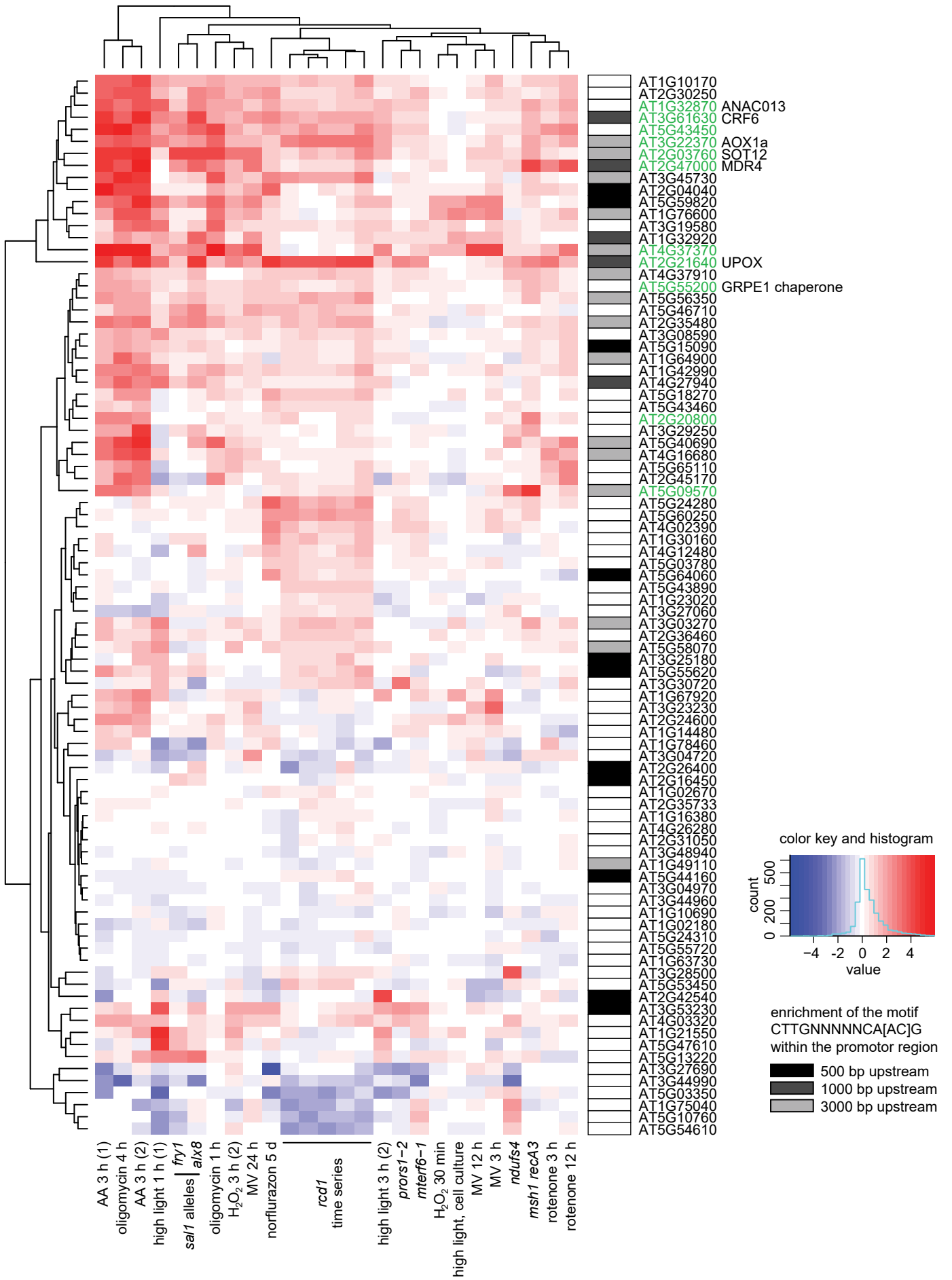


Figure 6 – figure supplement 1

Figure 6 – figure supplement 1. Clustering analysis of genes mis-regulated in *rcd1* (with cutoff of $\log_{2}FC < 0.5$) in published gene expression data sets acquired after perturbations of chloroplasts or mitochondria. Mitochondrial dysfunction stimulon (MDS) genes are labeled green. Enrichment of the ANAC013/ ANAC017 *cis*-element CTTGNNNNCA[AC]G (De Clercq et al. 2013) in promoter regions is shown by shaded boxes next to the gene names. Notably, MDS genes represent only a subclass of all genes whose expression is affected by RCD1. For example, a cluster of genes that have lower expression in both *rcd1* and *sal1* mutants and are mostly associated with defense against pathogens did not have enrichment of ANAC motif in their promoters. This is likely a consequence of interaction of RCD1 with about forty different transcription factors belonging to several families (Jaspers et al. 2009).

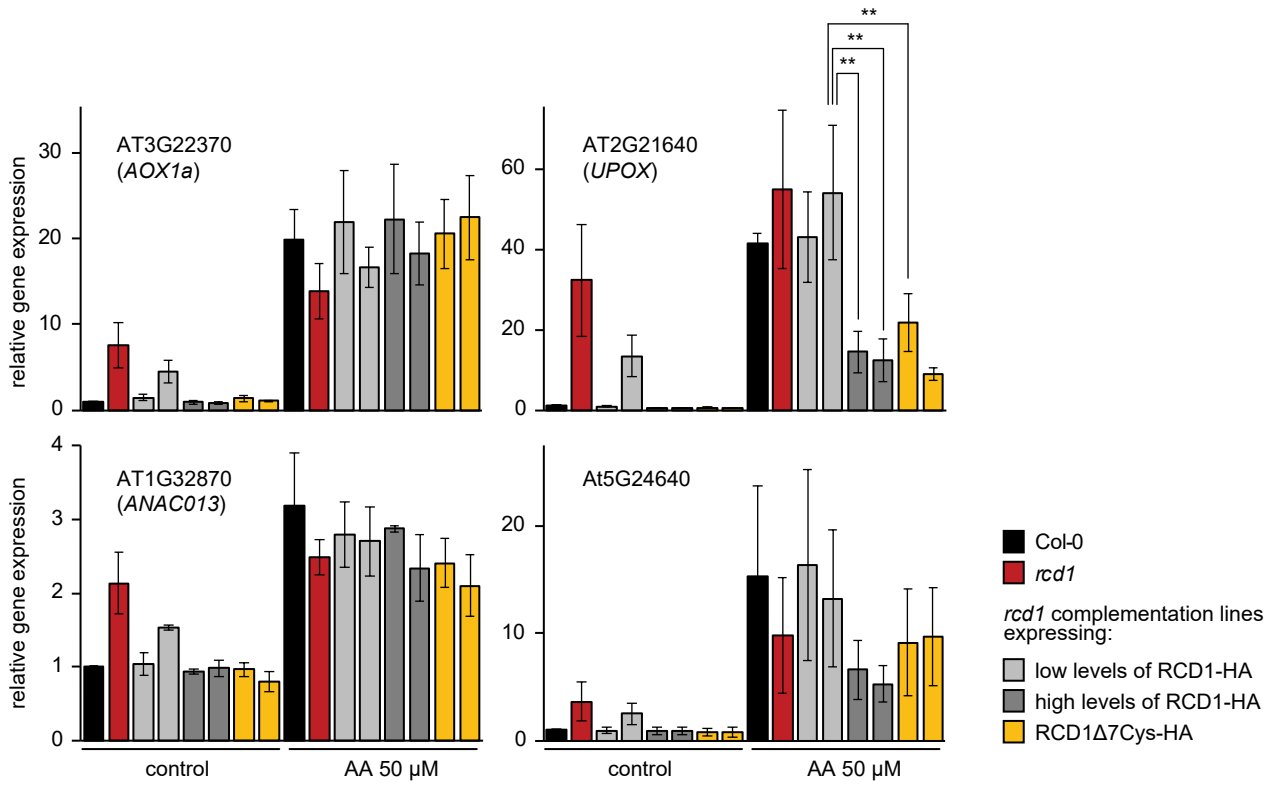


Figure 6 – figure supplement 2

Figure 6 – figure supplement 2. Induction of MDS genes in *rcd1* and *rcd1* complementation lines. To address the role of RCD1 in transcriptional response to AA, plant rosettes were sprayed with water solution of 50 μ M AA (or of DMSO as the control). Noteworthy, even though this concentration of AA has been widely used for the studies in mitochondria, AA \geq 20 μ M was shown to cause side effects including inhibition of chloroplast cyclic electron flow (Watanabe et al. 2016). Thus, the obtained results should be interpreted with caution. After 3-hour incubation under growth light, relative expression of the selected MDS genes was measured by real time quantitative PCR. Similar induction of *AOX1a* or *ANAC013* was observed in *rcd1*, Col-0, *rcd1*: RCD1-HA, and *rcd1*: RCD1 Δ 7Cys-HA lines. Interestingly, induction of another tested MDS gene, *UPOX*, was suppressed in the *rcd1*: RCD1-HA lines expressing higher levels of RCD1 and in the *rcd1*: RCD1 Δ 7Cys-HA lines. Analogous effect was observed for the MDS gene *At5G24640*, although with low statistical power. Suppressed MDS induction in the lines with higher levels of RCD1 was in line with the observation that RCD1 abundance *in vivo* inversely correlated with different tolerance of plants to MV (Figure 1 – figure supplement 1). Four rosettes were pooled together for each sample. Relative expression was calculated from three biological repeats and the data was scaled relative to control Col-0. Source data and statistics are presented in Figure 6 – supplemental dataset 1.

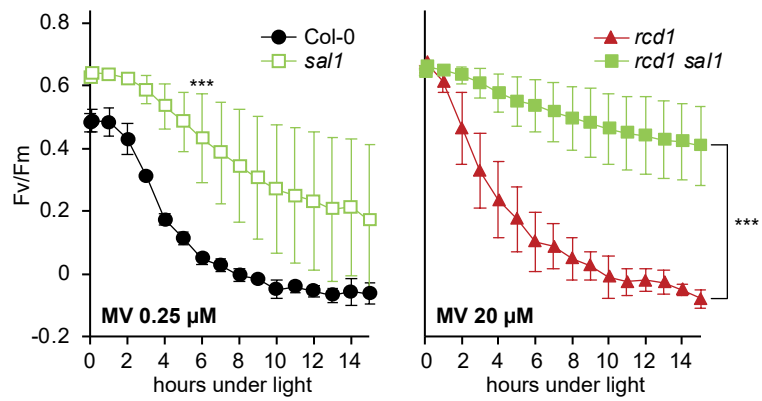


Figure 6 – figure supplement 3

Figure 6 – figure supplement 3. Tolerance of PSII to chloroplastic ROS in *sal1* mutants. MV-induced PSII inhibition was tested in 2.5-week rosettes. The single *sal1* mutant was more tolerant to MV than the wild type (left panel). The double *rcd1 sal1* mutant was more tolerant to MV than *rcd1* (right panel). Note different concentrations of MV used in the two panels. For source data and statistics see Fig. 6 – supplemental dataset 1.

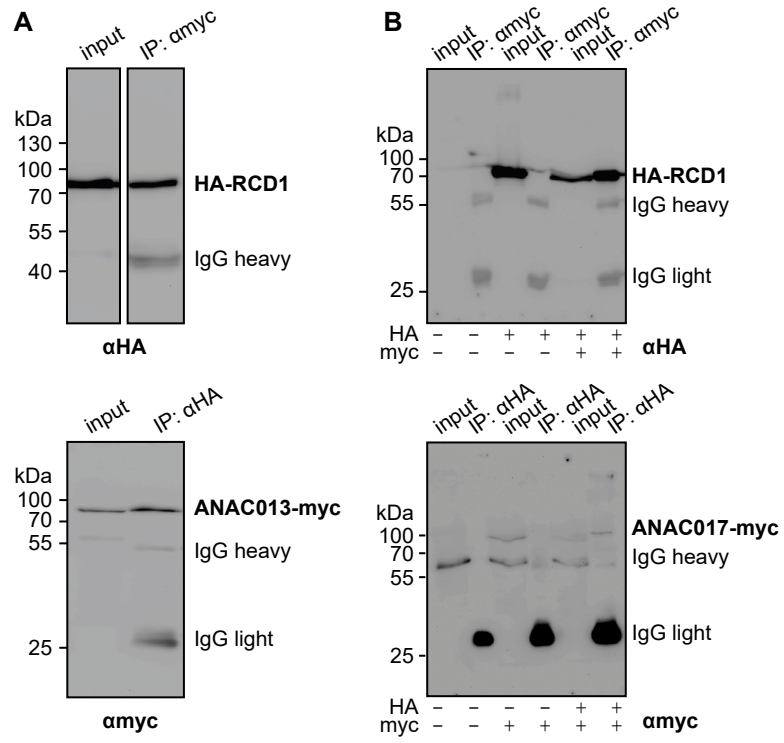


Figure 7 – figure supplement 1

Figure 7 – figure supplement 1. Biochemical interaction of RCD1 with ANAC013/ANAC017 transcription factors in human embryonic kidney (HEK293) cells. HA-RCD1 was co-expressed with ANAC013-myc (A) or ANAC017-myc (B) (IP – eluate after immunoprecipitation).

(A) Co-immunoprecipitation of HA-RCD1 with α myc antibody (top) and of ANAC013-myc with α HA antibody (bottom) indicated complex formation between HA-RCD1 and ANAC013-myc.

(B) Co-immunoprecipitation of HA-RCD1 with α myc antibody (top) and of ANAC017-myc with α HA antibody (bottom) indicated complex formation between HA-RCD1 and ANAC017-myc.

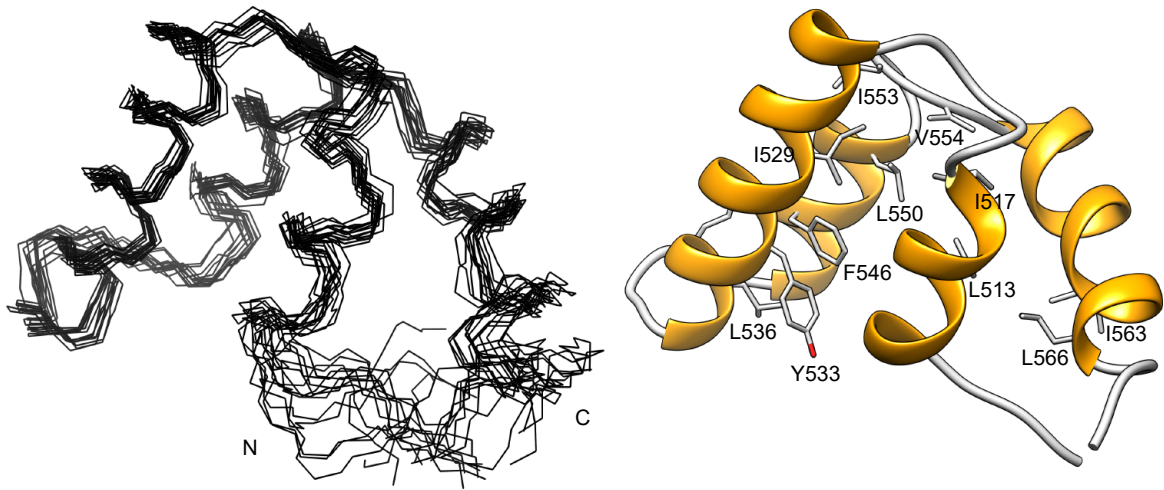


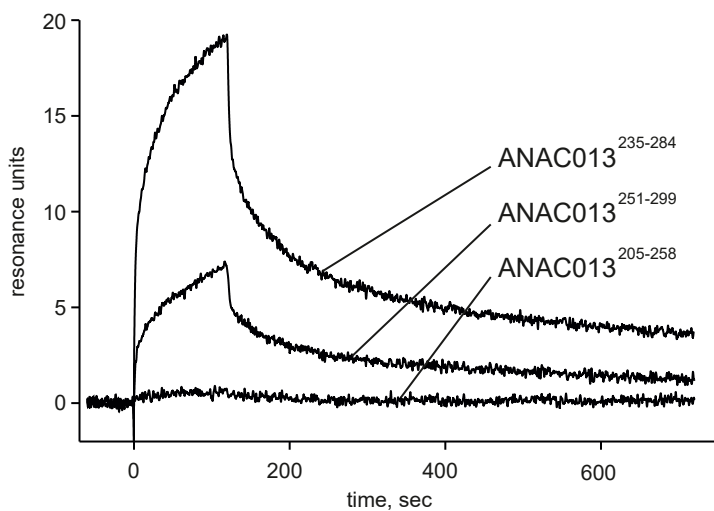
Figure 7 – figure supplement 2

Figure 7 – figure supplement 2. Structure of the RST domain of RCD1. Structure of the C-terminal domain of RCD1 (residues G468-L589) was determined by NMR spectroscopy. The first 38 N-terminal and the last 20 C-terminal residues are devoid of any persistent structure, hence only the structure of the folded part (residues P506-P570) is shown. The ensemble of 15 lowest-energy structures is on the left and a ribbon representation of the lowest-energy structure is on the right. The folded part represented by the RST domain is entirely α -helical and consists of four α -helices, F510-I517, E523-R537, R543-V554 and D556-L566. The structured region ends at position N568, which corresponds to the necessary C-terminal part for the interaction with transcription factors (Jaspers et al. 2010). The structure of the beginning of the first helix is dispersed in the ensemble due to sparseness of distance restraints. This arises from several missing amide chemical shift assignments (Tossavainen et al. 2017) as well as the presence of four proline residues in this region (P503, P506, P509 and P511), which severely hindered distance restraint generation. The many conserved hydrophobic residues (Jaspers et al. 2010), shown in stick representation, form the domain's hydrophobic core. Mutagenesis experiments identified hydrophobic residues L528/I529 and I563 as critical for RCD1 interaction with DREB2A (Vainonen et al. 2012). I529 and I563 are constituents of the hydrophobic core, and substitution of these residues probably disrupts the core of the RST domain thus abolishing the interaction. The atomic coordinates and structural restraints for the C-terminal domain of RCD1⁴⁶⁸⁻⁵⁸⁹ have been deposited in the Protein Data Bank with the accession code 5N9Q.

A

205 LWGKGLNQSELDDNDIEELMSQVRDQSGPTLQQNGVSGLNSHVDTYNLENLEEDMYLEINDLMEPEPEPTSVEVMENNWNEDGSGLLNDDDFVGA 299
205 LWGKGLNQSELDDNDIEELMSQVRDQSGPTLQQNGVSGLNSHVDTYNLENLEED 258
235 LQQNGVSGLNSHVDTYNLENLEEDMYLEINDLMEPEPEPTSVEVMENNWN 284
251 NLENLEEDMYLEINDLMEPEPEPTSVEVMENNWNEDGSGLLNDDDFVGA 299

B



C

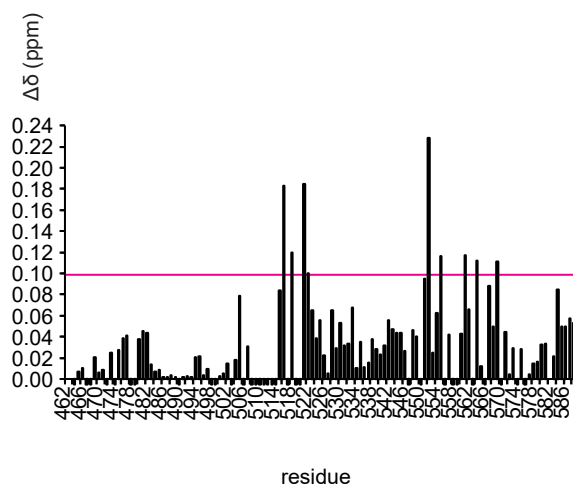


Figure 7 – figure supplement 3

Figure 7 – figure supplement 3. Analysis of interaction of the ANAC013-derived peptides with the RST domain of RCD1.

- (A) According to yeast two-hybrid data (O'Shea et al. 2017), ANAC013 residues 205-299 are responsible for interaction with RCD1. To narrow down the RCD1-interacting domain, three overlapping peptides ANAC013²⁰⁵⁻²⁵⁸, ANAC013²³⁵⁻²⁸⁴, ANAC013²⁵¹⁻²⁹⁹ were designed and tested for their binding to RCD1 by surface plasmon resonance.
- (B) Surface plasmon resonance interaction analysis of three ANAC013-derived peptides with the C-terminal domain of RCD1. The strongest binding was detected for ANAC013 peptide 235-284 (red in panel A), which was further used for the NMR titration experiment with the purified C-terminal domain of RCD1 (RCD1⁴⁶⁸⁻⁵⁸⁹).
- (C) Histogram depicting the changes in ¹H and ¹⁵N chemical shifts in RCD1⁴⁶⁸⁻⁵⁸⁹ upon addition of the ANAC013²³⁵⁻²⁸⁴ peptide. Changes were quantified according to the “minimum chemical shift procedure”. That is, each peak in the free form spectrum was linked to the nearest peak in the bound form spectrum. An arbitrary value -0.005 ppm was assigned to residues for which no data could be retrieved. The largest changes ($\Delta\delta \geq 0.10$ ppm) were found for residues located on one face of the domain, formed by the first and last helices and loops between the first and the second, and the third and the fourth helices. These residues probably representing the peptide interaction site are highlighted on the RST_{RCD1} structure in Fig. 7A inset. In addition, relatively large perturbations were observed throughout the RST domain, and notably, in the unstructured C-terminal tail, which might originate from a conformational rearrangement in the domain induced by ligand binding.

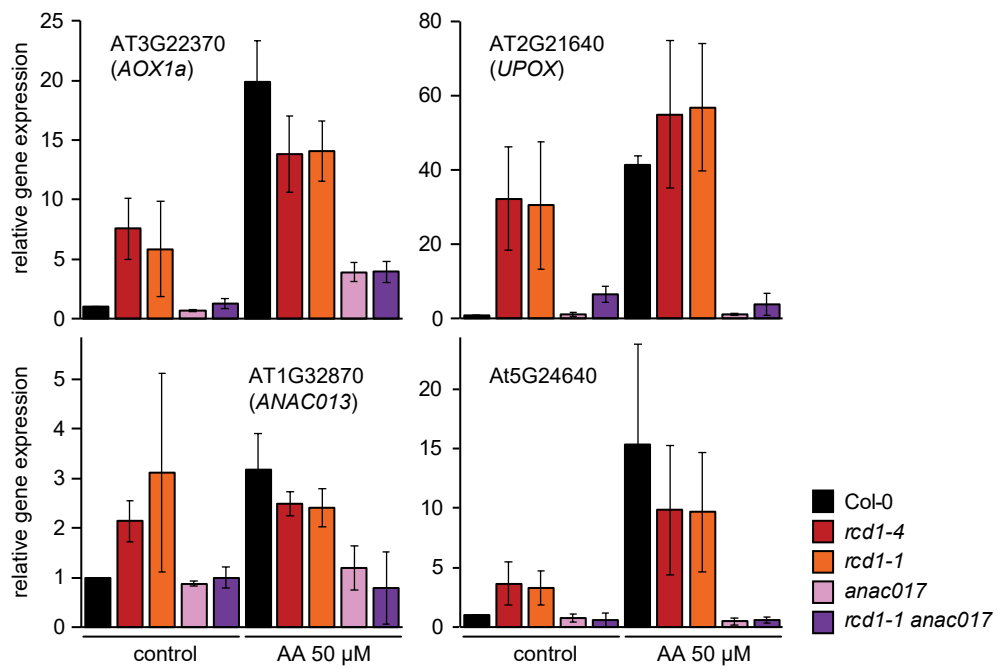


Figure 8 – figure supplement 1

Figure 8 – figure supplement 1. Induction of MDS genes in *anac017* and *rcd1 anac017* mutants. Expression of the selected MDS genes was assessed in rosettes 3 hours after spraying them with 50 μ M AA, as described in Figure 6 – figure supplement 2. The *anac017* mutation strongly suppressed induction of MDS genes in *rcd1* both under control conditions and after AA treatment. Relative expression was calculated from three biological repeats and the data was scaled relative to control Col-0. Source data is presented in Figure 6 – supplemental dataset 1.